Thermal performance of foam concrete structural façade elements with cavities

by

Hannelie Marais

Thesis presented in partial fulfilment of the requirements for the degree of Master of Engineering in Structural Engineering in the Faculty of Engineering at Stellenbosch University

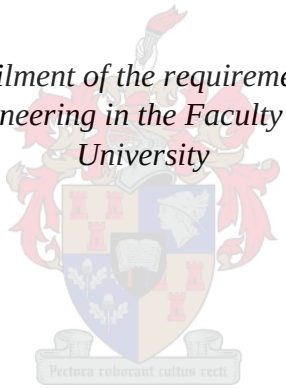

Supervisor: Prof. GPAG van Zijl

Co-supervisor: Dr. WI De Villiers

December 2020

The financial assistance of the National Research Foundation (NRF), Thuthuka Grant (99304), towards this research is hereby acknowledged. Opinions expressed and conclusions arrived at, are those of the author and are not necessarily to be attributed to the NRF.

Declaration

By submitting this thesis electronically, I declare that the entirety of the work contained therein is my own, original work, that I am the sole author thereof (save to the extent explicitly otherwise stated), that reproduction and publication thereof by Stellenbosch University will not infringe any third party rights and that I have not previously in its entirety or in part submitted it for obtaining any qualification.

Date: December 2020

Abstract

Thermal performance of foam concrete structural façade elements with cavities

H. Marais

Department of Civil Engineering,
University of Stellenbosch,
Private Bag X1, Matieland 7602, South Africa.

Thesis: MEng (Structural Engineering)

December 2020

The housing backlog in South Africa is an ever growing problem. Efforts are put together to study this problem and to reach a sustainable economical solution. Increased interest in the use of foam concrete in the building environment leads to renewed research in its use in structural housing elements where outside temperatures are the main influencing factor.

Foam concrete is a low density and lightweight material with excellent thermal properties. The Centre for Development of Sustainable Infrastructure has worked on increasing durability and strength of foam concrete while still maintaining a low density and 3D printing of this low density material. This study focusses on the detailed analysis of foam concrete cavity walls in terms of the cavity geometry and sizes for thermal comfort.

Parameters that greatly influence the thermal performance of foam concrete include its material density and its thermal conductivity. Other parameters include its porosity and effective pore size, specific heat, moisture content, core temperature rises and radiation inside the pores. These parameters also have an influence on each other. In some existing theoretical models pore volume fractions of the pore structure matrix are used to determine the effective thermal conductivity of foam concrete.

Heat exchange between the environment and the concrete surface occurs through convection and radiation and heat exchange that happens inside the concrete material occurs through conduction. In foam concrete, convection and radiation also takes place in the pores of the material. These heat transfer principles are analysed through finite element modelling of foam concrete wall sections.

An existing 3D printed foam concrete wall with air cavities is analysed using finite elements to determine the effect of conduction, convection and radiation on the thermal performance of the wall. A heat flux of 342 W/m^2 is applied on one side (the outside) of the wall section in different heat transfer analysis cases. When convection and radiation is included on the outer sides of the wall section and conduction in the wall section, the outside temperature is 41.798 °C and the inside temperature is 20.216°C. Heat is transferred through the foam concrete only and not through the air cavities which results in a non-uniform heat transfer. When the effects of cavity radiation is added to the air cavities, the outside temperature is 40.690°C and the inside temperature is 21.407°C. A more uniform heat transfer occurs through the wall. When heat transfer through cavity convection is also added, the outside temperature is 40.540°C and the inside temperature is 21.573°C. The slight decrease in the outside temperature is due to the release of some heat in the first cavity and as heat gathers closer to the inside of the wall section, the inside temperature increases slightly compared to when only cavity radiation is added to the wall section. When only heat transfer through conduction in the foam concrete and in the air cavities are modelled, the outside temperature is 42.022°C and the inside temperature is 20.407°C. Here it is evident that the effects of cavity radiation and cavity convection are neglected.

The effect of different cavity sizes and geometries of walls with equal total thicknesses is also researched. For fixed distances between rectangular cavities, the inside temperature is reduced by increasing the number of cavities. More cavities result in a reduced cavity thickness and thus a reduced void ratio which is the ratio between the total thickness of the air cavities and the total thickness of the wall. However, when a wall section with one set thickness between cavities and another wall section with another set thickness between cavities, are compared, the different void ratios as a result of the different thicknesses between cavities, can result in similar inside temperatures. Thus, a trend of reduced efficiency is suggested.

An analytical verification is done on the numerical results of some of the wall sections with rectangular cavities. A thermal resistance network is used which only accounts for conduction of the wall and the air cavities. Results are 3% higher than the numerical results.

It is thus concluded that the effect of cavity radiation and to a lesser extent cavity convection should not be neglected. Negligence of the effect of cavity radiation and cavity convection may lead to the prediction of a better thermal performance results than the reality. It is also concluded that cavity walls with more cavities rather than less, and thinner cavities give rise to an increased thermal performance.

Uittreksel

Termiese gedrag van skuimbeton strukturele fasade elemente met holtes

H. Marais

Departement Siviele Ingenieurswese,
Universiteit Stellenbosch,
Privaatsak X1, Matieland 7602, Suid Afrika.

Tesis: MIng (Struktuuringenieurswese)

Desember 2020

Die behuisingsagterstand in Suid-Afrika bly ‘n groeiende probleem. Daar is gesamentlike pogings om die probleem te bestudeer en ‘n volhoubare ekonomiese oplossing te vind. Dit veroorsaak onder andere verhoogde belangstelling in die gebruik van skuimbeton in die behuisingsomgewing asook nuwe navorsing oor die gebruik daarvan as strukturele behuisingselemente, waar buite-temperature ‘n bepalende rol speel.

Skuimbeton is ‘n lae digtheid, liggewig materiaal met uitstekende termiese eienskappe. Die Sentrum vir Ontwikkeling van Volhoubare Infrastruktuur werk daaraan om die duursaamheid en sterkte van skuimbeton te verhoog terwyl lae digtheid steeds behou word, en ook aan die 3D druk van dié liggewig materiaal. Hierdie studie fokus op die gedetailleerde analise van die geometrie en grootte van skuimbeton mure met holtes vir termiese gemak.

Parameters wat die termiese gedrag van skuimbeton grootliks beïnvloed, sluit die materiaaldigtheid en termiese geleidingsvermoë in. Porositeit, die effektiewe poriegroottes, spesifieke hitte, voginhoud, kerntemperatuurstygings en radiasie binne die porieë beïnvloed ook die termiese gedrag. Hierdie parameters het ook ‘n invloed op mekaar. Bestaande teoretiese modelle wat die effektiewe konduktiwiteit bepaal, sluit porie struktuur-matrikse in, waar die porievolumefraksies bepaal word.

Hitte-uitruiling wat tussen die omgewing en die beton-oppervlakte plaasvind, gebeur deur konveksie, en radiasie en hitte-uitruiling wat binne die betonmateriaal plaasvind, gebeur deur konduksie. In skuimbeton vind konveksie en radiasie ook plaas in die porieë. Hierdie hitte-uitruilingsmeganismes word ge-analiseer in die eindige elementmodellering van skuimbeton muurdele.

‘n Bestaande 3D-gedrukte skuimbetonmuur met lugholtes word ontleed met eindige elemente om die effek van konduksie, konveksie en radiasie op die termiese gedrag van die muur te bepaal. Hitte van 342 W/m^2 word aan die buitekant van die muurdeel toegepas vir die ontleding van verskillende hitte-uitruilingsgevalle. Wanneer konveksie en radiasie op die buitekante van die muurdeel toegepas word, en konduksie binne-in die muurdeel, is die buitenste temperatuur 41.798°C en die binneste temperatuur 20.216°C. Hitte wat dus net oorgedra word deur die skuimbeton en nie ook deur die lugholtes nie, lei tot ‘n nie-eenvormige hitte-oordrag. Wanneer die effek van radiasie in die lugholtes bygevoeg word, is die buitenste temperatuur 40.690°C en die binneste temperatuur 21.407°C. ‘n Meer eenvormige hitte-oordrag vind dan plaas deur die muur. Wanneer die effek van konveksie in die lugholtes ook bygevoeg word, is die buitenste temperatuur 40.540°C en die binneste temperatuur 21.573°C. Daar is ‘n effense afname in die buitenste temperatuur as gevolg van die hitte wat in die eerste holte vrygestel word, en namate die hitte nader aan die binnekant van die muurgedeelte versamel, verhoog die binne-temperatuur

effens, in vergelyking met wanneer slegs radiasie in die lugholtes bygevoeg word. Wanneer daar net hitte-uitruiling deur konduksie in die skuimbeton van die lugholtes gemodelleer word, is die buitenste temperatuur 42.022°C en die binneste temperatuur 20.407°C. Hier is dit duidelik dat die effek van radiasie en konveksie in die lugholtes nie in ag geneem word nie.

Die effek van verskillende groottes en geometrieë lugholtes van mure met gelyke totale diktes, word ook bestudeer. Vir ‘n vaste afstand tussen reghoekige lugholtes, word die binne-temperatuur verminder deur die hoeveelheid lugholtes te vermeerder. Dit het ‘n dunner lugholte tot gevolg en dus ‘n laer holte-tot-skuimbeton verhouding. ‘n Holte-tot-skuimbeton verhouding word gedefinieer as die verhouding tussen die totale dikte van die lugholtes en die totale dikte van die muur ‘n Muur met een vaste afstand tussen lugholtes en ‘n muur met ‘n ander vaste afstand tussen lugholtes het verskillende holte-tot-skuimbeton verhoudings, maar kan steeds dieselfde binne-temperatuur hê. (of eerder: Wanneer 'n muurgedeelte met een vaste dikte tussen holtes en 'n ander muurgedeelte met 'n ander dikte tussen holtes vergelyk word, kan die verskillende leemteverhoudings as gevolg van die verskillende dikte tussen holtes egter lei tot soortgelyke binnetemperature. ‘n Tendens vir afname in effektiwiteit word dus voorgestel.

‘n Analitiese verifikasie is ook gedoen op die numeriese resultate van sommige van die muurdele met reghoekige lugholtes. ‘n Termiese weerstandnetwerk is gebruik wat net konduksie van die muur en die lugholtes in ag neem. Resultate is 3.082% hoër as die numeriese resultate.

Daar word dus tot die gevolgtrekking gekom dat die effek van radiasie in lugholtes en, tot ‘n mindere mate, konveksie in lugholtes, nie geïgnoreer kan word nie. Wanneer hierdie hitte-uitruilingsmeganismes wel geïgnoreer word, kan die voorspelde resultate beter termiese gedrag gee as in werklikheid. Verder moet mure eerder meer lugholtes hê as minder en dunner lugholtes gee aanleiding tot ‘n toename in termiese gedrag.

Acknowledgements

I would like to thank the following people who contributed in this journey:

- My supervisor, Prof Gideon van Zijl, and my co-supervisor, Dr Wibke De Villiers. Thank you for your guidance and for sharing your knowledge and for being such incredible role models.
- My parents and especially my father for his ear to listen.
- My fellow colleagues to make this journey more memorable.
- Every friend and family member that prayed during this time.

Lastly, I would like to thank my Lord and Saviour, Jesus Christ. You are my rock and my strong foundation.

Table of Contents

Figures

Tables

Equations

Nomenclature

Latin variables

A	Area [m^2 or mm^2]
c	Specific heat [J/kgK or J/kg°C]
d_e	Pore diameter [nm]
E_c	Stiffness [GPa]
f_{cu}	Compression strength [MPa]
$f_{flexure}$	Flexural strength [MPa]
f_t	Tension strength [MPa]
F_{12}	View factor between surface 1 and surface 2
G_f	Fracture energy [N/m]
h	Convection heat transfer coefficient [W/m^2]
k	Thermal conductivity [W/mK]
k_g	Effective thermal conductivity of the gas [W/mK]
k_{hom}	Homogeneous thermal conductivity [W/mK]
k_m	Thermal conductivity of matrix [W/mK]
k_s	Thermal conductivity of the solid [W/mK]
k^*	Effective thermal conductivity of the gas [W/mK]
k_1	Thermal conductivity of spherical particles [W/mK]
l	Length [m or mm]
n	Normal vector
N	Coefficient of transmittance
P	Porosity
$P_{1,2}$	Pore volume fraction of material 1 or 2
q	Heat flux [W/m^2]
$\dot{q}$	Heat flux in terms of time [W/m^2]
q''	Heat flux in terms of spatial differentials [W/m^2]
q_{conv}	Heat flux in terms of convection [W/m^2]
q_r	Prescribed volume heat flux per volume [W/m^2]
q_{rad}	Heat flux in terms of radiation [W/m^2]
$q_{uniform}$	Uniform heat flux [W/m^2]
r	Heat supplied externally into the body per unit volume

R_{int}	Interfacial thermal resistance [°C/W or K/W]
R_{jk}	Thermal resistance between nodes k and j [°C/W or K/W]
S_1	Surface 1
S_2	Surface 2
S_3	Surface 3
t	Time [s]
T	Temperature [°C or K]
T_a	Ambient temperature [°C or K]
T_{cold}	Temperature on the cold side [°C or K]
T_{hot}	Temperature on the hot side [°C or K]
T_j	Temperature at node j [°C or K]
T_k	Temperature at node k [°C or K]
T_s	Surface temperature [°C or K]
T_0	Initial temperature [°C or K]
T^Z	Absolute zero temperature [-273.15°C or 0 K]
T^0	Sink temperature [°C or K]
$\dot{U}$	Material time rate of internal energy
V	Volume [m^3]
W_{dry}	Weight of oven-dried sample [kg]
W_{sat}	Weight in air of saturated sample [kg]
W_{wat}	Weight in water of saturated sample [kg]
x	Thickness [m or mm]

Greek variables

α	Thermal diffusivity [m^2/s]
α_{abs}	Absorptivity
α_i	Inside surface coefficient of heat transfer
α_o	Outside surface coefficient of heat transfer
β	Number of nodes adjacent to node j
ε	Emissivity
$\emptyset$	Volume fraction
φ	Configuration factor

ρ	Material density [kg/m^3]
σ	Stefan-Boltzmann constant [W/m^{2}K^4]
σ_d	bond stress [kPa]

Abbreviations

AAC	Autoclave Aerated Concrete
CDSI	Centre for Development of Sustainable Infrastructure
CFD	Computational Fluid Dynamics
CLC	Cellular Lightweight Concrete
CMU	Conventional Masonry Units
HGP	Hot Guarded Plate
ITR	Interfacial Thermal Resistance
LWC	Lightweight Concrete
LWFC	Lightweight Foam Concrete
MIP	Mercury Intrusion Porosymmetry
NBR	National Bureau of Standards
OPSFGC	Oil Palm Shell Foam Geopolymer Concrete
OPSNFGC	Oil Palm Shell Non-Foam Geopolymer Concrete
PCM	Phase Change Material
RDP	Reconstruction and Development Programme
SABS	South African Bureau of Standards
TBR	Thermal Boundary Resistance
TCR	Thermal Contact Resistance

Chapter 1

1 Prelude

This chapter discusses the topic that is being researched in the thesis. The background, scope and objective of the thesis are given and research limitations are identified.

1.1 Introduction

The bill of rights in the constitution of South Africa states that everyone has the right to have access to adequate housing. There is however an ever growing demand for adequate housing. The topic of housing has become closely knitted with mainly economic opportunities, safety and mobility amongst other issues (Jackson, 2015).

Single low-cost dwelling units in South Africa are built with conventional masonry units (CMU) which consist of concrete or burnt clay (De Villiers, 2019). Residential units in the Western Cape are currently constructed from unreinforced masonry. Quality, durability and temperature control of such houses remain challenging. Masonry walls are one of the major energy consuming components of buildings (Reddy et al., 2003). In order to increase the thermal capacity of masonry walls, the masonry layers can be thickened although this is uneconomical. Walls can also be sandwiched to provide better insulation. Typical pre-fabricated concrete sandwich elements are thick and heavy. These elements usually consist of an 80 to 100 mm thick outer panel made from reinforced concrete, a 100 to 200 mm thick insulation layer and an inner load-bearing panel of 100 to 150 mm reinforced concrete. It has been established that the thermal insulation capacity of a material is inversely proportional to its material density (Tada, 1986) (Silva et al., 2015). For buildings with high thermal performance requirements, while still maintaining a good strength performance, lightweight concrete can be used (Dunn et al., 2017). Thus, a decrease in the weight and thickness of walls affects the need for masonry mortar, masonry labour and transport cost.

To date there are limited set requirements and guidelines for housing projects in South Africa. The National Building Regulations (NBR) regulate the structural design of housing in South Africa (Act No. 103, 1977). The National Housing Code (NHC, 2009) and the National Building Regulations are used for national standard construction projects. For non-standard construction products Agrément certification may be obtained (Agrément, 2019). The National Building Regulations make provision for obtaining Agrément approval and thus one is still adhering to the requirements of the National Building Regulations if obtaining Agrément certification.

The use of foam concrete has become an excelling research topic in the building environment. Due to its low density which makes it easy to be precast and transported, and its low thermal conductivity which enhances its thermal performance, it can potentially be a competitor with other building materials.

Many studies have been done on the suitability of foam concrete as a building material. A few of these are Kearsley & Mostert (2005), Oginni (2017) and Van Zijl & Van Rooyen (2018). This thesis attempts to bring different characteristics of foam concrete like its excellent thermal performance into the building façade design world.

There have been no reported successes in the building industry to use foam concrete in façade design. There are also no certified standards about façade design. Therefore, guidelines for good façade design are identified in order to measure the performance of foam concrete as a suitable façade structure. A specific focus is laid on the necessary thermal performance of a building façade and what the use of foam concrete as a structural (load bearing) facade can do to meet these necessities.

1.2 Background

According to a General Household Survey that was conducted in 2017, 80.1% of South African households live in formal dwellings, 13.6% live in informal dwellings and 5.5% live in traditional dwellings (Government of South Africa, 2019). The survey also states that 13.6% of South Africans live in RDP (Reconstructive Development Programme) or state subsided dwellings (Government of South Africa, 2019). Tomlinson et al. (2015) report that although the government has provided over 2.5 million houses since 1994, the housing backlog increased from 1.5 million units to 2.1 million units.

The South African Bureau of Standards (SABS) published the first National Building Regulations (NBR) in 1985. From there numerous updates were made until SANS 10400 was published in 2010. A Home Building Manual first formed in 1999 was updated in 2015 to include Category 1 buildings in the NBR. Category 1 buildings include a floor area of less than 80 m^2, wall lengths of less than 6 m between lateral supports, single storey dwellings with wall thicknesses of 90 mm (NHBRC, 2015). The NBR (SANS 10400) states that non-standardised construction should take place on a performance-based criteria or a competent professionally registered person should submit a design or assessment to a body performing assessments of non-standardised building materials, being alternative masonry units, which is called Agrément South Africa.

For low cost housing (single storey Category 1 houses), normal concrete blocks still compete strongly against the use of lightweight concrete wall elements due to cost implications. A middle cost house is between R1.2 million and R 1.4 million and has an area of 141 m² to 220 m² (Business Tech, 2015). For loadbearing masonry middle cost housing there is still a great risk of the effect of seismic loads especially on multi storey units.

The focus of this study leans more toward middle cost housing with multiple stories due to the lightweight nature of lightweight concrete and due to the cost uncertainty in low cost housing when using lightweight concrete. Figure 1-1 shows a middle cost house located in Blackheath on the Cape Concrete premises called the Ukuzwana Building System constructed from cellular lightweight concrete (CLC). This Building System have received Agrément South Africa certification. Table 1-1 summarises the CLC mix design.

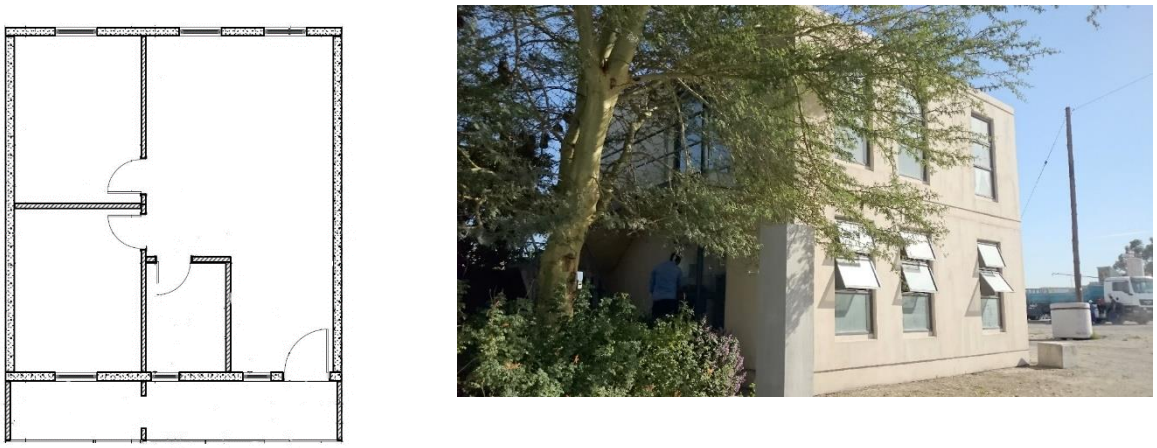

Figure 1-1: CLC two storey house in Blackheath

Table 1-1: Mix design of 1400kg/m^3 Ukuzwana Building System.

Sand	950 kg
Cement	380 kg
Water in mortar	150 kg
Quantity of foam	370 L
Water in foam	30 kg
Maximum strength	10 – 12 N/mm^2
Average thermal conductivity	0.45 W/mK

1.3 Scope

Research has been done on the structural properties of foam concrete (Dunn, 2017 and De Villiers et al., 2017) and the structural properties and construction of 3D printed foam concrete (Cho et al., 2019a). The focus of this research is on the suitability of foam concrete as a façade structure for middle cost houses. The project aims to use existing and developing knowledge of the mechanical behaviour and thermal properties of foam concrete to investigate whether foam concrete can increase the thermal performance of a building by using commercial FE software (Dassault Systémes, 2017).

The problem statement is thus the limited understanding regarding the thermal performance of printed foam concrete façade applications.

Existing models from Zhou et al. (2014), Al-Tamimi et al. (2017), Huang et al. (2018) and Del Coz Diaz et al. (2014) are used to gain a better understanding of the thermal performance of foam concrete. Other influencing parameters including the heat transfer parameters (heat conduction, heat convection and heat radiation), material density, porosity and pore structure, moisture content and high internal and external temperatures influencing thermal performance, are also researched through literature. These parameters are then used to form a model to predict the affect it has on the thermal performance of foam concrete.

1.4 Research objectives

Research objectives are to:

i. Identify influencing parameters on and existing predictive models of the thermal performance of foam concrete.
ii. Gain insight into the accurate thermal performance modelling of the heat transfer through walls with layered materials and hollow core structures by means of case studies.
iii. Effectively predict the thermal performance of foam concrete wall sections identified in (ii) using finite element (FE) software wall sections.
iv. Simulate the building model of an existing 3D printed wall with known foam concrete properties, by taking a representative section through the thickness of the wall and adding thermal parameters.
v. Determine effective cavity sizes and arrangements of hollow wall sections by FE modelling for thermal performance.
vi. Analytically verify FE models.

1.5 Outline

Chapter 2: Literature review
Lightweight foam concrete is broadly defined in terms of its microstructure and mechanical behaviour. Research then mainly aims on the thermal performance of lightweight foam concrete and heat transfer through a wall section.

Chapter 3: Finite element modelling of heat transfer
Advanced FE modelling programs are identified and the way in which these FE modelling programs evaluate heat transfer through wall elements are stated. Furthermore, case studies regarding cavity walls and layered walls are researched and analysed using FE modelling.

Chapter 4: FEA of 3DP foam concrete wall section
An existing 3D printed foam concrete wall section is modelled with the background of heat transfer through wall sections from the case studies discussed in Chapter 3.

Chapter 5: Cavity size and arrangement
Simple wall sections with different cavity sizes and numbers are analysed by FE modelling. The numerical models are analytically verified through the use of thermal resistance networks.

Chapter 6: Conclusions
An overview of findings is presented and recommendations for further research are proposed.

Chapter 2

2 Literature review

This chapter discusses current literature on lightweight concrete (LWC) and specifically foam concrete with focus on its thermal characteristics. Background on foam concrete is given including what it comprises of, what it is commonly used for and what the advantages and disadvantages are. Research is also done on the microstructure and the mechanical behaviour of foam concrete.

2.1 Background on lightweight foam concrete

2.1.1 History of lightweight foam concrete

The use of lightweight concrete (LWC) dates back almost a century, but renewed research intensity is evident. The ancient Romans introduced the idea of adding animal blood into concrete. This would allow air bubbles to form in the concrete which in turn makes it lighter and a better insulator. This idea of air entrapped concrete made the concrete more workable and durable (Aldridge, 2005).

Later, in the early 1900's air entrained materials began to be explored. Sweden, with its extreme weather conditions, introduced lightweight concrete that has a thermally efficient building characteristic and it was thus mainly used as insulation material (Aldridge, 2005).

The idea of air entrainment was accidentally re-discovered in America in the 1930's when it was observed that certain concrete pavements were more durable and frost damage resistant than other concrete (Dodson, 1990). The concept of air entrainment was then formed; the process whereby small air bubbles are entrained into concrete. These bubbles then become part of the matrix where it is surrounded by the skeleton formed by the paste that binds the aggregate together in the hardened concrete.

Cellular concrete blocks, wall boards, and floor slabs for commercial and residential structures were created in the 1930's in the Soviet Union. In the 1940's and 1950's equipment and standards were developed (Panesar, 2013).

2.1.2 What is lightweight concrete

Lightweight concrete consists of water, binder and inorganic aggregates, cement or agents. It is characterised as a low density, porous material with good thermal properties. A study has been done to determine the types of lightweight concretes and their properties. After researching the types of lightweight concretes and how they are formed, it is concluded that many lightweight concretes with different forming methods, being air entrained or foamed, and with different curing treatment by autoclaving versus simple air-curing or wrapping, have been given the same name although not necessarily referring to the same material. Therefore a clear distinction is made in the diagram in Figure 2-1.

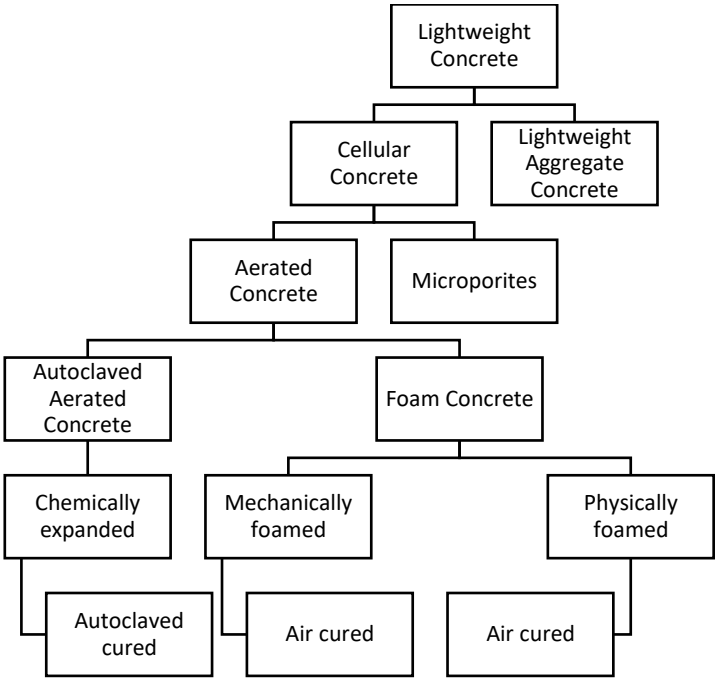

Figure 2-1: Diagram of types of lightweight concretes

Lightweight concrete can be divided into lightweight aggregate concrete or cellular concrete. Cellular concrete is formed through either foaming, air-entraining or a pore forming method. Cellular concrete is divided into aerated concrete and microporites. Aerated concrete has a closed system of macroscopic pores due to air-entraining or foaming agents. Microporites on the other hand do not contain either of these agents, but results from mortar mixed with water that retracts to form homogeneous pores (Rudnai, 1963).

Aerated concrete, made from mineral bound foams, can either be classified as autoclaved aerated concrete (AAC), or foam concrete (Just & Middendorf, 2008). When concrete is autoclaved, it is cured in a chamber at high temperatures and high pressures to develop high strength and reduced shrinkage. This process is however energy-intensive and may not be a sustainable method of forming lightweight concrete.

Foam concrete, also known as foamcrete or cellular lightweight (aerated) concrete, is a material with a minimum of 20% by volume of mechanically or physically entrained foam. It is defined as a cement based slurry of foam mixed with or entrained into plastic mortar. The foaming agents, which may be synthetic or protein based, create enclosed air bubbles by increasing the stability of the bubbles and reducing the surface tension of the solution. Foam concrete consists of water, cement or cement and fly ash (and/or slag blend), sand and a foaming agent. The cement generally used is ordinary Portland cement, but cement replacements can be used (Aldridge, 2005).

Notable characteristics of foam concrete are low density, low thermal conductivity and low embodied energy. Due to its low density of between 800 to 1600 kg/m^3 (normal concrete has a density of 2400 kg/m^3), foam concrete has a lower inertia for seismic accelerations during an earthquake (Kearsley, 1996). The low density of foam concrete also makes it possible for entire walls to be manufactured as a single uniform precast panel in scalable factory conditions. This presents better quality control associated with factory conditions (Kearsley, 1996).

Although AAC is advantageous for fast strength development and minimal shrinkage, it has been decided not to focus on autoclaving due to its high energy demand. Also, South Africa has limited

resources of lightweight aggregate that needs to be mined using financial and energy resources. The focus of this study will thus fall on air-cured foam concrete. A team at Stellenbosch University has been working on a mix design method of lightweight foam concrete and efforts are put together to study the mechanical performance of the material. This study focusses on the thermal performance of lightweight foam concrete and the effectiveness thereof as a façade structure to control the thermal performance of a building.

2.1.3 Common uses of foam concrete

Today, foam concrete is mostly non-structural as reported in a review publication by Van Zijl & Van Rooyen (2018). Common applications include insulation and backfill for drainage. Other applications include pre-cast wall blocks and panels, high volume void filling, floor and roof screeds, trench reinstatement and road foundations (Oginni, 2017). Cellular concrete is also used for provision of fire protection or soil stability in building and other precast elements and grouted tunnel walls.

Significant improvement of the mix of foam concrete and improved quality of the surfactants or foaming agents over the last two decades have enabled the use of foam concrete on a larger scale in a wider variety of applications. Kearsley and Mostert (2005) designed foam concrete with high fly ash contents to use foam concrete in construction and Van Zijl and Van Rooyen (2018) studied chloride profiling of integral and non-integral surface treated foam concrete. Van Zijl and Van Rooyen (2018) also introduced small amounts of micro fibre in the foam concrete mix to increase its durability.

2.1.4 Advantages and disadvantages of foam concrete

Foam concrete has many advantages. These include its ability to flow, its self-compacting and self-levelling nature and its low weight. Although strength has been a concern in the past, improvement of foam stability, whereby entrained air void dispersion and size is better controlled, together with refining of mixes and the addition of fly ash, the material exhibits controlled strength, sufficiently high for structural application and good load-bearing capacity (Van Rooyen, 2013). Furthermore, foam concrete exhibits excellent thermal insulation properties. Disadvantages still are high shrinkage and creep strains. Fillers like sand and fly ash and other additives like propylene glycol can reduce these strains, but still not to a significant level to compete with ordinary concrete (Do Amaral, 2019).

The most important reason for air entrainment in standard normal weight concrete is for durability purposes. The inclusion of air voids in the concrete leads to increased resistance to freeze-thaw damage, a deterioration mechanism of concrete in cold regions (Van Rooyen, 2013). However, the research focus here is on foam concrete, which contains significantly more entrained air than normally included purely for freeze-thaw resistance.

As for normal weight concrete, the properties of foam concrete deviate with age, temperature and humidity (Mydin, 2013). The advantage of the use of normal concrete is the vast pool of experience and data collected over the last century. Therefore standards like Eurocode (EN 1992-1-1:2004) offer time dependent equations for strength and stiffness relations. For foam concrete, like any new construction material, guidelines are still minimal. Characteristic values and material factors have yet to be determined with greater certainty.

Nonetheless, it is postulated that foam concrete is a useful construction material due to its low mass, which is advantageous for tall buildings, precast panels and the use of more cost effective low capacity cranes to hoist these precast panels, and in seismic regions. Furthermore, foam concrete promises a high insulation capacity and high durability due to its closed pore system. Foam concrete can increasingly compete with structural masonry and normal density concrete due to an increasing understanding of the material and foam technology.

2.2 Material characteristics of foam concrete

2.2.1 Microstructure

Foam concrete has a closed pore structure. According to Ramamurthy et al. (2009) pores between 1.5 and 2 nanometres are called gel pores, pores between 5 and 5000 nanometres are called capillary pores and pores having an irregular compaction shape are called macro pores. The pores at the various scales affect the composite mechanical properties of strength, creep and shrinkage. For 28-day dry densities lower than approximately 1000 kg/m^3 the 28-day compressive strength decreases for larger air voids and for 28-day dry densities higher than approximately 1000 kg/m^3 the 28-day compressive strength is not influenced by the air-void sizes (E Kearsley & Visagie, 2002).

Furthermore, according to Visagie & Kearsely (2002), for mixtures with dry densities lower than 1000 kg/m^3, 90% of the spacing distances are larger than approximately 35 micrometers and 50% of the spacing distances are larger than approximately 100 micrometers. Spacing distances increase for the higher dry densities. There is no clear relationship between the 28-day dry densities and the air-void spacing.

Foam concrete pores are either synthetically or protein based. Protein based pores or air bubbles are formed as a result of degradation of protein peptide linkage of large protein breaks which results in small hydrophobic molecules. The small molecules reduce the surface tension of the solution while creating an interface for bubbles and hydrogen bonds between molecules, which helps develop stable bubbles (Panesar, 2013). Synthetic based pores are created using a hydrophobic amphiprotic substance which is dissolved in water. This process forms air bubbles (Panesar, 2013).

Mubatapasango (2017) computed tomography scans on foam concrete with surface treated agents, namely integral surface treatment and non-integral surface treatment. His results showed that integral surface treated foam concrete has a lower total void volume compared to non-integral surface treated foam concrete. A uniform void distribution was discovered in each foam concrete but non-integral surface foam treated concrete has larger voids (7.04×10^{-3} mm^3) than integral surface treated foam concrete (4.36×10^{-3} mm^3). Furthermore, as seen in Figure 2-2, for non-integral surface treated foam concrete the largest network of connected air voids is 21.96 mm^3 at 3.52 mm from the top surface where for integral surface treated foam concrete the largest network of connected air voids is 6.49 mm^3 at 13.44 mm from the top surface. The connectivity of voids may weaken the foam concrete, and form transport channels for deleterious substances in the foam concrete which may impair its durability. Thus, it was concluded that smaller, well-dispersed voids should be entrained to avoid weak areas and access routes in the concrete.

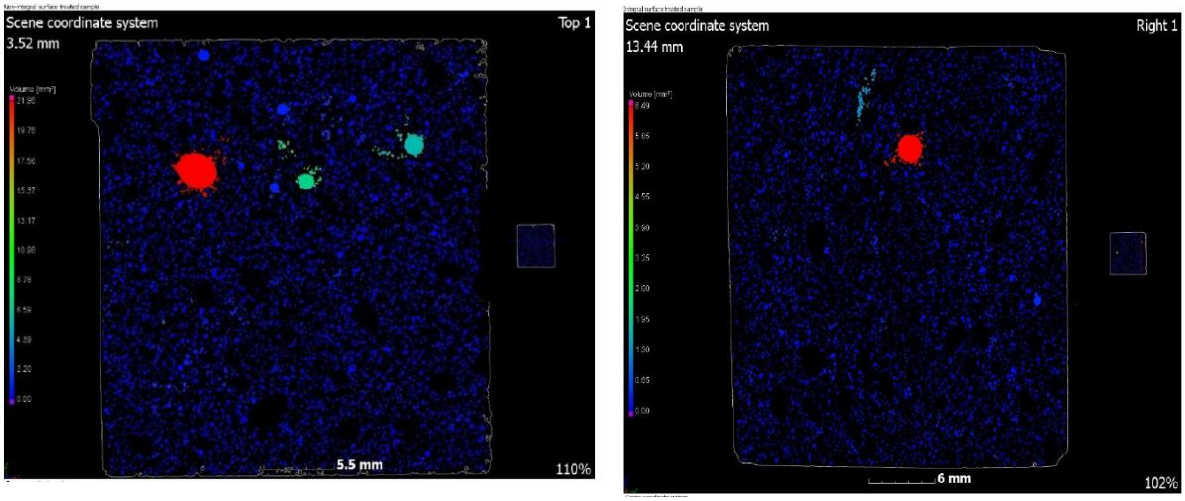

(a) (b)

Figure 2-2: Illustration of void connectivity in (a) non-integral surface treated concrete and (b) integral surface treated concrete (from (Mubatapasango, 2017)*)*

2.2.2 Mechanical behaviour

As with normal concrete the greater the air content the weaker the foam concrete. The strength of foam concrete can also be ascribed to the cement/water ratio for any given mix as it influences the density and strength of the skeleton.

The amount of air entrained in foam concrete may compromise the compressive strength and durability properties. For normal weight concrete the water to cement ratio governs the compressive strength, but for foam concrete the air void content and thus the composite density dominates the compressive strength (EP Kearsley & Wainwright, 2001). More entrained air reduces the distance between the entrained air voids, which increases the possibility of more interconnectivity, hence weaker and less durable foam concrete. However, it has been shown that less connected air voids results in a lower reduction in compressive strength (Vinith Kumar et al., 2018).

According to Wee (2006) an increase in air content does not lead to an increase in air void size, but leads to an increase in the number of air voids per unit volume. In this way the density is decreased without substantially decreasing the compressive strength. Also, when air voids are disconnected (thus having a closed pore structure), the compressive strength is reduced less. The skeleton composition and the fineness of the air voids therefore are important factors in determining strength (Van Zijl & Van Rooyen, 2018). These disconnected air voids are closed voids and are discussed in Section 2.2.3.

Figure 2-3 shows the normalised compression strength (f_{cu}), tension strength (f_t), stiffness (E_c), fracture energy (G_f) and bond stress (σ_d) of foam concrete with densities of 1200 kg/m^3, 1400 kg/m^3 and 1600 kg/m^3 compared to normal weight concrete (standard class 40MPa) (De Villiers et al., 2017). From the graph it can be seen that the compression and tension strengths are both disproportionate to density, and the stiffness is proportionate to density. However, the fracture energy is very low, an improvement for 1400 kg/m^3 foam concrete is made by including 0.35 % by volume of polypropylene fiber with a length of 12 mm and a diameter of 0.04 mm (Dunn et al., 2017).

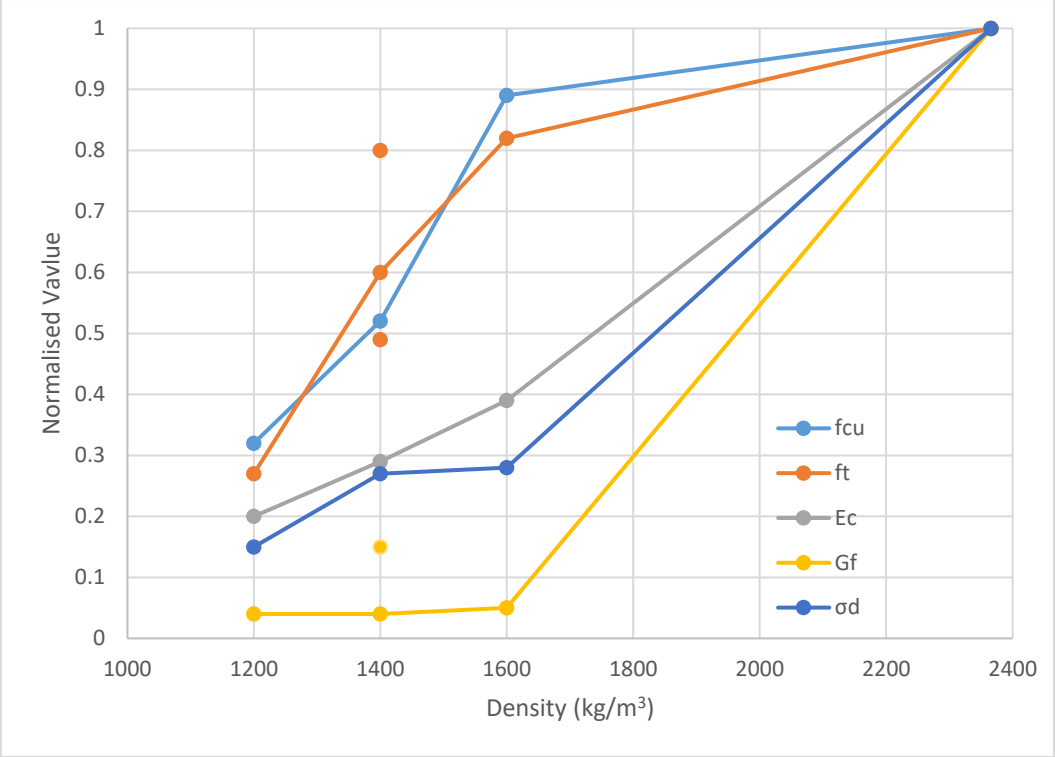

Figure 2-3: Normalised compression and tensile strength, stiffness, fracture energy and bond stress of concrete with different densities with improvements for 1400 kg/m³ in f_{cu} and G_f (reworked from De Villiers et al. (2017)*).*

2.3 Thermal characteristics of foam concrete

Concrete can be seen as a thermal conductor (Marshall, 1972). Temperature changes occur through heat exchange, being source or sink, between the concrete and the environment and inside the concrete. Heat exchange that happens between the environment and the concrete surface occurs through convection and radiation heat transfer and heat exchange that happens inside the concrete material occurs through conduction heat transfer. In foam concrete, convection and radiation also take place in the pores of the material. Heat transfer is thus divided into conduction, convection and radiation and is illustrated in Figure 2-4 for a walling system with one side exposed to the outside environment and one side exposed to the indoor environment.

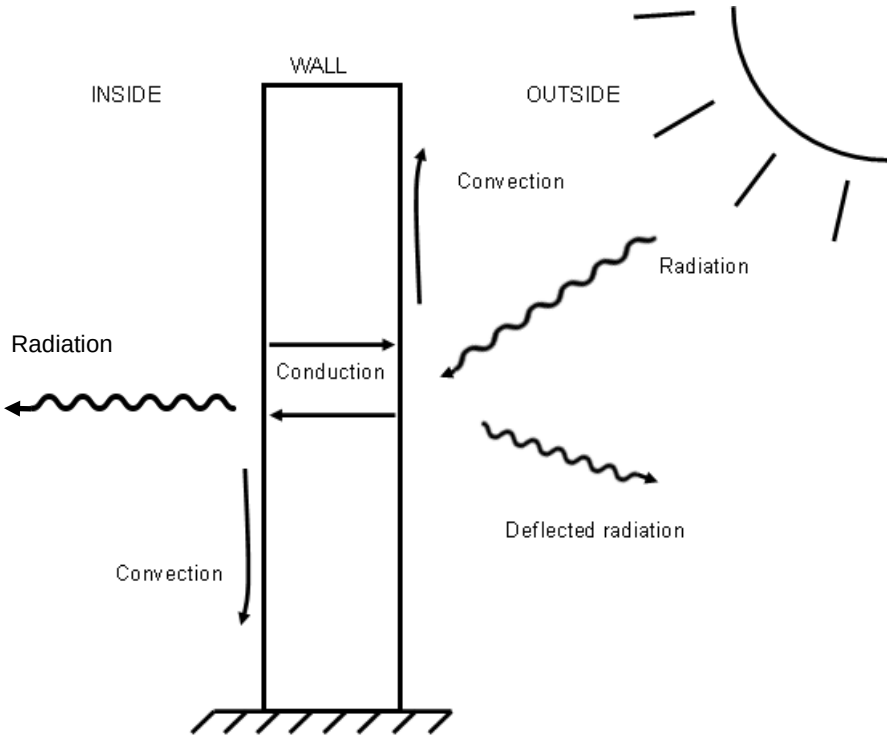

Figure 2-4: Heat transfer through a wall

According to Marshall (1972), thermal expansion, thermal conductivity (k), specific heat (c) and thermal diffusivity (α) are important roleplayers in the thermal characteristics of normal concrete. These properties change with age, temperature and humidity.

In order to understand the modes of heat transfer that occur in and around a foam concrete wall element, the general concept of these modes need to be studied thoroughly. In thermodynamics, the internal energy of a system (U) is the sum of the heat exchanged between the system and its surroundings and the work done by or on the system. Heat flows spontaneously from areas with high temperatures to areas with lower temperatures to reach thermal equilibrium. The way in which heat flows is by heat transfer through the modes of conduction, convection and radiation heat transfer.

The conservation of energy principle states that energy can neither be created nor destroyed but can only change from one form to another (Cengel & Ghajar, 2015). Thus, the total energy that enters a system minus the total energy that leaves a system must be equal to the change in the total energy of the system. During steady state form the rate of net energy transfer into a system is thus equal to the rate of net energy transfer out of the system. The heat transfer analysis of a system follows energy balance due to the conservation of energy principle so that the heat going into a system plus the heat generated in the system equals the heat going out of a system plus the heat stored in the system. The heat transfer follows the mode of conduction, convection and radiation as mentioned and the energy that is generated is put into thermal energy. When the heat of a system increases, the thermal energy will be stored in the system as the product of the density, the specific heat and the difference in temperature over time at a specific location in the system.

Thermal conduction is the transfer of heat through microscopic collisions of particles. The rate of heat conduction is dependent on the geometry of the medium (its thickness), the material type and the temperature difference across the medium. Heat conduction can be expressed as a heat flux with unit W/m^2 and is proportionate to the area and temperature difference of a medium and inversely proportionate to the thickness of a medium.

$$rate\ of\ heat\ conduction \propto \frac{area \times temperature\ difference}{thickness}$$

To translate the rate of heat conduction (heat flux with symbol q) to a usable equation, the difference in temperature over the difference in thickness is multiplied by a constant called the thermal conductivity having a symbol k and unit W/mK. Thermal conductivity is further explained in Section 2.3.1. The rate of heat conduction can thus be expressed using Equation 2.1 where the heat flux is described in terms of time ($\dot{q}$) and spatial (q'') differentials. When the difference in thickness (Δx) is infinitesimally small ($\Delta x \to 0$), Equation 2.1 can be changed to Equation 2.2 which is called the Fourier heat flow equation or the Fourier law.

$$\dot{q}'' = -k\frac{\Delta T}{\Delta d} \tag{2.1}$$

$$\dot{q}'' = -k\frac{dT}{dx} \tag{2.2}$$

Thermal radiation is electromagnetic radiation emitted from a material due to the heat of the material and is relatively independent of a material's thickness and the area of air the material is exposed to. However, radiation is very much dependent on the reflectance of material surface. Radiation can be expressed using Equation 2.3.

$$\dot{q}'' = \alpha_{abs}\varphi\varepsilon\sigma\Delta T^4 \tag{2.3}$$

where φ is the configuration factor, σ is the Stefan-Boltzmann constant with a value of $56.7\text{x}10^{-9}$ W/m^{2}K^4, ε is emissivity between 0 and 1 and α_{abs} is the absorptivity which is a fraction of radiation energy incident on a surface absorbed by the surface between 0 and 1. In order to consider radiation on the material surface, a radiation boundary condition is set for Equation 2.3. This boundary condition is expressed by Equation 2.4. The symbol n is the normal vector to the surface and T_s and T_a are the panel surface temperature and ambient air temperature respectively.

$$-k\frac{\partial T}{\partial n} = \varepsilon\sigma(T_s^4 - T_a^4) \tag{2.4}$$

Thermal convection is the transfer of heat through fluid motion. Convection can be expressed using Equation 2.5.

$$\dot{q}'' = h\Delta T \tag{2.5}$$

where h is the convection heat transfer coefficient (W/m^2). Another boundary condition, a convection boundary condition is set to solve Equation 2.2 and is expressed by using Equation 2.6.

$$-k\frac{\partial T}{\partial n} = h(T_s - T_a) \tag{2.6}$$

The convection heat transfer coefficient can be associated with the convection of air. Factors that influence the convection heat transfer coefficient include the type of surface (i.e. how smooth or how rough), the type of material of the formwork and flow characteristics. According to Rastrup (1954) the heat transfer coefficient ranges between 5 to 35 W/m^{2}K. The convection heat transfer coefficient also increases as the wind speed increases. More heat is released through convection than through conduction, that is from the centre of the material to the surface (Lee et al., 2009).

Thermal conduction along a building envelope panel with dimensions dx, dy and dz, as shown in Figure 2-5, is expressed by Equation 2.7.

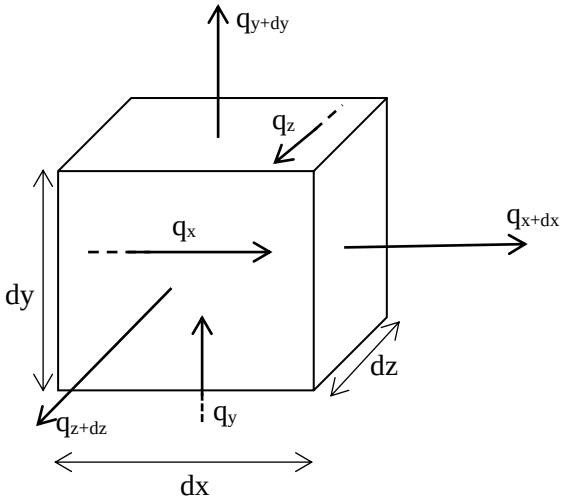

Figure 2-5: Thermal conduction along a building envelope panel (reworked from del Coz Diaz et al. (2012)*).*

Heat inflow during a specific time plus the heat generated by internal sources during the specific time is equal to the heat outflow during the specific time plus the change in internal energy during the specific time.

$$(q_x + q_y + q_z)dt + \dot{q}dxdydzdt = (q_{x+dx} + q_{y+dy} + q_{z+dz})dt + \rho c dT dxdydz \tag{2.7}$$

Where q_x and q_{x+dx} are as follows:

$$q_x = -k_x A_x \frac{\partial T}{\partial x} = -k_x \frac{\partial T}{\partial x} dydz \tag{2.8}$$

$$q_{x+dx} = -k_x A_x \frac{\partial T}{\partial x} - \frac{\partial}{\partial x}\left(k_x A_x \frac{\partial T}{\partial x}\right) dx = -k_x \frac{\partial T}{\partial x} dydz - \frac{\partial}{\partial x}\left(k_x \frac{\partial T}{\partial x}\right) dxdydz \tag{2.9}$$

Similar expressions for q_y, q_z, q_{y+dy} and q_{z+dz} can be created and by dividing by *dxdydz* one obtains:

$$\rho c \frac{\partial T}{\partial t} = \frac{\partial}{\partial x}\left(k_x \frac{\partial T}{\partial x}\right) + \frac{\partial}{\partial y}\left(k_y \frac{\partial T}{\partial y}\right) + \frac{\partial}{\partial z}\left(k_z \frac{\partial T}{\partial z}\right) + \dot{q} \tag{2.10}$$

The material density is symbolised as ρ and c is the specific heat. The symbol T is temperature and k_x is the thermal conductivity in the x-direction. The heat source $\dot{q}$ is expressed as power per unit volume with unit W/m^3. When considering foam concrete as an isotropic medium, the thermal conductivity in the different directions is the same, i.e. $k = k_x = k_y = k_z$. Thus, Equation 2.10 can be rewritten as Equation 2.11.

$$\frac{\partial^2 T}{\partial x^2} + \frac{\partial^2 T}{\partial y^2} + \frac{\partial^2 T}{\partial z^2} + \frac{\dot{q}}{k} = \frac{\rho c}{k} \frac{\partial T}{\partial t} \tag{2.11}$$

During steady state, Equation 2.11 can be reduced to the Poisson Equation (Equation 2.12). Thus, heat flow during steady state heat transfer is independent of the material density ρ and the specific heat c.

$$\frac{\partial^2 T}{\partial x^2} + \frac{\partial^2 T}{\partial y^2} + \frac{\partial^2 T}{\partial z^2} + \frac{\dot{q}}{k} = 0 \tag{2.12}$$

When a body is in steady state without any heat source, the Poisson Equation reduces to Laplace's Equation. The boundary conditions on surfaces S_1, S_2 and S_3 (see Figure 2-6) are then defined in Equations 2.13 to 2.15.

$$T(x, y, z, t) = T_0 \text{ for } t > 0 \text{ on } S_1 \tag{2.13}$$

$$k_x \frac{\partial T}{\partial x} l_x + k_y \frac{\partial T}{\partial x} l_y + k_z \frac{\partial T}{\partial x} l_z + q = 0 \text{ for } t > 0 \text{ on } S_2 \tag{2.14}$$

$$k_x \frac{\partial T}{\partial x} l_x + k_y \frac{\partial T}{\partial x} l_y + k_z \frac{\partial T}{\partial x} l_z + h(T - T_\infty) = 0 \text{ on } S_3 \tag{2.15}$$

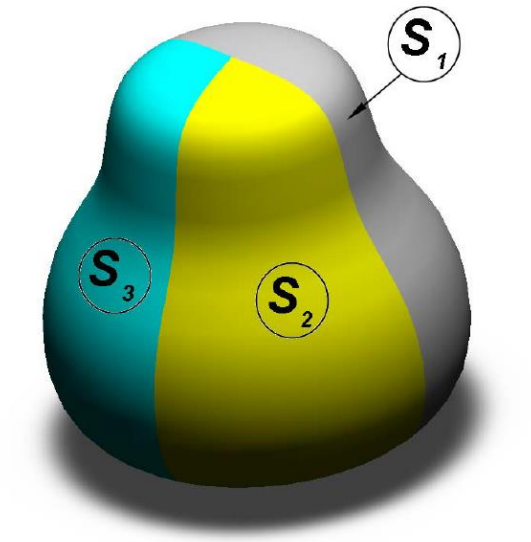

Figure 2-6: 3D model with surfaces S_1, S_2 and S_3 (from del Coz Diaz et al. (2012)*)*

The initial condition is:

$$T(x, y, z, t = 0) = \overline{T_0}(x, y, z) \; in \; V \tag{2.16}$$

Thus, for steady state heat flow the thermal conductivity, pore size and pore structure, moisture content and amount of air influence the thermal performance. For transient heat flow the specific heat and the material density also influence the thermal performance. These parameters also influence each other. Each of the mentioned parameters is defined and/or analysed in terms of its relationship with the thermal performance of foam concrete.

2.3.1 Thermal conductivity

According to Mydin et al. (2012) thermal conductivity is the property of a material describing its ability to conduct heat. Thermal conductivity k is defined as the time rate of steady state heat flow through a

surface area of a homogeneous material as a result of a temperature gradient in the direction perpendicular to that area (Cengel & Ghajar, 2015). Thus, a good insulating material will have a low thermal conductivity. Due to the fact that foam concrete has a low density, it has good thermal properties (by lowering the density, a lower thermal conductivity can be reached). Equivalent thermal conductivity is the total thermal conductivity of different materials calculated either in series or in parallel. According to Aldridge (2005) a typical sand cement screed has a thermal conductivity of 1.8 W/mK and foam concrete with a density of 1000 kg/m^3 has a thermal conductivity of 0.3 W/mK. Thus, foam concrete is six times less conductive, however it may not necessarily be more thermally efficient because some factors may have a more adverse effect.

Thermal diffusivity α is how fast heat diffuses through a material and is measured in m^{2}s. Specific heat c is the measure of the ability of a material to store thermal energy and is measured in J/kgK. Thermal conductivity (W/mK) is the result of thermal diffusivity (m^2/s), specific heat (J/kgK) and density as seen in Equation 2.17. It is influenced by its own material characteristics, pore structure, chemical composition, moisture and temperature.

$$\alpha = \frac{Heat\ conducted}{Heat\ stored} = \frac{k}{\rho c} \tag{2.17}$$

Tada (1986) used the coefficient of thermal transmittance (symbol N in W/m²K) to determine the optimal thickness of a wall of dwelling units in Tokyo for monolithic AAC. The thermal conductivity of the AAC was determined through experimentally determining its relationship with bulk density ($k = 2.43 \times (10)^{-4}\rho + 4.62 \times (10)^{-3}$ W/mK) as seen in Figure 2-7. The thermal conductivity of AAC is then used in Equation 2.18 with α_i and α_o, the surface coefficients of heat transfer (9.3 W/m^{2}K and 23 W/m^{2}K respectively), and x the wall thickness. Thermal transmittance is taken as smaller than 0.4 for cold regions and smaller than 0.6 for warm regions (see Table 2-1).

$$N = \frac{1}{\frac{1}{\alpha_i} + \frac{x}{k} + \frac{1}{\alpha_o}} \tag{2.18}$$

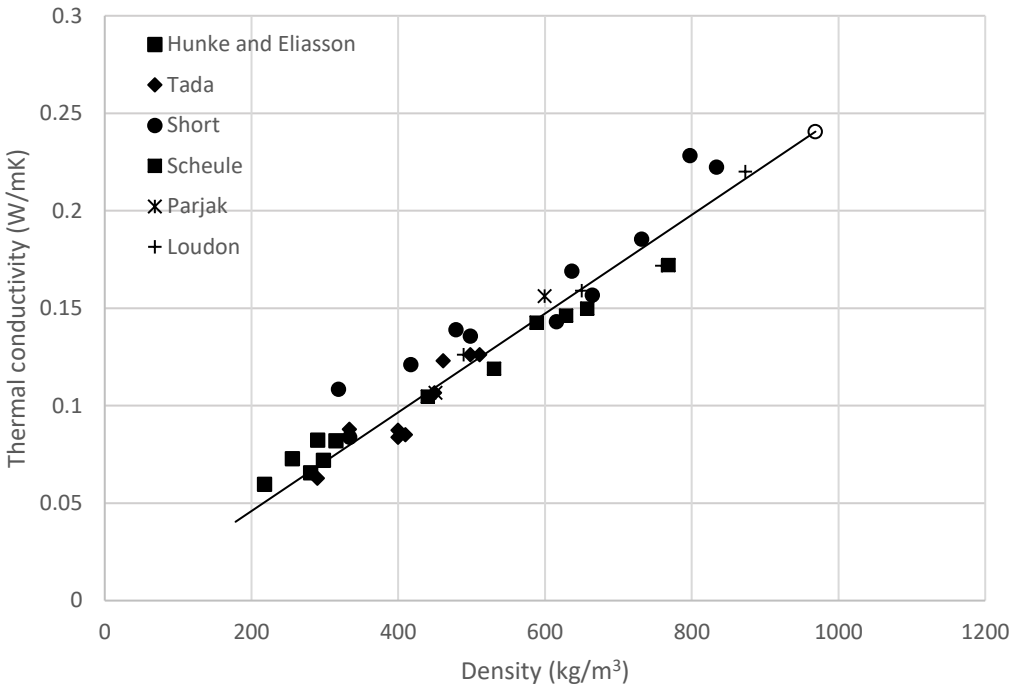

Figure 2-7: Thermal conductivity of AAC as a function of bulk density (reworked from Tada (1986)*).*

Table 2-1: Minimum thermal transmittance for outer walls of dwellings (reworked from Tada (1986)*)*

Countries	Heating degree – days (℃ day)		
	2000	3000	4000
England	0.6	0.6	0.6
France	0.57	0.41	-
W. Germany	-	0.76	-
Sweden	-	-	0.3
USA	0.45	0.4	0.3

Panesar (2013) conducted a study to determine the relationship between plastic density and types of foaming agents (synthetic and protein based). Results show that all relationships are linear, but that the rate of increase in thermal conductivity for foam concrete with synthetic foaming agents with increase in plastic density is lower than the rate of increase in thermal conductivity for foam concrete with protein based foaming agents. These results show that the thermal conductivity of protein based foam is more sensitive to change than the thermal conductivity of synthetic foam.

2.3.2 Effect of material density

An increase in density leads to an increase in thermal conductivity. Silva et al. (2015) conducted a study where test samples with different densities were used to determine if there is a relationship between the density of foam concrete and thermal conductivity. Their results show that there is a fairly good linear correlation between these two parameters (see Figure 2-8). Mydin (2011) also determined that the relationship between material density and thermal conductivity is positively linear.

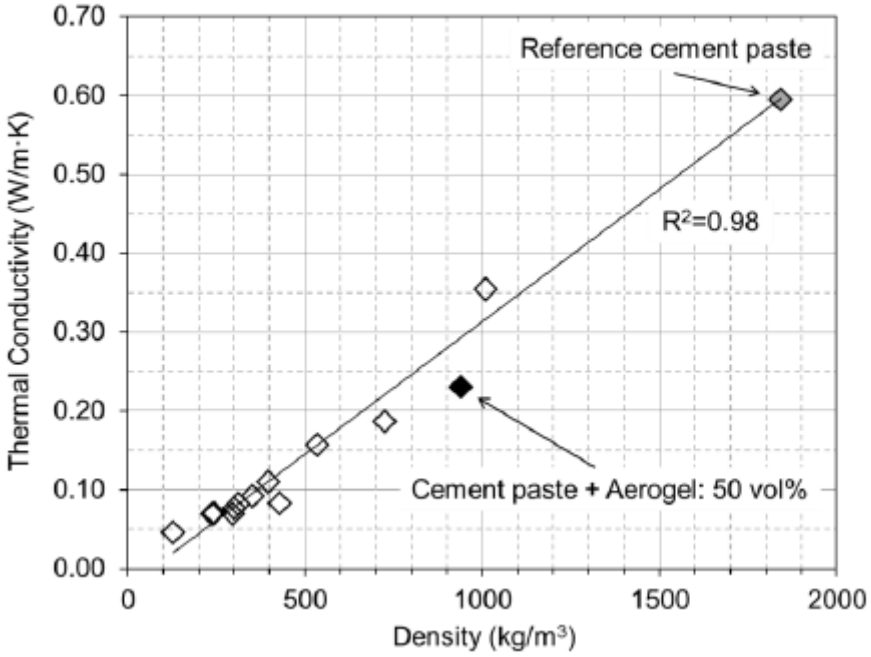

Figure 2-8: Thermal conductivity of foam concrete at different densities (Silva et al., 2015).

Liu et al. (2014) performed an experiment to determine the thermal conductivity of oil palm shell foam geopolymer concrete (OPSFGC) at densities of 1300, 1500 and 1700 kg/m^3 and were compared to the thermal conductivity of oil palm shell non-foam geopolymer concrete (OPSNFGC), blocks and bricks. Panels of every material at a 28 day strength were surrounded by a hot plate (40°C) from the one side and a cold plate (18°C) from the other side. The temperature of each panel was recorded every 10 minutes for 24 hours. The thermal conductivity for each material was then calculated using the Fourier heat flow equation (Equation 2.2). The results in Figure 2-9 show a lower density material has a lower thermal conductivity.

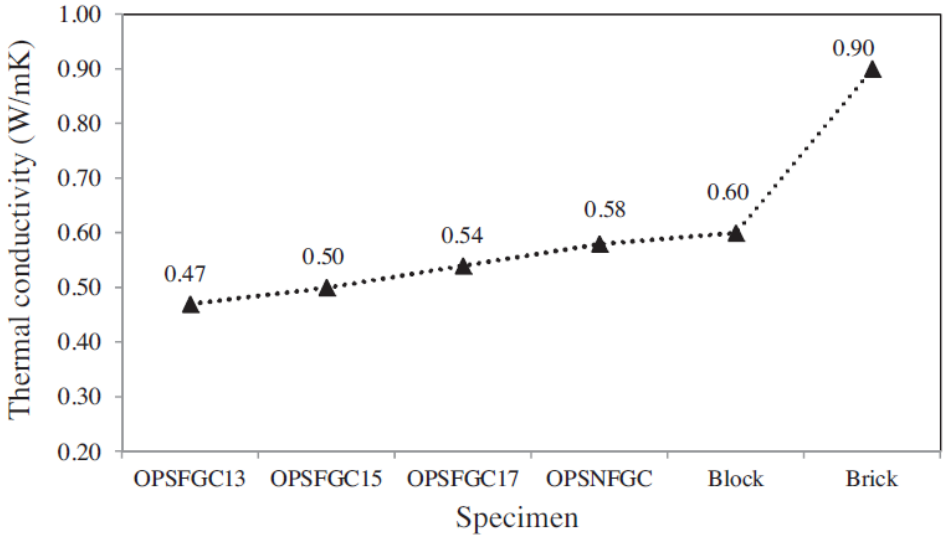

Figure 2-9: Thermal conductivity of specimens (Liu et al., 2014).

Wei et al. (2013) also conducted a study on the thermal performance of foam concrete through the use of the Fourier heat flow equation. A sample foam concrete plate was placed between two plates with temperatures of 0°C and 40°C respectively. Their results also show a near linear relationship with material density and thermal conductivity.

2.3.3 Porosity and pore structure

Foam concrete has a pseudo-homogeneous dispersed pore structure that is created by entraining air voids, of roughly 0.1 to 1 mm, into the concrete mix (Hilal et al., 2015). Porosity of concrete can be measured through apparent, total vacuum saturation and mercury intrusion porosymmetry (MIP) (Amran et al., 2015). Porosity depends on the degree of infusion characteristics including water absorption, sorption and permeability and the amount of fine materials in the mix. Lime powder may reduce porosity more than fly ash and other pozzolanic additives like silica fume may enhance cement past aggregate bonds which also reduces porosity (Amran et al., 2015).

Porosity, determined by a gravimetric method such as water saturation, can be calculated using Equation 2.19.

$$P = \frac{W_{sat} - W_{dry}}{W_{sat} - W_{wat}} \times 100 \tag{2.19}$$

where P is the vacuum saturation porosity in %, W_{sat} is the weight in air of the saturated sample, W_{wat} is the weight in water of the saturated sample and W_{dry} is the weight of the oven- dried sample.

Porosity influences the compressive strength, flexural strength and durability of concrete. Othuman & Wang (2011) conducted experiments to determine the effect of porosity on the thermal conductivity of foam concrete. Their experiments included determining the relationship between density and porosity, effective pore size and thermal conductivity. Their results show that for an increase in material density the porosity and effective pore size decrease. Figure 2-10 summarises the Othuman & Wang (2011) findings. Thus, because porosity and pore size influence the density of a material, they also influence the thermal conductivity of a material.

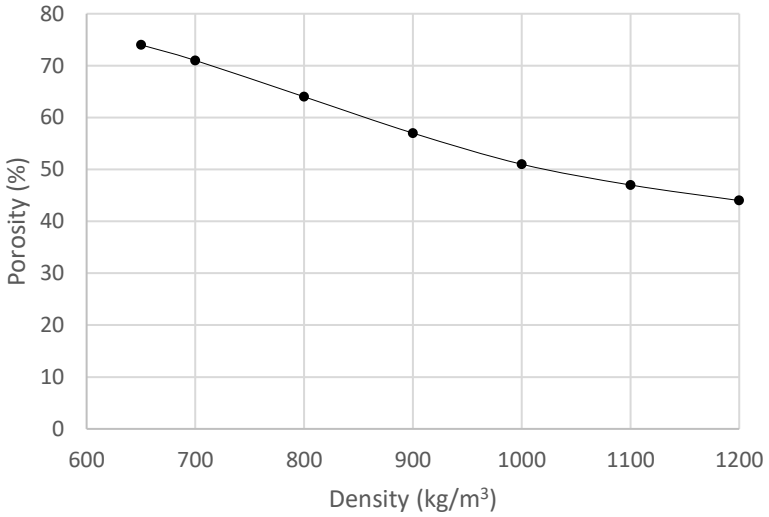

(a)

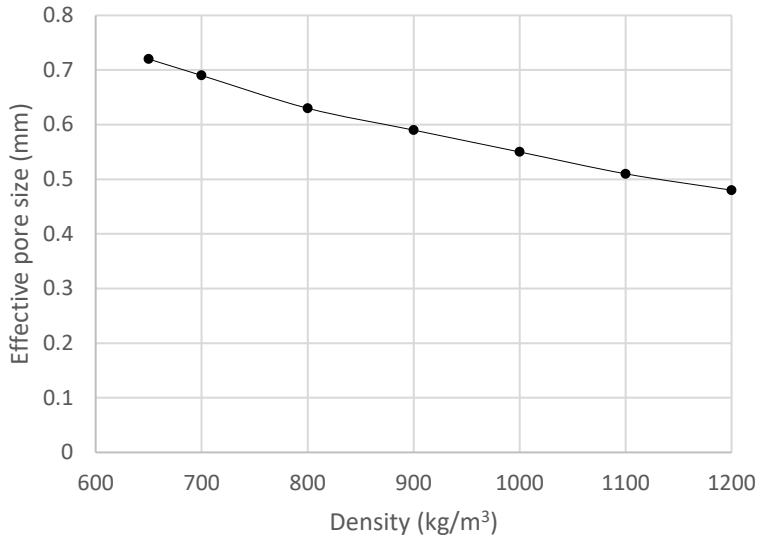

(b)

Figure 2-10: The relationship of porosity and effective pore size with density of foam concrete (reworked from Othuman & Wang (2011)*).*

Less connected air voids yield a lower reduction in compressive strength, but an increase in air voids yield an increase in thermal resistance. Vinith et al. (2018) conducted a study to see what the effect of the amount of air voids in foam concrete is on the thermal conductivity of the concrete. Six batches with different cement, fly ash, water and foam densities were prepared. These batches where then exposed to heat (45°C for 6 hours) on the one side and open atmosphere to the other side (measured with a laser thermometer). The measured temperature was then used to calculate the difference in temperature in order to determine the thermal conductivity (see Equation 2.2). It was found that M4 (see Figure 2-11) with the highest percentage of foam (20% foam), yielded the lowest thermal conductivity (0.021 W/mK).

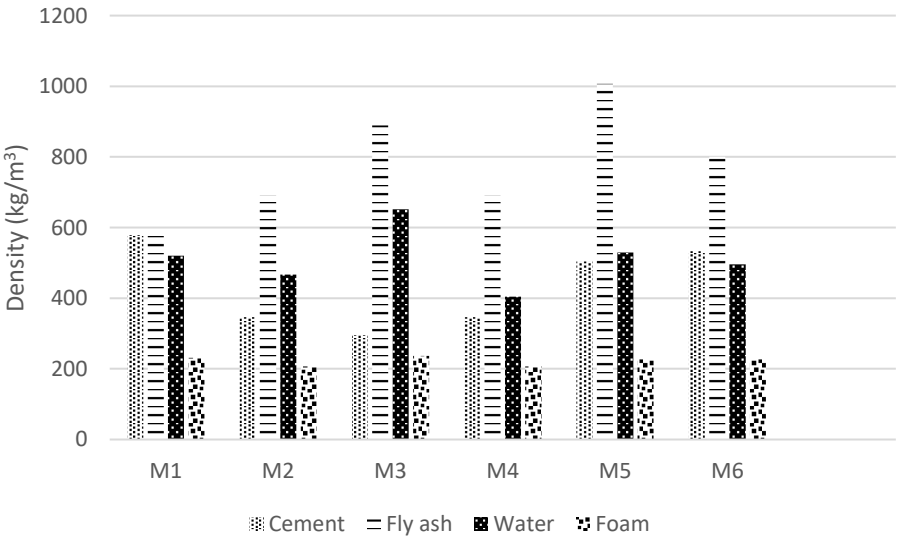

Figure 2-11: Mix proportions of different batches of foam concrete (reworked from Vinith et al. (2018)*)*

Vinith et al. (2018) compared the thermal conductivity of brick with foam concrete. It was found that the thermal conductivity of brick with a density of 1600 - 1920 kg/m^3 is 0.6 – 1 W/mK compared to 0.021 - 0.035 W/mK of foam concrete with a density of 860 - 1245 kg/m^3. Their results are summarised as follows: Foam concrete is highly insulating and light weight when compared to the clay bricks. Vinith et al. (2018) concludes that if foam concrete blocks are used for building construction rather than clay bricks, the energy consumption of air conditioning and costs involving transportation, labour and foundation can be reduced.

It is safe to say that the lower the density of foam concrete, the higher its porosity. Thus, because a material with a lower density has a lower thermal conductivity, thermal conductivity also changes with porosity of a material. This is because air is a poorer conductor compared to solid and liquid due to its molecular structure.

Wei et al. (2013) also conducted a study to determine the relationship between thermal conductivity and porosity of foam concrete by creating a theoretical 2D model based on geometrical simplification of the microstructure of foam concrete. First the pore size distribution of 300, 800 and 1700 kg/m^3 foam concrete was determined as a log-normal distribution. The mean and standard deviation parameters from the log-normal distribution were used to create a two-phase porous structure where randomly distributed spheres in a solid matrix represent the pores of the foam concrete. Figure 2-12 shows the steps that were followed to generate the pores where N is the number of target pores. Numerical thermal conductivity values were determined by calculating the temperature at each pore centre. Nodes on the far left and right were assigned temperatures as follows:

$$T_j = T_{hot} \tag{2.20}$$

$$T_j = T_{cold} \tag{2.21}$$

Where j introduces the node number.

Nodes in the middle were analysed according to the conservation law of energy where the sum of heat flow towards a node is equal to the sum of heat flow away from the node. Equation 2.22 is used to determine the temperatures in the middle nodes.

$$\sum_{k=\beta_1}^{\beta_m} \frac{T_k - T_j}{R_{jk}} = 0 \tag{2.22}$$

β = number of nodes adjacent to node *j*

T_k = temperature at node *k*

T_j = temperature at node *j*

R_{jk} = thermal resistance between nodes *k* and *j*

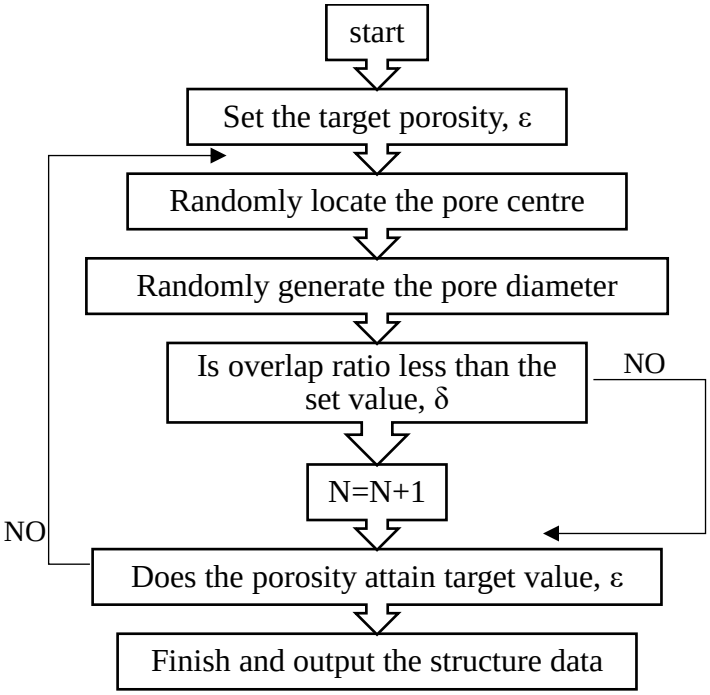

Figure 2-12: Flow chart of pore generation method (reworked from Wei et al. 2013)*).*

Figure 2-13 illustrates several theoretical models showing the relationship of the thermal conductivities and pore volume fraction of air and of the concrete particles (Wei et al., 2013). The numerical data was obtained from the procedure in Figure 2-12. Here it is clear that the so called EMPT (effective medium percolation theory) model shows the closest prediction of the numerical data. The EMPT model uses the void particles and material particles to form a continuous matrix (Hashin & Shtrikman, 1962) while also taking the connectivity of the void and material particles into account (Landauer, 1952). This theory is explained further in Section 2.3.7.

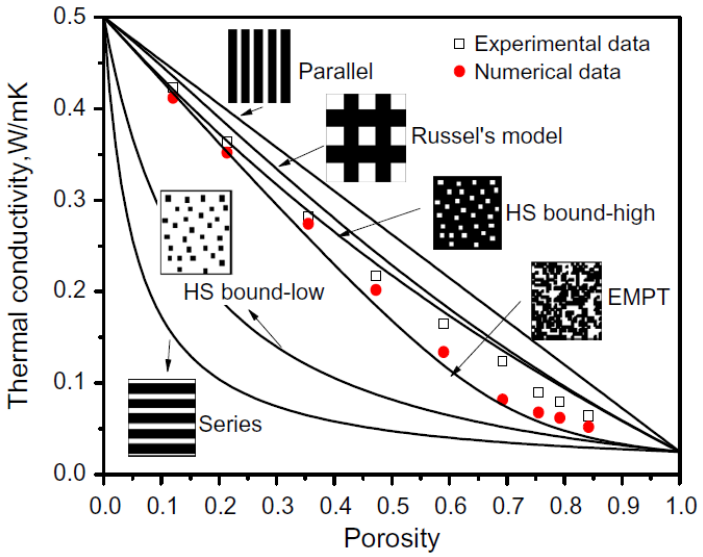

Figure 2-13: Comparison of experimental data with numerical data and existing thermal conductivity models (Wei et al., 2013)

2.3.4 Effect of high internal temperatures

According to Jones & McCarthy (2006) foam concrete with a high volume to surface area combined with a relatively high Portland cement content may lead to significant core temperature rises due to heat of hydration. They further say that if the core or surface thermal gradients are large enough, cracking may occur which then affects the concrete performance. Furthermore, core temperatures may be retained for a greater period of time in foam concrete than in normal weight concrete. This in turn may have an effect on its thermal performance.

Jones & McCarthy (2006) measured temperature profiles of test specimens subjected to near-adiabatic conditions in an insulated hot-box. Rises in temperature of between 29°C and 62°C from ambient at rates of rise up to 20°C/h. A reduction in cement content from 600 to 300 kg/m^3 helped reduce the temperature development during cement hydration.

2.3.5 Effect of moisture content and dehydration reactions

An increase in moisture content leads to an increase in thermal conductivity. Foam concrete consists of free water and chemically bonded water. The free water is dependent on the concrete's density. If the free water and some of the chemically bonded water evaporates, dehydration will occur in the foam concrete which will then affect the thermal properties of the foam concrete (Othuman & Wang, 2011).

Typically, at elevated temperatures, free water and some chemically bonded water in the cement paste is released. This process releases a large amount of energy. According to Mydin (2013) free water evaporates at around 100°C and chemically bonded water evaporates at 180 to 300°C through the decomposition of C-S-H and carboaluminate hydrates. Reactions in the hardened foam concrete may then occur at 400 to 600°C. These reactions include destruction of C-S-H gels and the decomposition of the hydration products (calcium hydroxide to lime and water) which in effect lead to damage due to lime expansion.

2.3.6 Effect of high external temperatures

Othuman & Wang (2011) studied the thermal properties of foam concrete at elevated temperatures and determined that the thermal conductivity of foam concrete at elevated temperatures depends on the thermal conductivity of the cement and air and also on the radiation inside the air pores. Foam concrete panels of 150 mm at densities of 650 kg/m^3 and 1000 kg/m^3 were tested using a Hot Guarded Plate (HGP) test and an electric kiln. For the HGP test, the average thermal conductivity was determined with the Fourier heat flow equation (Equation 2.2). This value is used in Equation 2.23 as k_s.

The results in Figure 2-14 were obtained by weighing samples after heating them at different temperatures. From Figure 2-13 it can be seen that there are three phases of dehydration and a final weight loss between 750°C and 850°C due to the release of carbon dioxide (Othuman & Wang, 2011).

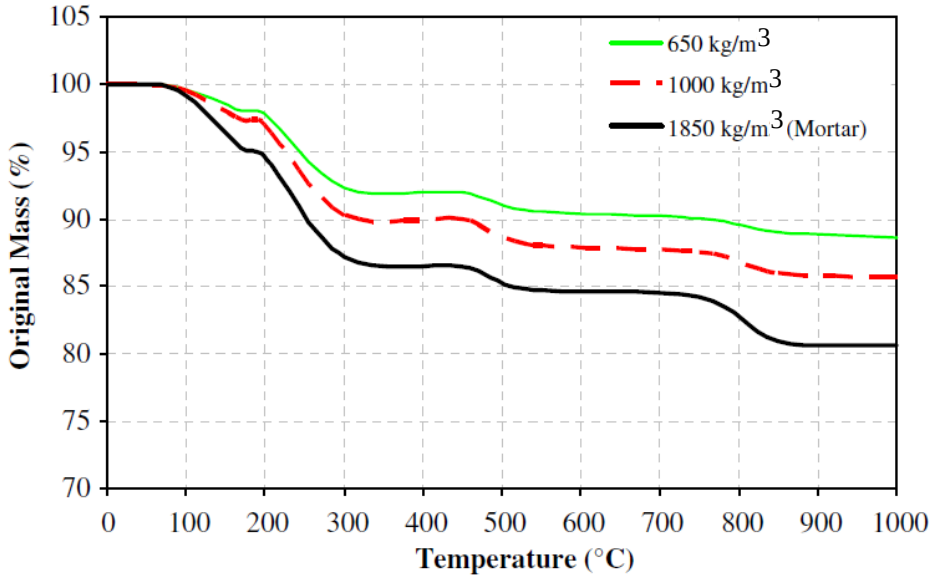

Figure 2-14: Percentage of original density at different temperatures (Othuman & Wang, 2011)

Othuman & Wang (2011) used Equation 2.23 to determine the effective thermal conductivity (k^*) of foam concrete at elevated temperatures. The effective thermal conductivity of gas (k_g) was determined using Equation 2.24 which includes the effect of radiation (the latter part of the equation).

$$k^* = k_s \frac{k_g P^{\frac{2}{3}} + \left(1 - P^{\frac{2}{3}}\right) k_s}{k_g \left(P^{\frac{2}{3}} - P\right) + \left(1 - P^{\frac{2}{3}} + P\right) k_s} \tag{2.23}$$

Where

k_s = thermal conductivity of the solid

k_g = effective thermal conductivity of the gas (accounting for heat transfer in the pores)

P = porosity of the material

$$k_g = 4.815 \times 10^{-4} T^{0.717} + \frac{2}{3} \times 4 d_e \sigma T^3 \tag{2.24}$$

Where

d_e = pore diameter (assuming a uniform distribution of spheres)

Equation 2.24 was then used to determine the third segment of the graph in Figure 2-15 when the temperature is above 170°C and radiation in the pores starts to take place. The middle part of Figure 2-14 shows the evaporation of water in the foam concrete which leads to a decrease in thermal conductivity until the foam concrete is dry.

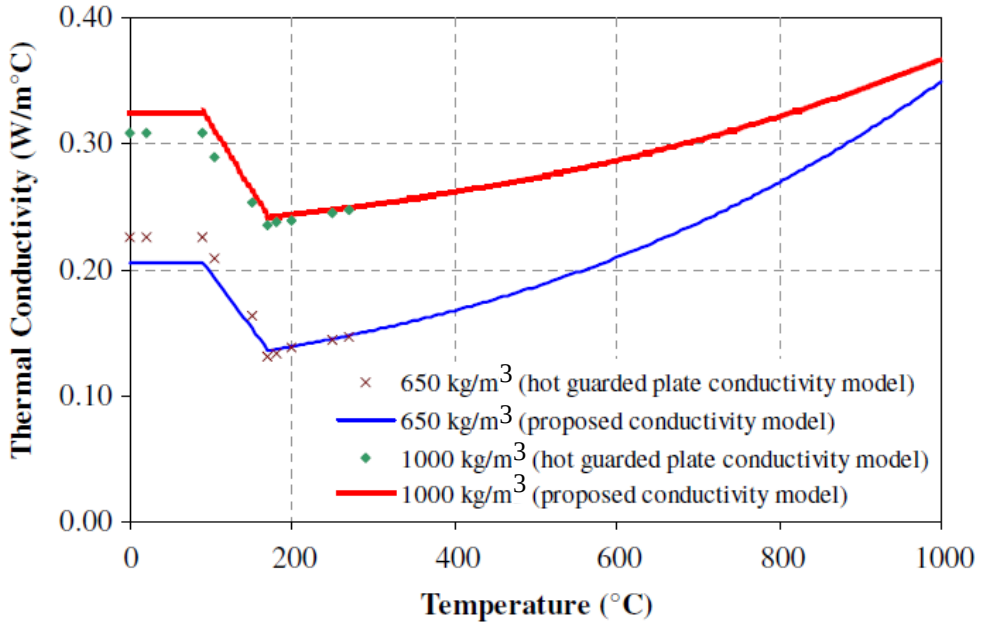

Figure 2-15: Effective thermal conductivity of foam concrete for 650kg/m³ and 1000kg/m³ densities (Othuman & Wang, 2011).

2.3.7 Existing theorems on calculating thermal conductivity

One of the first models to predict thermal conductivity is the Maxwell model and Rayleigh model (Pietrak & Winiewski, 2015). The Maxwell model (Equation 2.25) is based on spherical particles of conductivity k_1 embedded in a continuous matrix of conductivity k_m and $ø$ is the volume fraction of the filler. The Maxwell model is only valid for low $ø$ (<25%) and thermal interaction between particles is ignored.

$$\frac{k^*}{k_m} = 1 + \frac{3ø}{\left(\frac{k_1 + 2k_m}{k_1 - k_m}\right) - ø} \tag{2.25}$$

The Rayleigh Model is based on spherical inclusions arranged in simple cubic array embedded in continuous matrix. Thermal interaction between particles are taken into consideration.

$$\frac{k^*}{k_m} = 1 + \frac{3ø}{\left(\frac{k_1 - 2k_m}{k_1 - k_m}\right) - ø + 1.569\left(\frac{k_1 - k_m}{3k_1 - 4k_m}\right)ø^{\frac{10}{3}} + \cdots} \tag{2.26}$$

When heat flows through an interface between constituents of a composite material, a temperature drop occurs at the interface. The disturbance of heat flow is called the interfacial thermal resistance (ITR) and refers to the combined effect of two thermal resistances. One is called the thermal contact resistance (TCR) and causes poor mechanical and chemical bonding between constituent phases. The other is called the thermal boundary resistance (TBR) and occurs because of the difference in the physical properties of constituent materials. Johnson & Hasselman (1987) predicted the first expressions for effective thermal conductivity of composite materials including ITR. ITR is a ratio of temperature discontinuity ΔT at the interface to the heat rate $\dot{Q}$ per unit area A across the interface between two phases in contact and is determined using Equation 2.27.

$$R_{int} = \frac{\Delta T}{\mathrm{Q}/A} \tag{2.27}$$

Hashin and Shtrikman (1962) developed a theory where the most restrictive upper and lower limits of the effective thermal conductivity of a material is determined (see Equation 2.28 where P_1 and P_2 are the pore volume fractions). This theory makes use of a two-phase system where spherical inclusions are placed in a continuous matrix (Wei et al., 2013). Landauer (1952) derived an equation where the connectivity of a two-phase material is taken into account (see Equation 2.29). Both Hashin and Shtrikman's and Landauer's approaches however become limited when pore volume fractions increase (Wei et al., 2013).

$$P_1 \frac{k_1 - k}{k_1 + 2k} + P_2 \frac{k_2 - k}{k_2 + 2k} \tag{2.28}$$

$$k = k_1 + \frac{P_2}{\frac{1}{k_2 - k_1} + \frac{P_1}{3k_2}} \tag{2.29}$$

Miled & Limam (2016) summarised existing theorems on calculating the thermal conductivity of a homogeneous solid matrix consisting of an isotropic, porous material. These theorems include the Voight model, the Mori-Tanaka and Eshelby's model, the dilute scheme, the self-consistent scheme and the differential scheme. The Voight model provides the upper bound for the effective thermal conductivity of isotropic porous solids according to their porosity. According to the Mori-Tanaka model each pore is isolated in an infinite matrix and is subjected to its boundary to the average of the temperature gradient field over the matrix phase. The dilute scheme does not account for interactions between pores. Pores are isolated in an infinite matrix subjected to a uniform temperature gradient field on its boundary. The self-consistent scheme assumes that pores are embedded in a fictitious homogeneous, infinite matrix with a uniform temperature gradient field on its boundary. The differential scheme uses an infinitesimal formulation of the dilute scheme.

The different theorems on calculating the thermal performance of a material is summarised in Table 2-2 and is also illustrated in Figure 2-16. The homogeneous thermal conductivity k_{hom} is a function of the porosity, P, fraction of total volume and k_m, the thermal conductivity of the matrix.

Table 2-2: Existing theorems on calculating the thermal conductivity of a homogeneous solid matrix consisting of an isotropic, porous material

Voight Models	$\boldsymbol{k_{hom}(P) = k_m(1 - P)}$
Mori-Tanaka Model	$k_{hom}(P) = k_m \frac{(1-P)}{\left(1 + \frac{P}{2}\right)}$
Dilute Scheme	$k_{hom}(P) = k_m(1 - \frac{3}{2}P)$
Self-consistent Scheme	$k_{hom}(P) = k_m(1 - \frac{3}{2}P)$
Differential Scheme	$k_{hom}(P) = k_m(1 - P)^{\frac{3}{2}}$

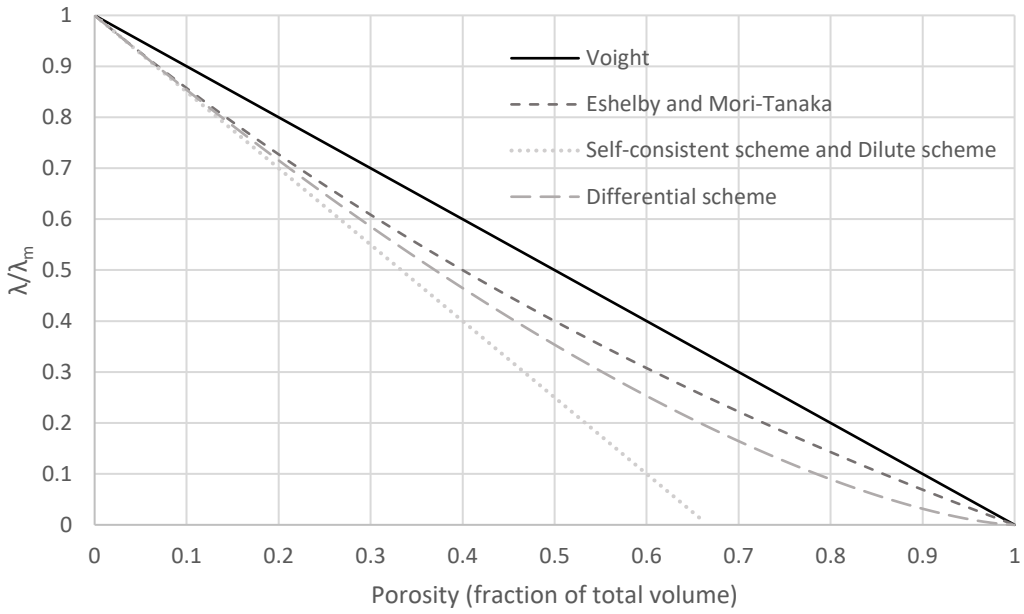

Figure 2-16: Existing theorems on calculating the thermal conductivity of a homogeneous solid matrix consisting of an isotropic, porous material at different porosities (Miled & Limam, 2016)

2.4 Concluding summary

This chapter gives an in depth definition of lightweight concrete and identifies different lightweight concretes. Focus is put on the thermal performance of lightweight foam concrete in collaboration with studies on its durability and strength.

Parameters that influence the thermal performance of foam concrete are identified in Section 2.3. For steady state heat flow the thermal conductivity, pore size and pore structure, moisture content and amount of air influence the thermal performance. For transient heat flow the specific heat and the material density also influence the thermal performance. These parameters also influence each other.

Lastly, the three principles of heat transfer, conduction, convection and radiation are studied in Section 2.3. Existing theorems on determining the thermal conductivity of a porous material are identified and given in Section 2.3.7.

Chapter 3

3 Finite element modelling of heat transfer

The aim of this chapter is to give background on walls with hollow core structures and elaborate on the finite element (FE) solution of heat flow to analyse thermal performance of structures with layered or hollow core walls. The further aim is to investigate case studies on layered wall sections and cavity wall sections. These case studies are analysed using FE software to gain a better understanding of the heat transfer principles and to compare their results with those of the case studies.

3.1 Advanced modelling of thermal performance

Modelling of thermal performance of materials and combination of materials can become a complex task (Sala, et al., 2008). The EN 1745 (2012) Annex D lists the capabilities that a heat transfer modelling program should have such as isotropic or anisotropic thermal conductivity, mass transfer and the type of voids being equivalent thermal conductivity or resistance or radiation exchange and equivalent thermal conductivity. Some of these heat transfer modelling programs that can perform finite element analyses (FEA) and computational fluid dynamics (CFD) analyses, include ANSYS, COMSOL, FloTHERM, ABAQUS and TRNSYS amongst others.

Researchers such as Zhou et al. (2014), Marx (2018) and Jeffers et al. (2013) have used FEA as implemented in ABAQUS (Dassault Systémes, 2015) in their thermal analysis of walls and this will also be used in the thermal analysis of walls in this thesis.

The three heat transfer modes, namely conduction, convection and radiation, discussed in Section 2.3, can be studied with FEM. Heat transfer through convection and radiation is implemented as interactions where the heat transfer coefficient and the radiative emissivity are defined. These interactions are defined either by specifying surface pairings or self-contact surfaces.

Using the Galerkin approach, the Fourier law and principle of energy balance can be expressed using Equation 3.1.

$$\int_V \rho \dot{U} \delta T dV + \int_V \frac{\partial \delta T}{\partial x} \cdot k \frac{\partial T}{\partial x} dV = \int_V \delta T r dV + \int_{S_q} \delta T q dA \tag{3.1}$$

The boundary conditions are as follows:

$T = T(x,t)$ is the temperature.

$q = q(x,t)$ is the prescribed surface heat flux per area.

$q_r = q_r(x,t)$ is the prescribed volume heat flux per volume.

$q_{conv} = h(T - T^0)$ is the surface convection.

$h = h(x,t)$ is the film coefficient.

$T^0 = T^0(x,t)$ is the sink temperature.

$q_{rad} = \varepsilon\sigma((T - T^Z)^4 - (T^0 - T^Z)^4)$ is the radiation.

Where:

V = volume of solid material

T = temperature

A = surface area

ρ = density of the material

$\dot{U}$ = material time rate of internal energy

q = heat flux per unit area of the body flowing into the body

r = heat supplied externally into the body per unit volume

T^Z = absolute zero temperature

The FE programme assumes that heat transfer models are uncoupled. Thus, $U = U(T)$ and q and q_r are independent of strains and displacements.

3.2 Finite element analysis of case studies

3.2.1 Background

Heat transfer through conduction takes place inside the solid parts of hollow wall elements as well as in the hollow parts. Radiation and convection heat transfer takes place between the outside air and wall elements exposed to the outside air, and the hollow cores and wall elements exposed to the hollow cores.

Bekkouche et al. (2013) determined the optimum thickness in cavity walls in buildings. They concluded that thermal emissivity and the thickness of air cavities are the main factors that influence the thermal resistance of a concrete block. By controlling the effectiveness of air inside a cavity the heat transfer coefficient can be controlled. The amount of air inside a cavity is governed by the thickness of the cavity and thus the thickness of a cavity becomes an important design parameter.

From Figure 3-1 it can be seen that radiation is independent of the thickness of a material and the thickness of the cavities but convection and conduction are dependent on the thickness. The lowest heat transfer value is achieved when the air layer is 42 mm thick. Bekkouche et al. (2013) conclude from Figure 3-1 that long wave radiation is the dominating heat transfer mechanism in closed air cavities bounded by ordinary building materials with an emissivity of 0.9.

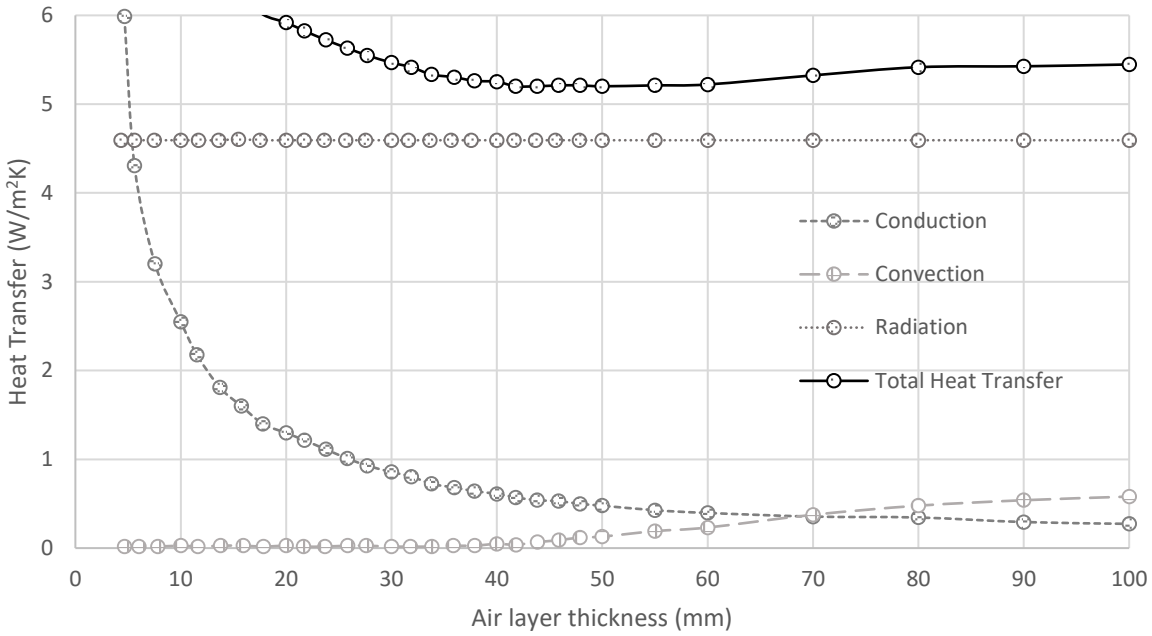

Figure 3-1: Estimated heat transfer in a closed air cavity (reworked from Bekkouche et al. (2013)*).*

Partition walls, recommended and widely used in Chinese industry, include walls with seven circular cylinder cavities for a 600 mm long partition wall as seen in Figure 3-2 (Ministry of Housing and Urban-Rural Construction of the People's Republic of China, 2016) (Standardization Administration of the People's Republic of China, 2009). Huang et al. (2018) proposed using five elliptical cylinders for the porous structure in a 600mm long partition wall. The reason for this geometry includes a reduction of the amount of cavity cylinders which makes fabrication easier and the control of the spacing of the cavity cylinders by controlling the eccentricity of the ellipse. When the spacing is controlled the thermal and mechanical performance of the partition wall is controlled (Huang et al., 2018). Also, heat flow which is the sum of the heat fluxes passing through a section, is an important parameter in evaluating the thermal performance of a structure (Huang et al., 2018). They concluded that for an increase in spacing between the cavity cylinders, the heat flow at that location increase and that for an increase in cavity size, and thus an increase in porosity, the heat flow at that location decreases. They also noted that the heat flow is nearly linearly proportional to the spacing between the cavity cylinders and the porosity, but that boundary conditions such as the heat transfer coefficient and the difference in temperature may cause deviations in these proportions and the heat flux is not uniformly distributed along the width of the wall.

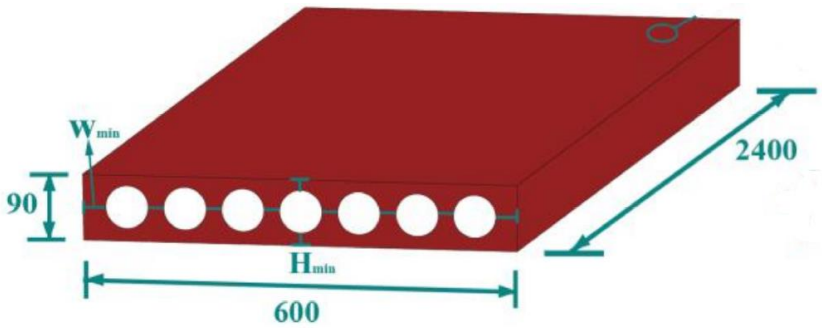

Figure 3-2: Partition wall with seven cylinder cavities widely used in Chinese industry (from Huang et al., 2018*)*

Del Coz Diaz et al. (2014) analysed the heat transfer of six hollow core blocks made from light weight concrete. Analyses were done using FEM and thermal resistances of the holes were determined from UNE-EN ISO 6946. Radiation and convection were present on either side of the blocks as well as inside the holes and were accounted for using the thermal resistance named the internal and external surface resistances with unit m^2K/W. Eight-node elements were used that can become triangular shaped elements to represent curved boundaries and that reproduce conduction heat transfer. Convection and radiation were simulated using surface elements with three nodes. These finite elements are shown in Figure 3-3. Both the elements that represent conduction and convection and radiation have one degree of freedom per node.

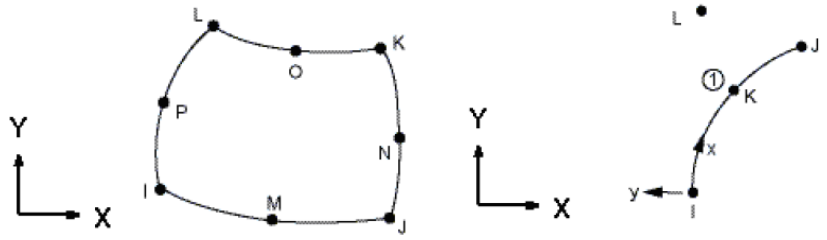

(a) (b)

Figure 3-3: (a) an 8-node quadrilateral finite element and (b) a 1D 3-node plus and extra node finite element (from Del Coz Diaz et al. (2014)*).*

Al-Tamimi et al. (2017) determined the optimum geometry of holes for concrete bricks for an increased thermal performance. Finite element analysis was done using ABAQUS to create 23 different models with different configurations of holes in masonry concrete bricks. They concluded that for bricks with the same hollow ratio, i.e. the total area of the holes divided by the cross-sectional area of the brick, there is an effect of the shape of the holes in reducing the thermal flow going through the bricks. The number of holes has a minimal effect on the average inner temperature of the bricks. When using circular holes in a staggered arrangement of four cavities, the inner temperature of the bricks reduces considerably and when using rectangular holes, the inner temperature does not reduce. However, rectangular cavities show a better thermal performance than cylindrical cavities.

Figure 3-4 illustrates the relationship between the average inner temperature and the hollow ratio of wall blocks (Al-Tamimi et al., 2017). Wall blocks with hollow ratios up to 52.5% were analysed.

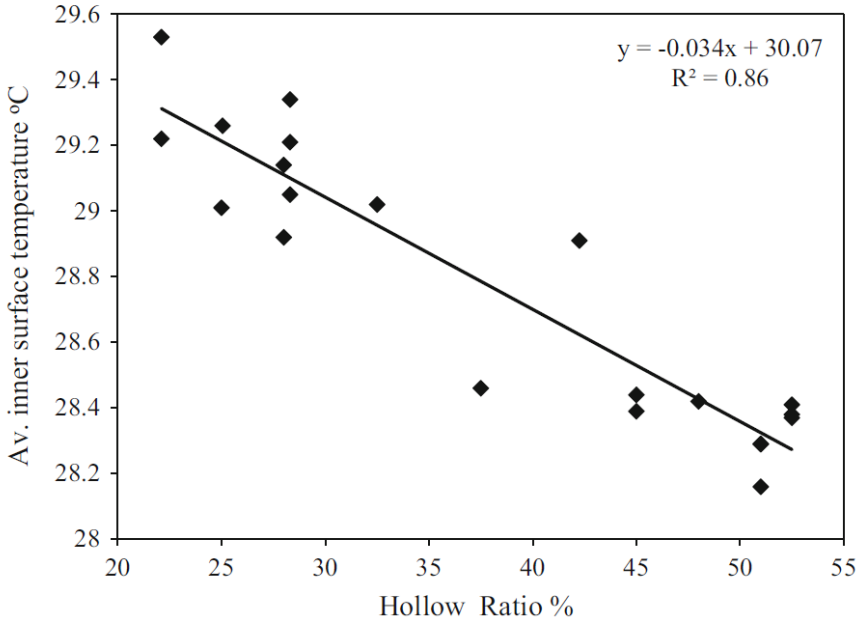

Figure 3-4: Relationship between hollow ratio and average inner surface temperature (Al-Tamimi et al., 2017)

A study by Zhou et al. (2014) was done to determine the thermal effectiveness of sandwich wall elements. The study included an experimental analysis and a finite element analysis. The experiment involved the thermal testing of layers of concrete, concrete and solid gypsum and concrete and gridded gypsum. The thermal testing involved the heating through radiation of one side of the layered specimen while allowing the other sides to be exposed to an ambient temperature. The finite element analysis involved a simulation in ABAQUS. Both experimental procedure and simulation in ABAQUS were analysed for 12 hours.

The models by Zhou et al. 2014 and Al-Tamimi et al. 2017 were done in the FEA software ABAQUS and for this reason they are analysed further also in ABAQUS. The purpose is to verify modelling strategy and accuracy, in comparison with the experimental and numerical studies on thermal behaviour. Both cases are relevant to building facades, in either using combinations of building and thermal insulating materials in a sandwich layout, or patterns of cavities in wall panels, in order to reduce weight and improve thermal resistance.

3.2.2 Sandwich wall elements

The case study of Zhou et al. (2014) included an experimental procedure and the FE analysis of the concrete specimen and the layers concrete and solid gypsum specimen. The concrete specimen (C- specimen) has three layers of only concrete and the concrete and gypsum sandwich specimen (G- specimen) has two layers of concrete with a layer of gypsum in the middle. The inside temperature refers to the side that is not exposed to external heat and the outside temperature refers to the side that is exposed to external heat. Thus the terms inside and outside are either sides of an outer building wall.

Figures 3-5 and 3-6 illustrate the wall elements that were analysed by Zhou et al. (2014). This wall element is modelled and the results are compared to those determined by Zhou et al. (2014). Three solid homogeneous wall parts are created. All parts have densities, specific heat capacities and thermal conductivity values as shown in Table 3-1. The parts are meshed according to the heat transfer element DC3D8 3D 8-node linear isoparametric element which has 8 nodes in a linear formulation. Furthermore, the concrete wall element is initially exposed to a surrounding temperature of 25.1°C and the concrete and gypsum layered wall element is initially exposed to 25°C.

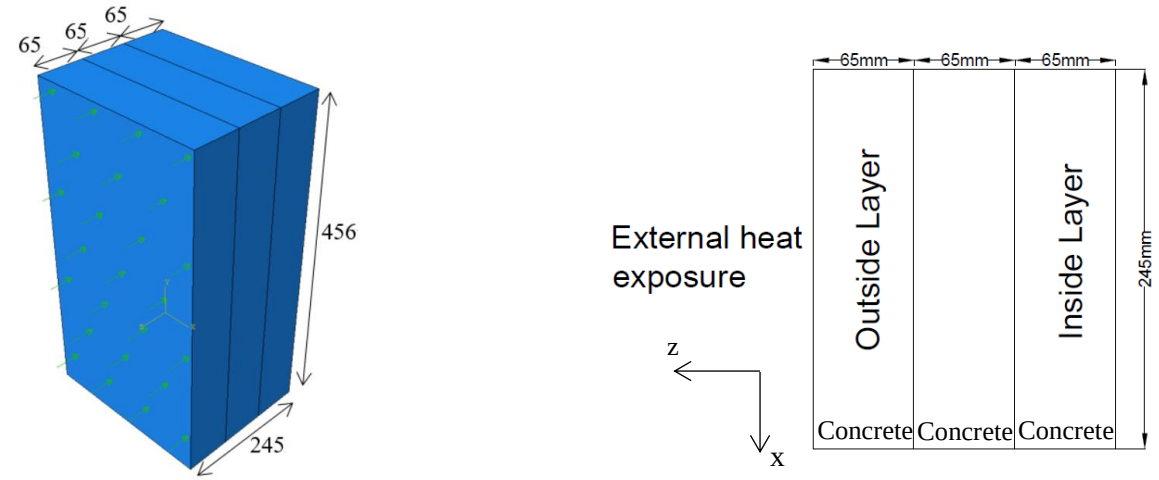

Figure 3-5: Diagram of layered concrete element (units in mm).

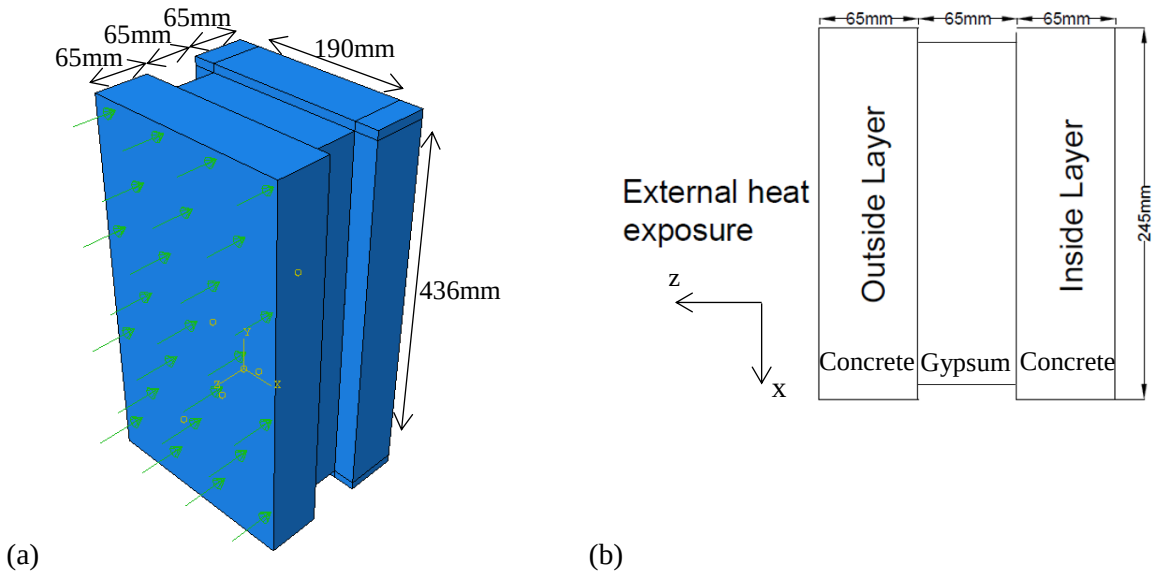

Figure 3-6: Diagram of layered concrete and gypsum layered element (units in mm).

Table 3-1: Properties of concrete from Zhou et al. (2014).

Material	**Concrete**	**Gypsum**
Density (ρ) [kg/m^3]	2300	1500
Specific heat capacity (c) [J/kgK]	750	1090
Heat convection coefficient (h) [W/m^{2}K]	8.9	9.0
Emissivity (ε)	0.85	0.85
Thermal conductivity (k) [W/mK]	1.05	0.5

Radiation and convection with the air are present on both sides of the wall element as seen in Figure 3-7. They are represented as an emissivity factor and a heat convection coefficient value in the FE model. The solar radiation is represented by a halogen lamp conducting a 1000 W at a 300 mm distance from the outside surface of the specimen.

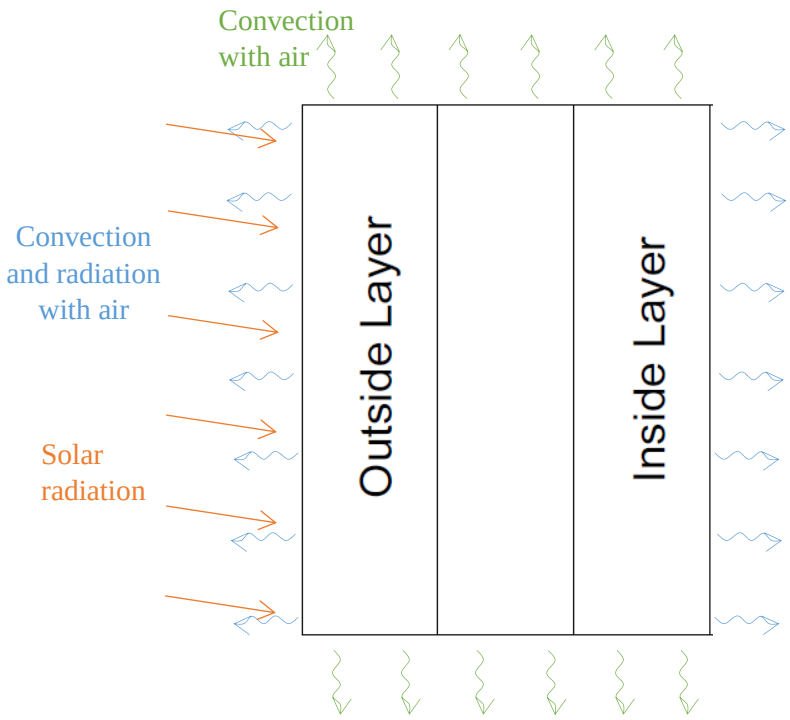

Figure 3-7: Diagram of layered concrete element with solar radiation as well as convection and radiation with air from Zhou et al. (2014).

A view factor is calculated to take into account the distance between the heat source and the specimen. Cengel et al. (2015) determined the radiative view factors between two different surfaces by calculating the explicit geometric dependence between one surface (1) to another (2). Equation 3.2 determines the view factor of surface 1 on surface 2 where both surfaces have equal areas ($A_1 \times A_2$) with a distance of H between the surfaces.

$$F_{12} = \frac{1}{\pi xy}\left[ln\frac{x_1^2 y_1^2}{x_1^2 + y_1^2 - 1} + 2x\left(y_1 \arctan\frac{x}{y_1} - \arctan x\right) + 2y\left(x_1 \arctan\frac{y}{x_1} - \arctan y\right)\right] \quad (3.2)$$

$$\text{with } x_1 = \sqrt{1 + x^2} \text{ and } y_1 = \sqrt{1 + y^2}$$

$$x = \frac{A_1}{H} \text{ and } y = \frac{A_2}{H}$$

When the approach of Equation 3.2 is used in the FE model, assuming that the surface area of the lamp and the surface area of the concrete exposed to radiation from the lamp are equal, the view factor is calculated to be 0.220.

Ehlert and Smith (1993) also determined an equation for the view factor between two rectangular plates that do not have the same area. The view factor from rectangular plate A_1 to rectangular plate A_2 at a distance z is shown in Equation 3.3 (see Figure 3-8). When assuming the lamp has a different surface area than the concrete exposed to the radiation from the lamp, the view factor is calculated to be 0.228. The larger of 0.220 and 0.228 is chosen.

$$F_{12} = \frac{1}{2\pi A_1}\sum_{l=1}^{2}\sum_{k=1}^{2}\sum_{j=1}^{2}\sum_{i=1}^{2}\left[(-1)^{(i+j+k+l)}B\left(x_i, y_j, \eta_k, \xi_l\right)\right] \tag{3.3}$$

$$\text{with } A_1 = (x_2 - x_1)(y_2 - y_1)$$

$$B = vp\arctan\left(\frac{v}{p}\right) + uq\arctan\left(\frac{v}{p}\right) - \frac{z^2}{2}ln(u^2 + v^2 + z^2)$$

$$u = x - \xi, \qquad v = y - \eta, \qquad p = \sqrt{u^2 + z^2}, \qquad q = \sqrt{v^2 + z^2}$$

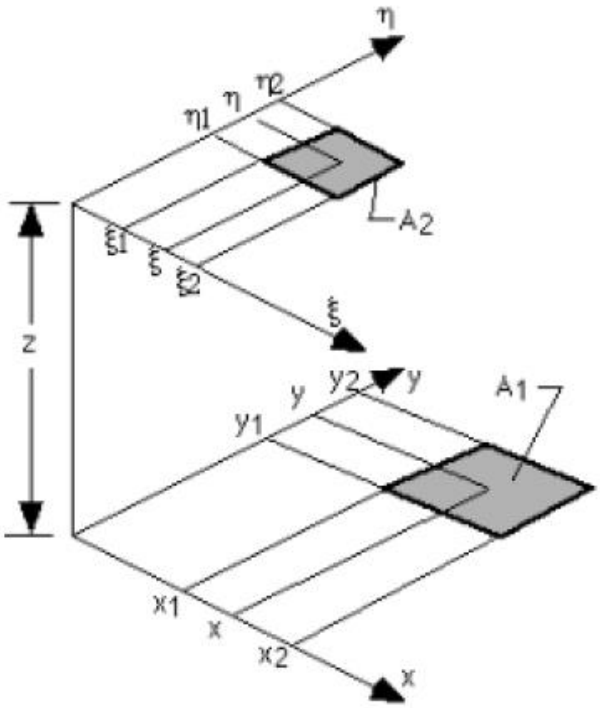

Figure 3-8: Illustration of parallel rectangular plates with difference areas at a distance z between each other (Ehlert and Smith, 1993).

Results from the FEA are taken at the centre of the inside and outside layers as was done by Zhou et al. (2014).

$$q_{uniform} = \frac{\text{power}}{A} \times F_{12} \times (1 - \text{reflectance}) \tag{3.4}$$

$$= \frac{1000}{0.41 \times 0.221} \times 0.228 \times (1 - 0.47)$$

$$= 1333.628\, W/m^2$$

Figure 3-9 illustrates the difference between the inside and outside temperatures computed and the Zhou et al. (2014) experimental results for the C-specimen. Figure 3-10 illustrates the difference between the computed inside and outside temperature and the Zhou et al. (2014) experimental results for the G-specimen.

Table 3-2 summarises the results from Zhou et al. (2014) and the FE of both the C-specimen and G-specimen after 12 hours. The computed temperature for the C-specimen at the outside layer is 13% lower and at the inside layer is 4% higher than that of Zhou et al. (2014). The computed temperature for the G-specimen at the outside layer is 8.8% lower and at the inside layer is 4% lower than that of Zhou et al. (2014). It is interesting to note that the difference between the computed and the experimental results for the G-specimen of the outside temperatures are greater than that of the C-specimen and the difference between the computed and the experimental results for the G-specimen of the inside temperature are smaller than that of the C- specimen.

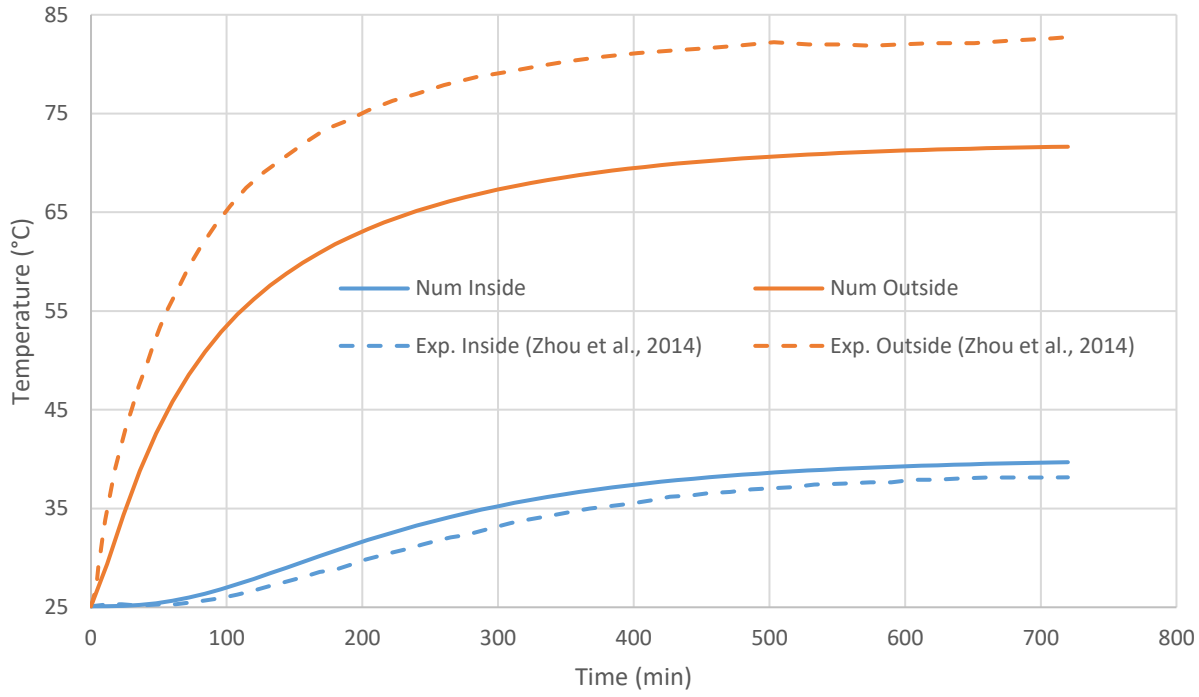

Figure 3-9: Numerical analysis temperature results of the inside and outside of C-specimen.

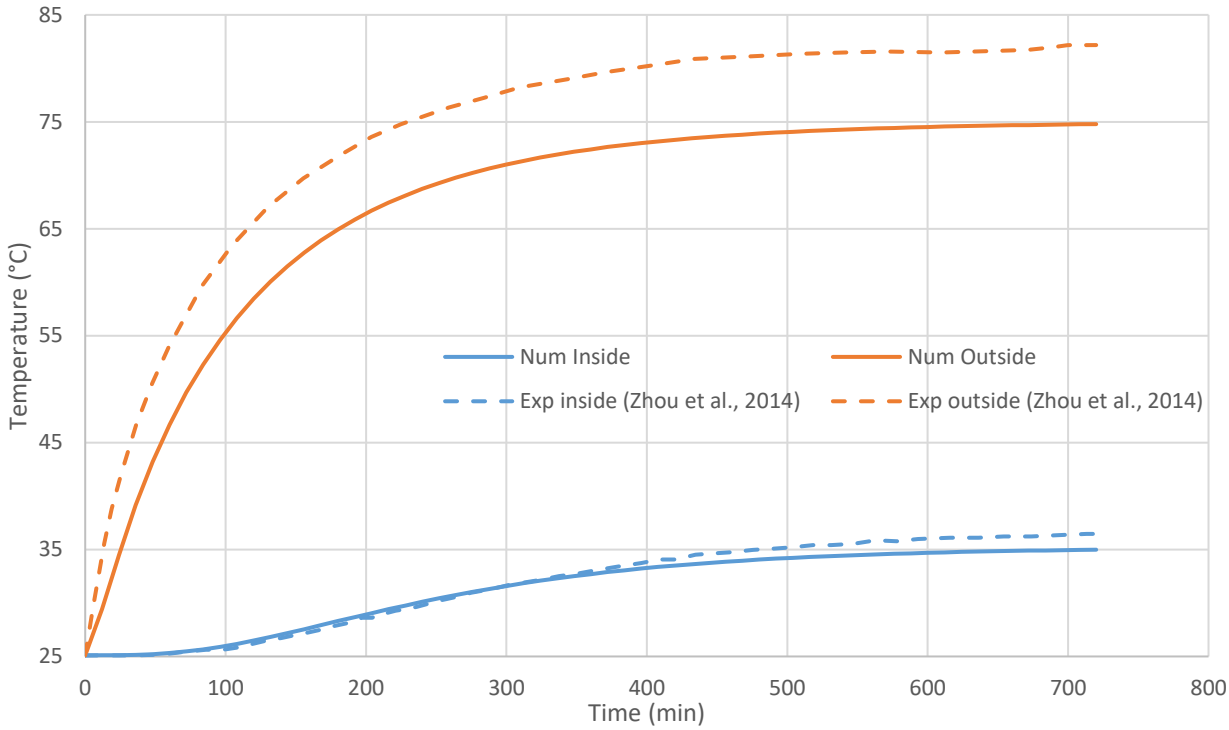

Figure 3-10: Numerical analysis temperature results of the inside and outside of G-specimen.

Table 3-2: Temperature results after 12 hours for the C and G wall in degrees Celsius of the experimental test by Zhou et al. (2014) *and the numerically computed results.*

		Ambient Temperature (°C)	**Outside layer (°C)**	**Inside layer (°C)**	**Difference between layers (°C)**
C-specimen	Zhou et al. (2014)	25.1	82.5	38.2	44.3
	Computed	25.1	71.6	39.7	31.9
G-specimen	Zhou et al. (2014)	25	82.0	36.3	45.7
	Computed	25	74.8	35	39.8

A time sensitivity analysis was also done to determine a realistic optimum time interval as seen in Figure 3-11. One can see that time intervals of 1 minute and 10 seconds are more accurate than for 1 hour. The smaller time increments portray a better representation of the temperature over time curve so that the curve is flatter at the start and at the end and peaks earlier than near the end of the time span. A difference of up to almost 1°C is seen at times between the 1 hour and 10 seconds intervals. However, there is not a significant difference between the 1 minute and 10 seconds intervals.

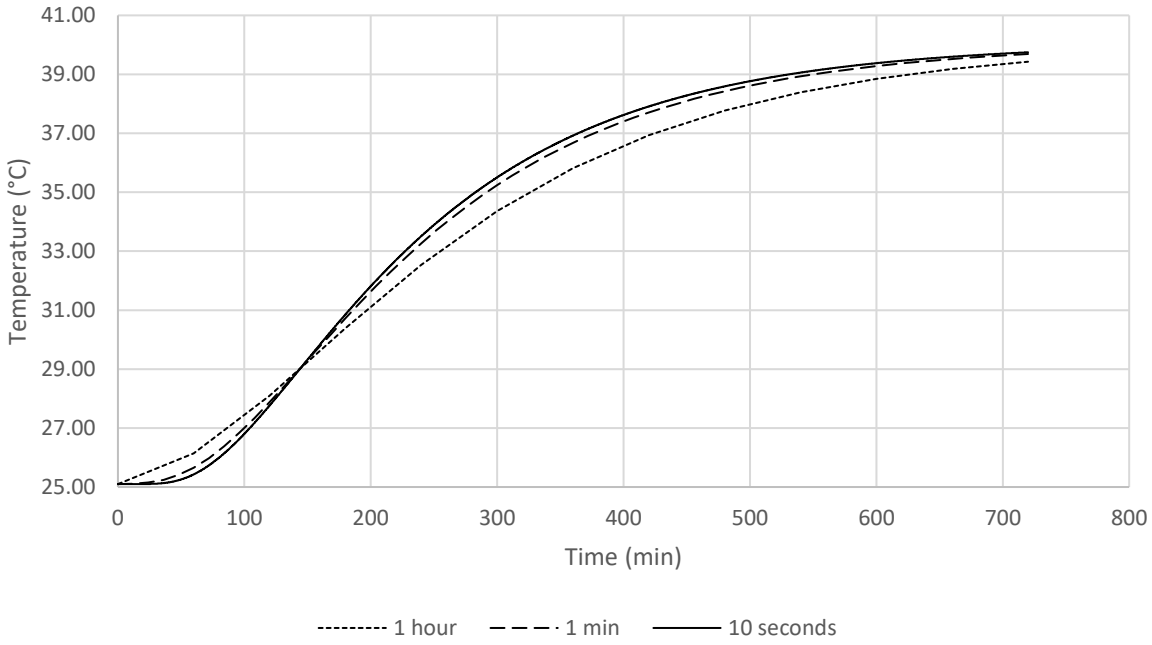

Figure 3-11: Time sensitivity analysis of the inside temperature of the C-specimen

Figures 3-12 and 3-13 show the temperature - time curve of the inside wall of both the C-specimen and G- specimen with different thermal conductivity values (Zhou et al., 2014).

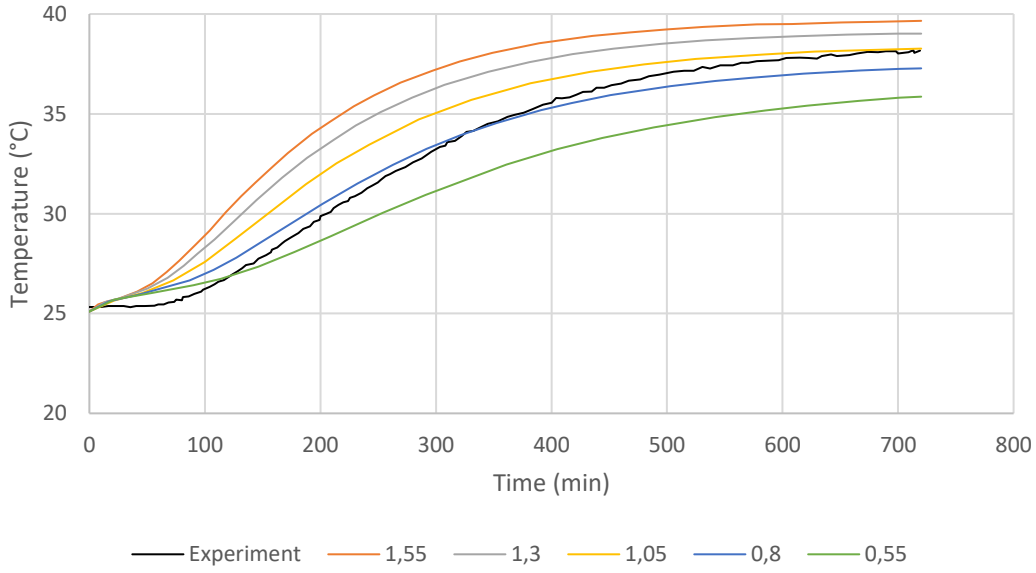

Figure 3-12: Numerical inside temperature results for different thermal conductivity values and experimental inside temperatures of the C-specimen (reworked from Zhou et al. (2014)*).*

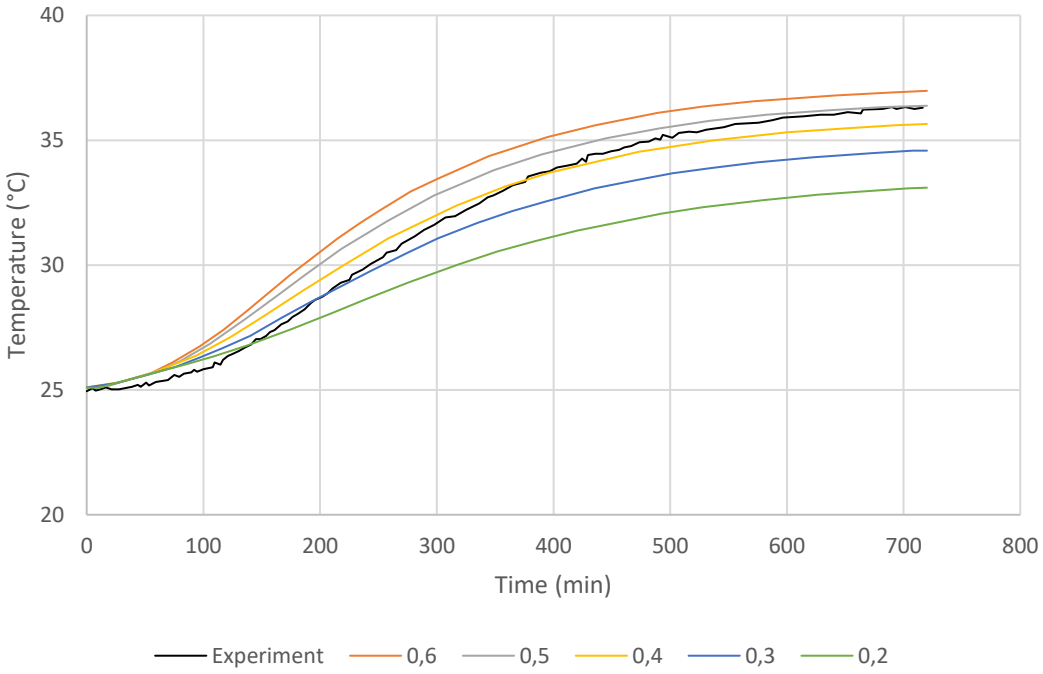

Figure 3-13: Numerical inside temperature results for different thermal conductivity values and experimental inside temperatures of the G-specimen (reworked from Zhou et al. (2014)*).*

Figure 3-14 compares the numerical results from Zhou et al. (2014) and the author of different thermal conductivities for the C-sepcimen and that G-specimen. The numerical analysis included a transient analysis with 12 minute increments. The numerical analysis done by Zhou et al. (2014) is not specified.

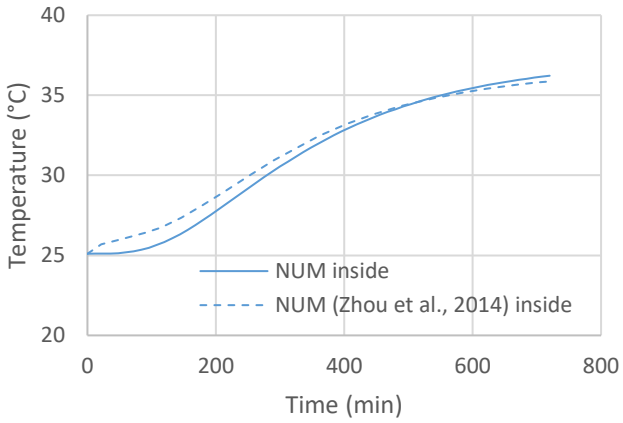

(a) k = 0.55

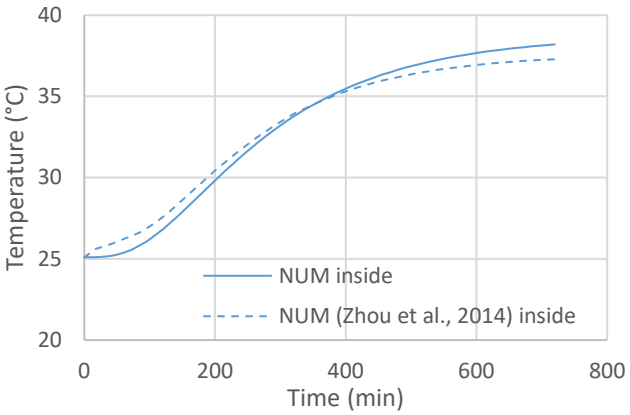

(b) k = 0.8

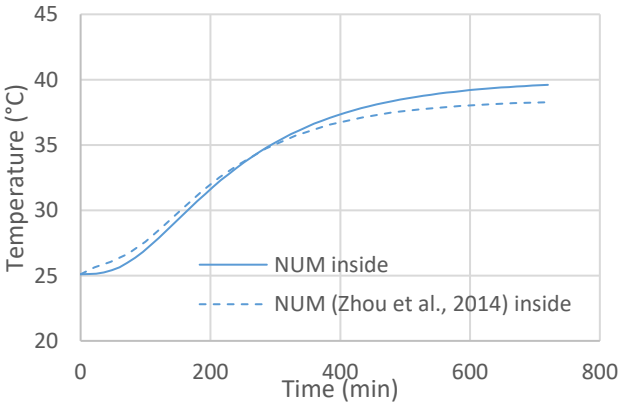

(c) k = 1.05

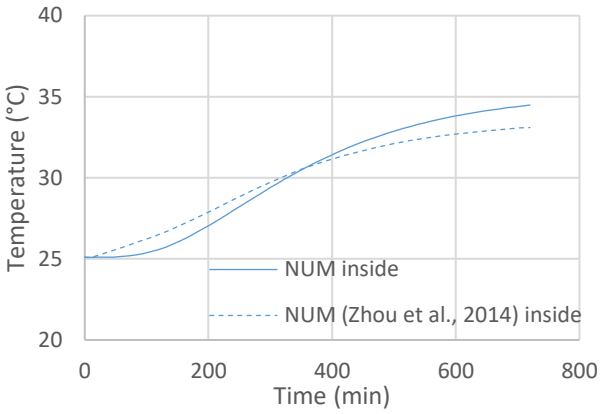

(f) k = 0.2

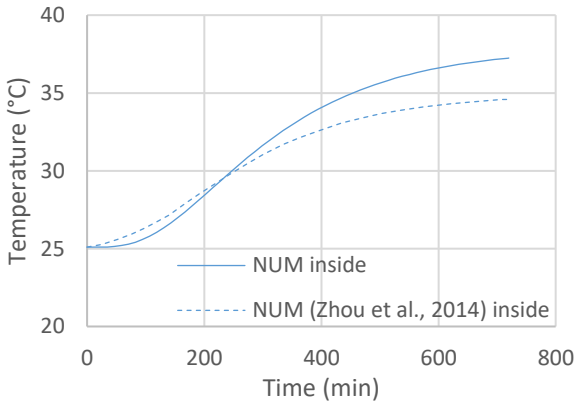

(g) k = 0.3

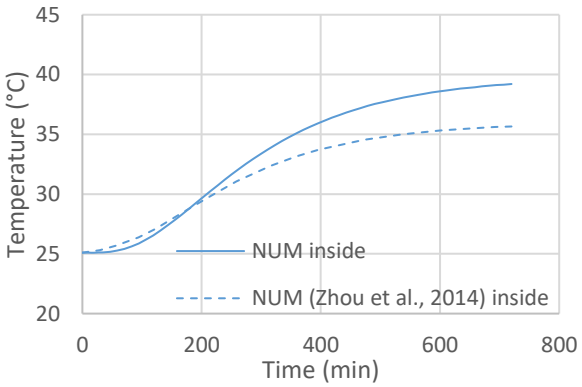

(h) k = 0.4

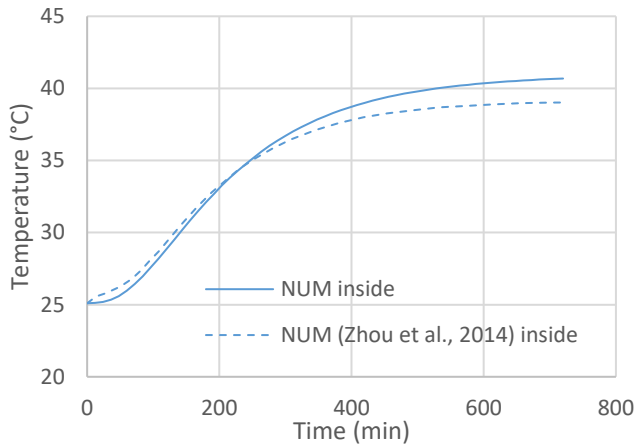

(d) k = 1.3

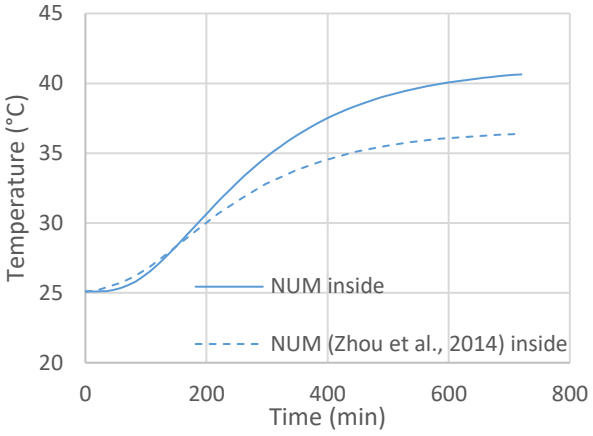

(i) k = 0.5

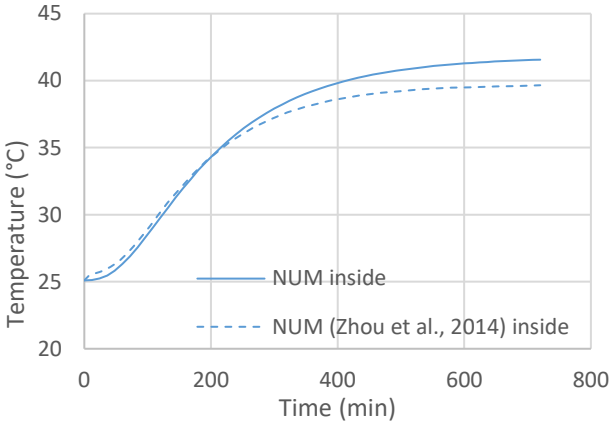

(e) k = 1.55

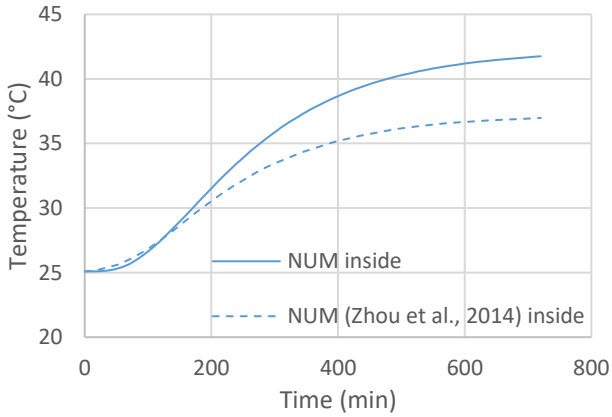

(j) k = 0.6

Figure 3-14: Difference between computed analysis results and Zhou et al. (2014) results for the inside temperature of the C- specimen (left) and the G-specimen (right) using different thermal conductivity values

There is uncertainty about experimental control in their laboratory test; their inability to numerically capture the distinct early thermal s-shape evolution shown in Figures 3-11 and 3-12, whereas the current computational results do. Hence, deviations between their computational and the current numerically computed results are not further investigated to improve agreement.

3.2.3 Hollow block thermal performance

Al-Tamimi et al. (2017) analysed hollow blocks by FEA to determine the most effective geometry for thermal performance. They analysed the hollow ratio (the area of void over the area of block material), the shape (square, rectangular and circular cavities), staggered and non-staggered voids and the cavity size for 400x200 mm blocks. All blocks were loaded with a heat flux of 746 W/m^2 on one surface to represent the outside of the wall. Thermal convection with a film condition of 8.9 W/m^{2}K and thermal radiation with an emissivity of 0.93 were applied on both sides of the wall with an ambient temperature of 46°C on the outside and 25°C on the inside of the wall. Convection and radiation in the cavities were determined according to EN ISO 6946 (2017). Results showed that out of the numerous models the geometry that showed the lowest inside temperature was with four equal rectangular cavities of 340x30 mm as shown in Figure 3-15. The equivalent film condition that was calculated from EN ISO 6946 for the cavities in Figure 3-15 was 6.52 W/m^{2}K which, according to Al-Tamimi et al. (2017) accounted for the radiation and convection inside the cavities.

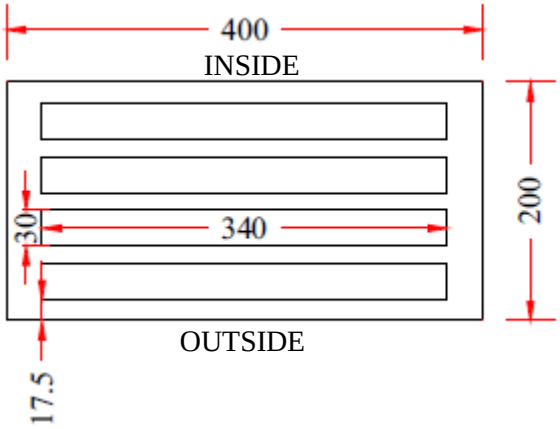

Figure 3-15: A 400x200 mm block with four equal 340x30 mm cavities from Al-Tamimi et al. (2017)

Al-Tamimi et al. (2017) determined the outside and inside temperature for the geometry in Figure 3-15 in ABAQUS to be 73.79°C and 28.16°C. The author of this thesis also performed the analysis using ABAQUS and reached the results shown in Table 3-3. Figure 3-16 shows the temperature distribution over the wall section from the author.

Table 3-3: Numerical results of the outside and inside temperatures from Al-Tamimi et al. (2017) and the author.

Surface	**Al-Tamimi et al. (2017) (°C)**	**The author (°C)**	**Temperature difference (%)**
Outside	73.79	86.76	14.95
Inside	28.16	28.15	0.04

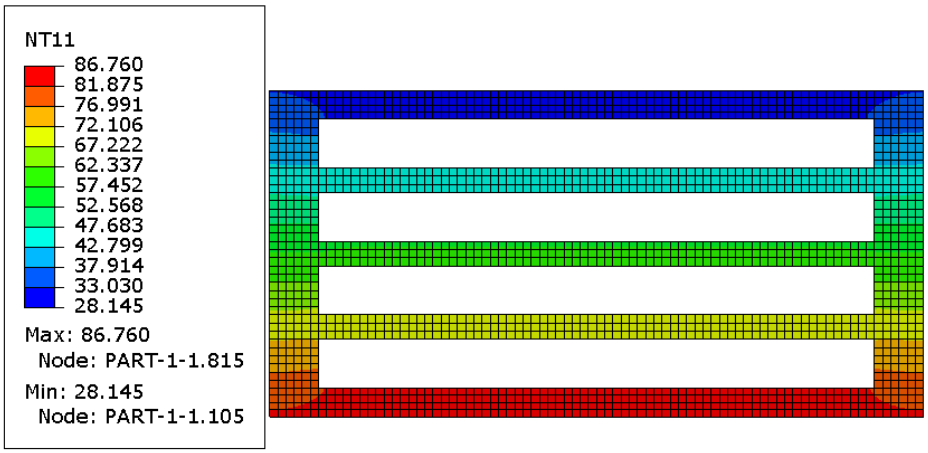

Figure 3-16: Numerical temperature results for the cavity wall section from the author.

3.3 Concluding summary

Case studies from literature were analysed. From the case studies it was found that radiation is independent of the width of the material and the width of the cavities. When the cavity sizes and the spacing between cavities increases, then the heat flow at those points increases as well.

Care should be taken when choosing the time interval for a transient heat transfer analysis. If the time increment is too large, the temperature curve shape will be inaccurate.

Lastly, after verifying the case studies that was modelled using FE the package ABAQUS, it was found that similar inside temperatures were reached although the outside temperatures differed from those of the case studies.

Chapter 4

4 FEA of 3DP foam concrete wall section

Background on 3DP foam concrete is provided in this chapter. An existing 3D printed foam concrete wall in the Stellenbosch University laboratory is analysed using the knowledge gained from the case studies. Heat transfer parameters are obtained from literature. The 3D printed wall is analysed using four different methods. First no heat transfer is accounted for inside the cavities, then the effect of radiation inside the cavities is added. After radiation is added the effect of cavity convection is added. Lastly, the wall is also analysed using pure conduction inside the air cavities where the thermal conductivity of air is used.

4.1 3DP foam concrete wall background

The Centre for Development of Sustainable Infrastructure (CDSI) at Stellenbosch University is a research institution that focusses, inter alia, on the research of 3D printing of concrete (3DPC) (Cho et al., 2019a). LWFC is 3D printed by Cho et al. n.d. whereby cement, other binders, fine aggregates, water and preformed foam are combined. Nano-SiO_2 particles with a diameter less than 30 nm are added to the mix for an increase in shear resistance and thixotropic behaviour (Cho et al., 2019b). Table 4-1 shows that although the fracture energy of 3DP nano-SiO_2 LWFC (3DP nSPP) is less than half of that of nano-SiO_2 LWFC, the flexural strength is significantly larger.

Table 4-1: Fracture energy and flexural strength of nSPP and nSPP(3D) LWFC (from Cho et al. n.d.*).*

	nSPP LWFC	**3DP nSPP LWFC**
Fracture energy G_f (N/m)	38.7	15.1
Flexural strength $f_{flexure}$ (MPa)	7.9	13.1

Foam concrete has the potential to be used as a seismic structural material due to its low self-weight and thus low inertia force (Dunn, 2017) and can compete as a structural element (De Villiers et al., 2017). Its weight, which can be further reduced by adding hollow cores, and its fast construction due to 3DP technology makes it a promising material in the housing industry. Thus, the focus on the thermal performance of foam concrete with cavities in this thesis may add to this promising material.

4.2 Finite element modelling of 3DP foam concrete wall

The foam concrete wall in Figure 4-1 was 3D printed by a team at Stellenbosch University. The height of each printed layer is 15 mm and the height of the wall is 810 mm. The entire wall section is 200 mm thick and about 990 mm in length. The thickness of the top layer was measured at 40 different places to reach a mean layer thickness of 37 mm (with a standard deviation of 2.80 mm).

An experimental hot box test was done on the wall to determine its thermal conductivity value (October, 2019). The thermal conductivity was determined as 0.3708 W/mK (October, 2019). The specific heat is determined from Mydin, (2013) to be 1100 J/kg°C and the density of the foam concrete is 1400kg/m^3 (Cho et al., 2019c).

4.2.1 Representative 2D finite element model

If the temperature is uniform along the outer area of the wall, the 3D problem can be reduced to a 2D problem, if the wall ends are ignored. Thus, Figure 4-1 is simplified to a 2D section shown in Figure 4-2. The ridged surface caused by the foam concrete layers is also approximated as a smooth surface due to the fact that the effect of the average area of the ridged surface is a smooth surface.

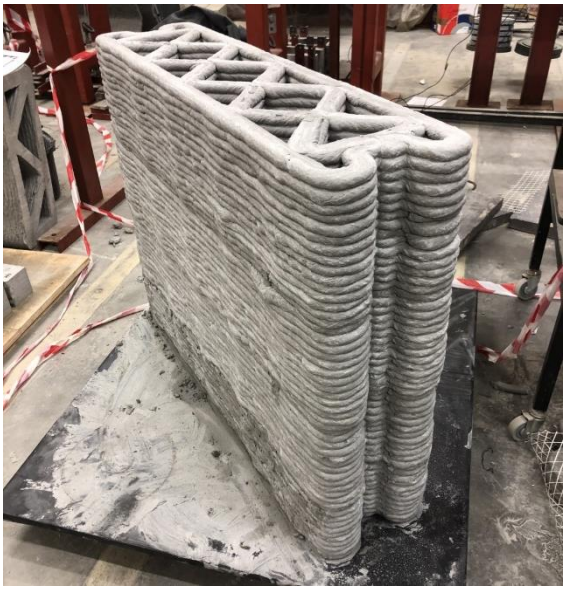

Figure 4-1: 3D printed foam concrete wall section

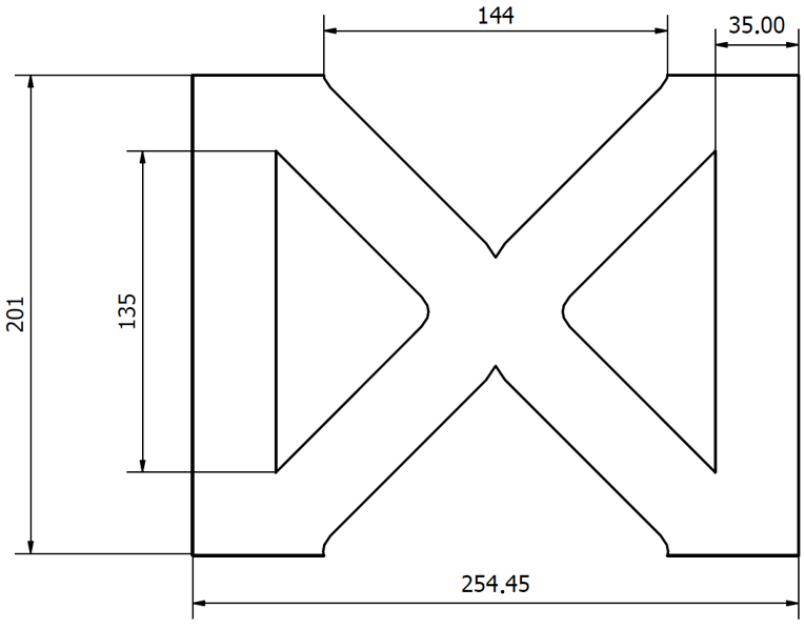

Figure 4-2: Main dimensions in mm of 3D printed foam concrete wall section

The direct normal irradiation is assumed to be 1000 W/m^2. The cosine law suggests that the relative intensity of radiation on a surface is equal to the cosine of the angle of incidence and that relative area over which it is distributed is the inverse of this value (Marsh, 2020). Thus, if the angle of incidence in

Figure 4-3 is taken as $\theta = 70°$, the incident heat flux acting perpendicular to the wall surface is 342 W/m^2.

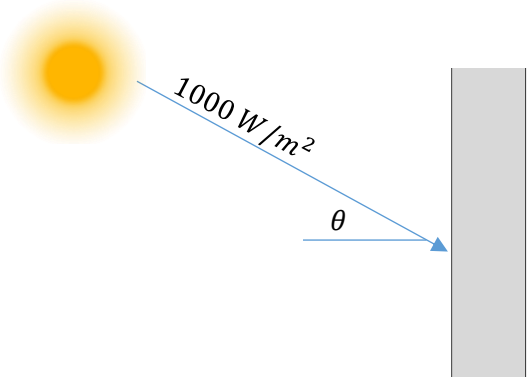

Figure 4-3: Diagram of the cosine law for solar radiation on a wall

4.2.2 Model parameters

A 2D plane was created in ABAQUS to represent a section of the 3D printed wall. The one side of the wall represents the outside of a building (exposed to solar radiation) and the other side of the wall represents the inside of a building. The wall section is solid homogeneous. The extrusion thickness of the layers is 35 mm which is the theoretical thickness to which the 3D printer extrudes the layers. A heating step was created including time intervals of 30 minutes for a duration of 24 hours.

Four different cases, including conduction and/or radiation and/or convection, were created and analysed against each other. Case A includes the modelling of only convection and radiation on the outer sides of the wall section and thus only including conduction in the wall concrete. Case B includes the addition of cavity radiation within the cavities of the wall and Case C includes the addition of both cavity radiation and convection. Case D involves creating a solid part inside each cavity and assigning to it heat transfer parameters of air. Table 4-2 summarises the heat transfer parameters of the 3D printed foam concrete wall.

Table 4-2: Heat transfer parameters of 3D printed foam concrete

Foam concrete properties	**Values**		**Reference**
Density	1400 kg/m^3	1.4E-6 kg/mm^3	given
Specific heat	1100 J/kg°C		(Mydin, 2013)
Thermal conductivity	0.3708 W/mK	0.000371 W/mmK	(October, 2019)
Heat transfer coefficient (outside)	10 W/m^{2}K	10E-6 W/mm^{2}K	(Mydin, 2013)
Emissivity	0.85		(Zhou et al., 2014)
Solar radiation	342 W/m^2	0.000342 W/mm^2	calculated
Cavity convection	2 W/m^{2}K	2E-6 W/mm^{2}K	(Del Coz Diaz et al., 2014)

A section cut representing a repeating pattern of the wall is analysed by FE. The section is shown in Figure 4-4 indicating the different boundary conditions and interactions for the different cases.

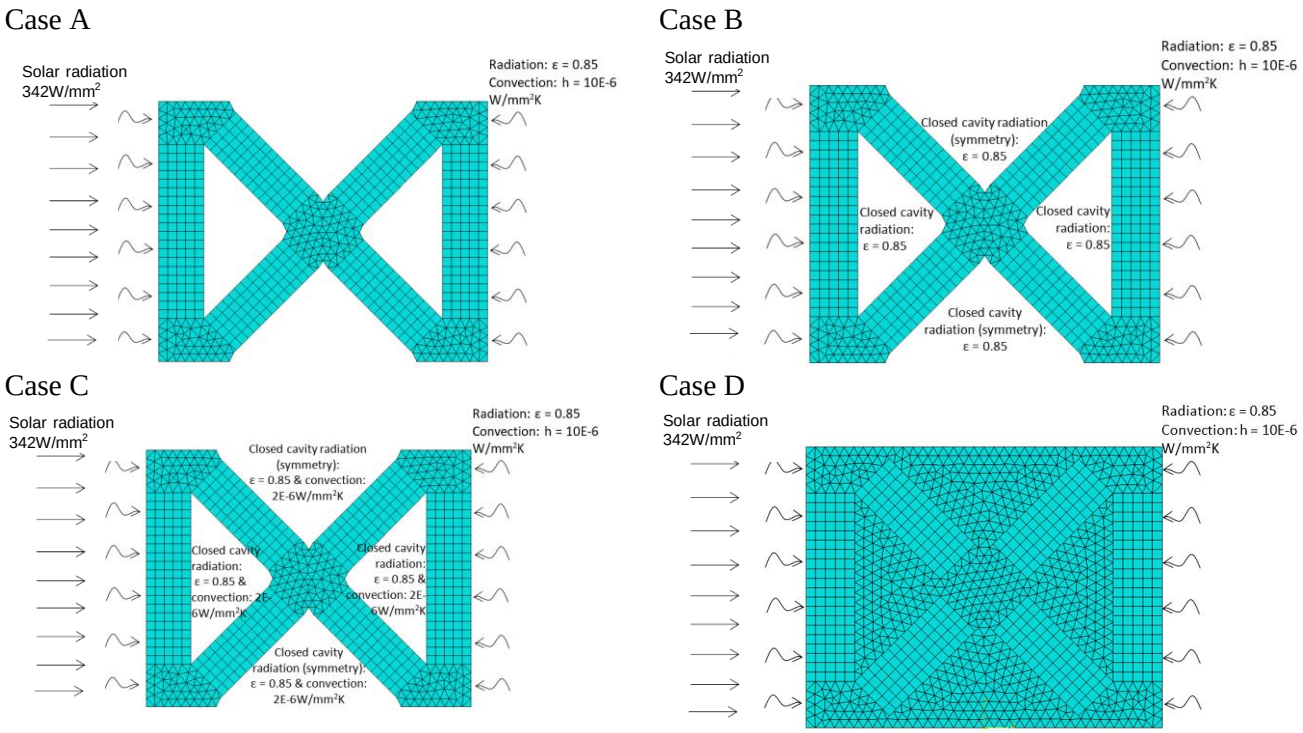

Figure 4-4: Heat transfer Cases A (only conduction inside the concrete), B (conduction inside concrete as well as closed cavity radiation), C (conduction and closed cavity radiation as well as convection inside the cavities) and D (conduction through the use of solid parts inside the cavities with heat transfer parameters of air assigned to the solid parts) of a section of the 3D printed foam concrete wall.

4.2.3 Results

As seen from Figure 4-4, Case A represents the wall section that is only analysed with conduction inside the concrete. Thus heat transfer through radiation and convection is ignored in the cavities. A solar radiation load is applied on the outside surface (left) of the wall section while both convection and radiation with air are applied on both the inside and the outside of the wall section. No interaction is applied inside the cavities. It was decided that the inside and outside of the wall section have a predefined temperature of 20 °C. As seen from Figure 4-5 after about 180 minutes (3 hours) the inside of the wall section starts to increase from 20°C. The curves having higher temperatures represent the nodes that are at the top and the bottom of the inside of the wall section and the curves having lower temperatures represent nodes that are closer to the middle of the inside of the wall section. Due to symmetry only the top half of the nodes on the inside of the wall, from nodes 1 to 14, are represented in Figure 4-5.

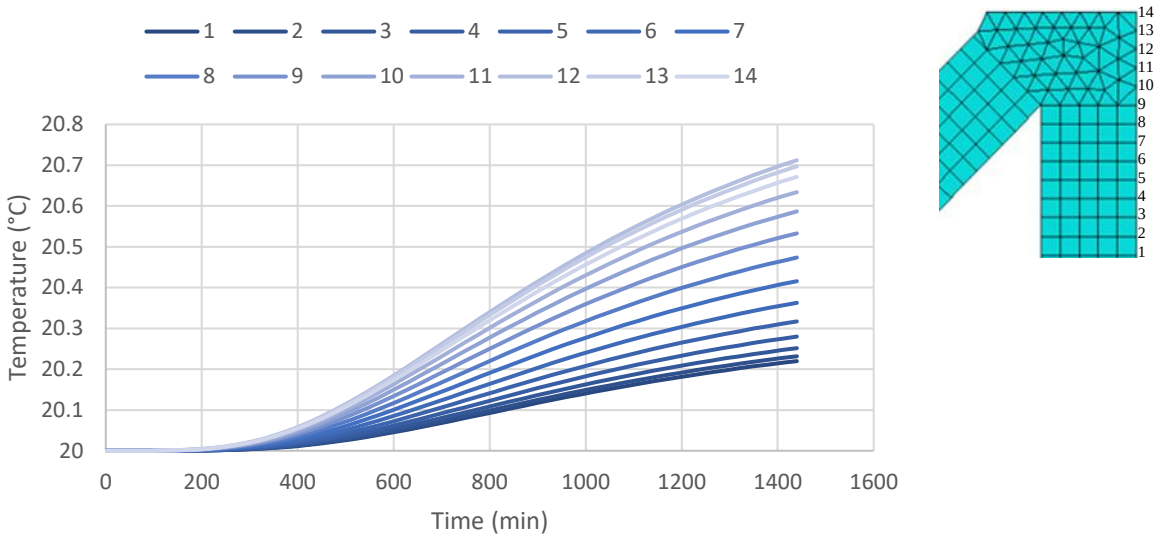

Figure 4-5: Nodal temperature of the inside of the wall section for Case A.

Figure 4-6 illustrates the nodal temperatures for the inside of the wall section for Case B. A solar radiation load is again applied at the outside of the wall section and radiation and convection with air is also applied on both sides of the wall section. A closed cavity radiation factor of 0.85 is applied in the cavities with an interaction temperature of 20°C. The cavities on the top and the bottom of the wall section are also analysed as closed cavities with symmetry due to the section cut being a repeating pattern. The nodal temperatures start to increase from 20°C after about an hour. The nodes with higher temperatures are once again more to the top and the bottom of the inside of the wall section and the nodes with lower temperatures are in the middle of the inside of the wall section. The average temperature of the nodes on the inside of the wall section is 21.6°C. Again, only nodes 1 to 14 are illustrated.

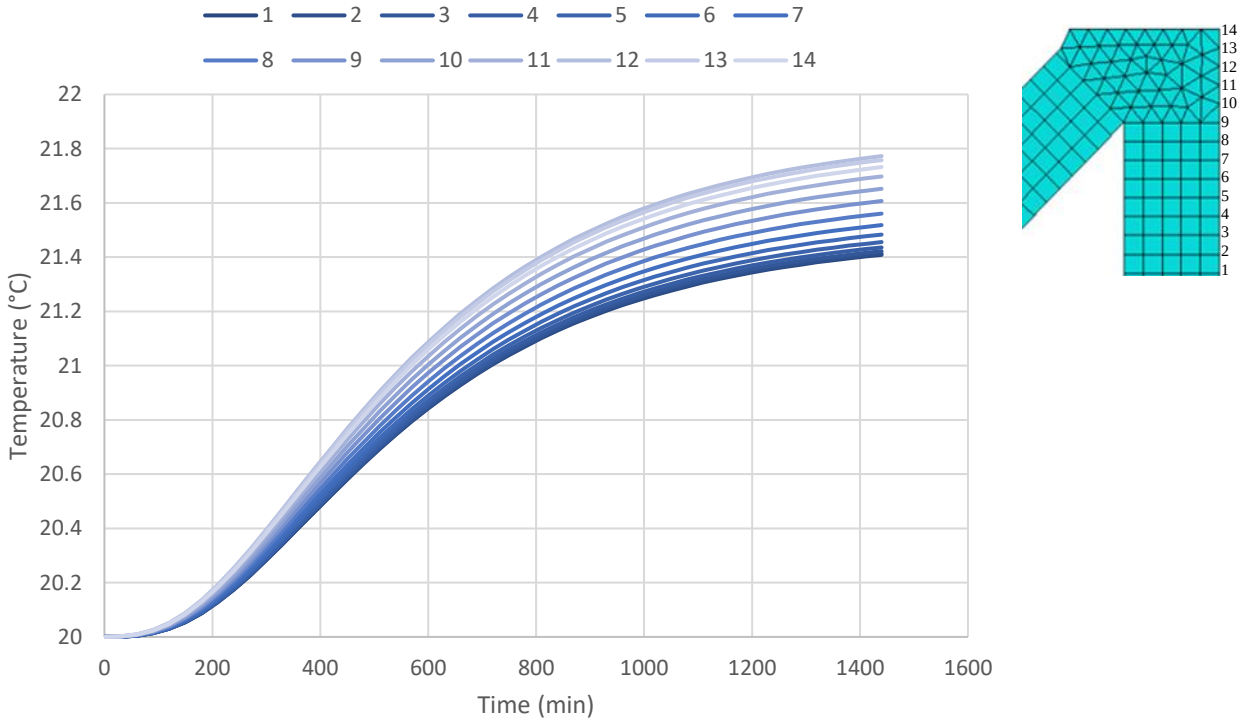

Figure 4-6: Nodal temperatures of the inside of the wall section for Case B.

Jeffers et al. (2013) reported verification cases for the thermal performance of fire resistive assemblies. In one of their cases they compared the addition of void radiation effect only to both void radiation and void convection effects. They modelled an I-beam protected by an insulation board in ABAQUS and added a thermal fire load on all four sides according to the ISO 834 (ISO 834-11 2014) time-temperature curve. This case study was first presented by Wickström and Palsson (1999). The results by Jeffers et al. (2013) and Wickström and Palsson (1999) show a good correlation and were also verified by Marx (2018). The procedure that was followed included a radiative heat transfer analysis within the cavities formed between the I-beam and the insulation board. The average temperature on the inside of the insulation board that was reached after the analysis was then used as amplitude values in a following analysis to include convection. The average time-temperature amplitude was used as an ambient temperature for convection on the I-beam surfaces of the cavities.

For Case C, the time-temperature amplitudes of the nodes on the surface of the cavities in the results of Case B were used as input parameters for the cavity convection interaction. The air inside the cavities is heated or cooled by the surfaces it is exposed to and thus in reality there is no uniform temperature inside these cavities. However, the air in the cavities is constantly mixing with temperatures from the surfaces forming the cavities. Hence, an approximation of the air as having a uniform temperature can be created. Heat transfer of the air is proportional to the area of contact and temperature difference and thus the temperature of the air can be said to become the temperature of the surfaces it is in contact with. Thus, the concept of using average temperatures on the surfaces of the cavities as done by Wickström and Palsson (1999), Jeffers et al. (2013) and Marx (2018) is used.

However, modelling the convection by using the air temperature will increase heat transfer through the section because a path for energy transfer is being added to the analysis. Hence, the perimeter temperature may increase, and the calculated air temperature from the first iteration is now lower. The air temperature can then be updated based on the increased section temperature based on the increased section temperature. This would need to be done iteratively until convergence, but that is probably not going to take more than one or two air temperature updates or iterations depending on the amount of heat transfer relative to conduction.

As seen in Figure 4-4 Case C, there are four triangular cavities in the wall section. Each cavity is treated separately when calculating the average time- temperatures of the nodes in each cavity. Figure 4-7 shows the temperature results of the nodes on the inside of the wall section after heat transfer through convection in the cavities is added to Case B. Figure 4-8 shows the second iteration and Figure 4-9 shows the third iteration.

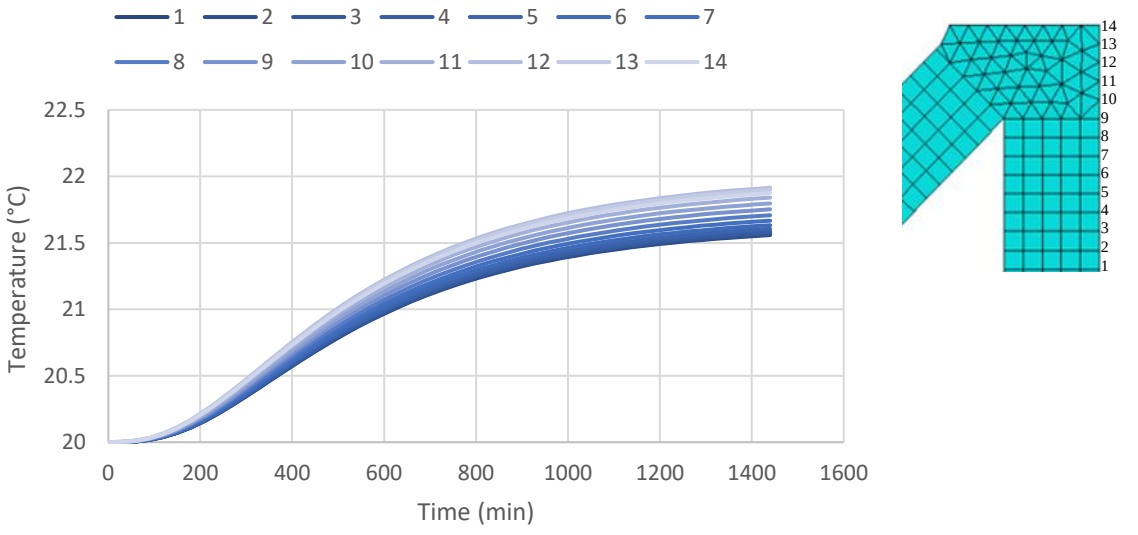

Figure 4-7: Nodal temperatures of the inside of the wall section for the first iteration of Case C.

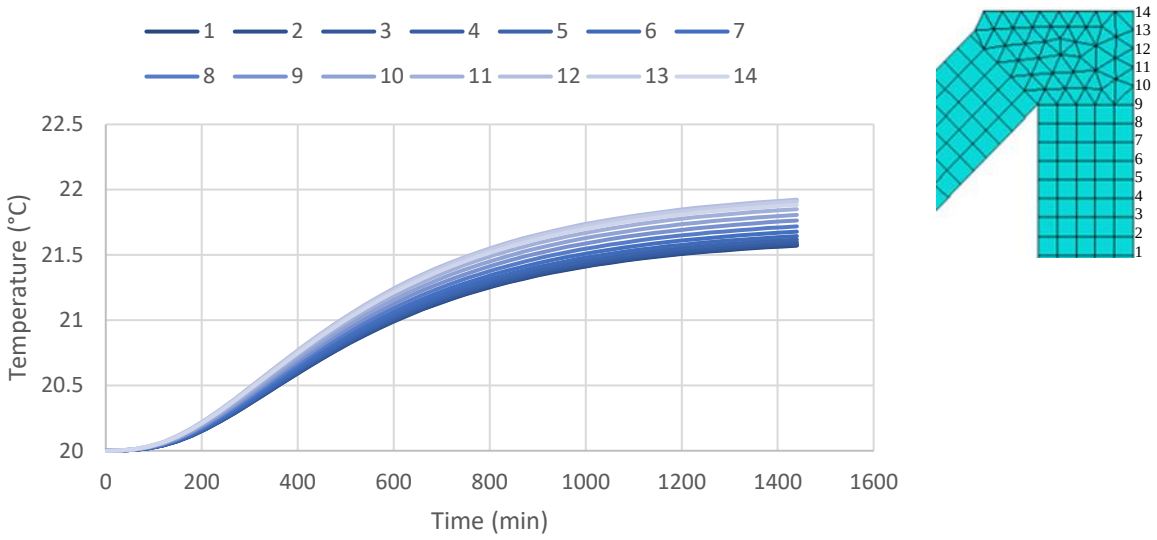

Figure 4-8: Nodal temperatures of the inside of the wall section for the second iteration of Case C

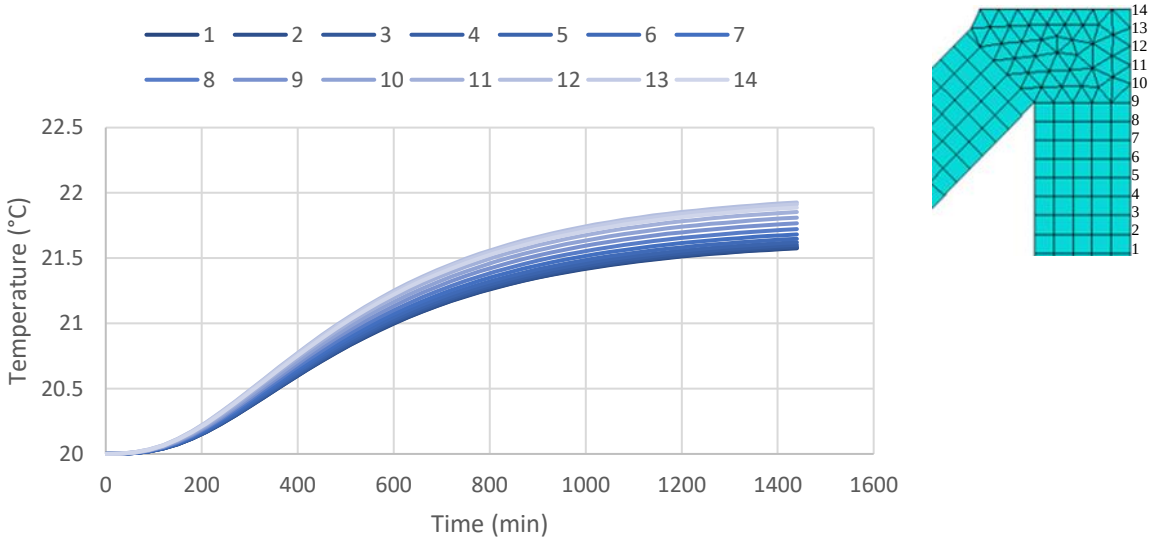

Figure 4-9: Nodal temperatures of the inside of the wall section for the third iteration of Case C

Figure 4-10 shows the nodal temperatures for the different iterations of the inside of the wall section after the wall is heated for 24 hours. Trial 0 represents the temperature results for Case B, thus no heat transfer through convection is added to the system. The largest temperature difference between Trial 0 and Trial 3 is 0.17°C and occurs in the middle of the inside of the wall section at 100.71 mm (thus a 0.788% increase from Trial 0 to Trial 3). The minimum temperature difference between Trial 0 and Trial 3 is 0.15°C and occurs at the ends of the inside of the wall section at 0mm and 201.42 mm (thus a 0.684% increase from Trial 0 to Trial 3) There is thus a gradual increase in temperature from the ends of the inside of the wall section to the middle of the inside of the wall section from adding only cavity radiation to the model to adding cavity radiation and convection to the model. The increase in temperature from Trial 0 to Trial 3 makes sense due to the addition of an energy transfer path when adding heat transfer through convection in the cavities. The temperature results from Trials 1 to 3 are close to each other and the temperature results between Trials 2 and 3 are nearly similar. Thus, the iteration process is stopped after Trial 3.

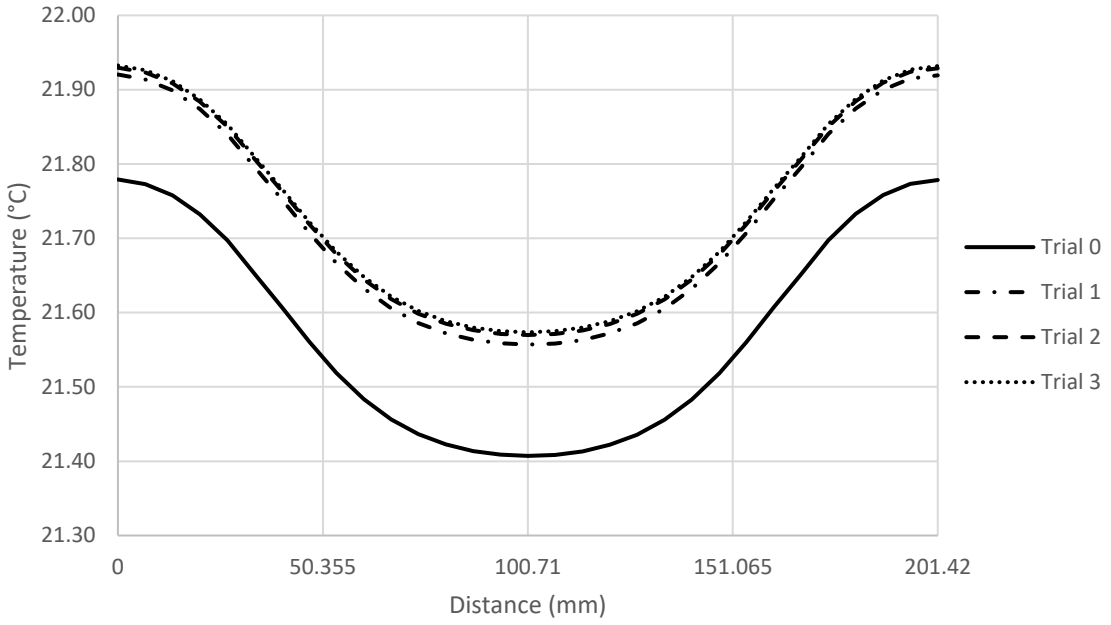

Figure 4-10: Temperature after 24 hours of the inside nodes of the wall section

The heat transfer parameters for air for Case D is summarised in Table 4-3. These parameters are assigned to a solid homogenous part and tied to the modelled wall section. The nodal temperatures on the inside of the wall section are shown in Figure 39. These nodes all have the same time-temperature values due to the uniform flow of heat from the outside of the wall section to the inside as seen in Figure 4-11 Case D.

Table 4-3: Heat transfer parameters of air at 1 atm and 20°C

Air properties	**Values**
Density	1.204E-9 kg/mm^3
Thermal conductivity	2.514E-5 W/mmK
Specific heat	1007 J/kg°C

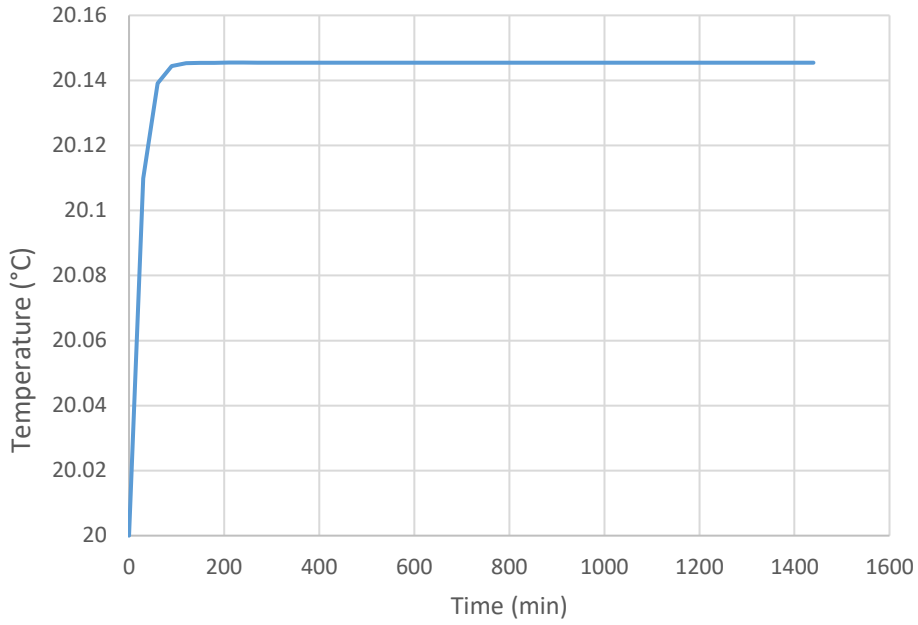

Figure 4-11: Nodal temperatures of the inside of the wall section for Case D.

The visualisation of the heat transfer analysis after 24 hours of Case A shown in Figure 4-12 indicates a non-uniform heat flow from the outside wall to the inside wall. Heat is only conducted through the concrete and not conducted through the cavities. The maximum temperature occurring on the outside wall is 41.798°C and the minimum temperature occurring on the inside of the wall is 20.216°C. As mentioned previously, heat transfer through radiation in the cavities is added in Case B. Hence, a more uniform heat flow occurs through the wall. The maximum temperature occurring on the outside in Case B is 40.690°C and the minimum temperature on the inside is 21.407°C. For Case C, the addition of heat transfer through convection in the cavities, the maximum temperature is 40.540°C and the minimum temperature is 21.573°C. Thus, with the addition of heat transfer through convection in the cavities, as the heat flows through the wall section the temperature on the outside of the wall is initially colder due to the release of some heat in the first cavity, but then heat is gathered more near the inside than with Case B and thus has a higher inside temperature than Case B. Case D shows a maximum outside temperature of 42.022°C and a minimum inside temperature of 20.145°C.

The outside and inside temperatures of Case D are respectively the highest and lowest. Case D only accounts for conduction in the air cavities and in the foam concrete. When cavity radiation and convection is added, as in Case B and C, the outside temperature decreases and the inside temperature increases. This is due to heat being transported faster from the outside to the inside with respect to Case A and D. Therefore, cavity radiation and convection cannot be neglected.

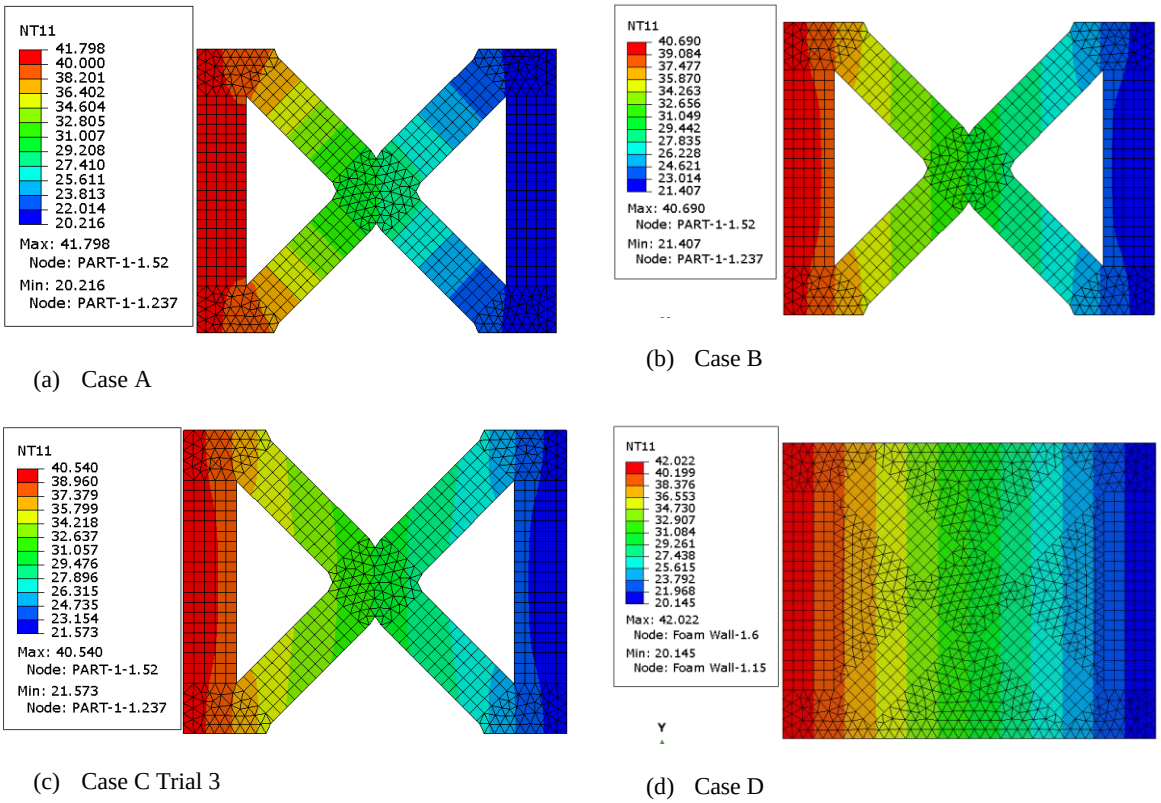

(a) Case A

(b) Case B

(c) Case C Trial 3

(d) Case D

Figure 4-12: Visualisation of the heat transfer (a) Case A (only conduction inside the concrete), (b) Case B (conduction inside concrete as well as closed cavity radiation), (c) Case C Trial 3 (conduction in the concrete and closed cavity radiation as well as convection inside the cavities) and (d) Case D (conduction through the use of solid parts inside the cavities with heat transfer parameters of air assigned to the solid parts) of a section of the 3D printed foam concrete wall after being heated for 24 hours (NT11 units in degrees Celsius).

4.3 Concluding summary

When doing a heat transfer analysis on a hollow wall system, it is important to take the effects of both radiation and convection in the hollow parts into account. The addition of the effect of radiation and convection in the cavities decreases the outside temperature of the wall and increases the inside temperature. Thus, the inside temperature may in reality be higher than the simulation if cavity radiation and cavity convection is not taken into account.

3D printed facade walls should be adjusted to benefit from thermal resistance of smaller voids as depicted in Figure 3-3, and large cavities that contribute to poorer thermal insulation through cavity radiation and convection should be avoided.

Chapter 5

5 Cavity size and arrangement

The aim of this chapter is to determine what the influencing parameters are on a wall section with air cavities (such as the size and number of cavities) to obtain an optimum thermal performance. The FE simulation models for wall sections with different numbers and sizes of air cavities are studied. Furthermore, the numerical results are compared to analytical verifications determined with thermal resistance networks.

5.1 Numerical analysis

Given the significant influence of cavity radiation and convection highlighted in the previous section, the role of cavity size and layout is investigated further here. Geometrically simple rectangular cavities are studied, given the pool of experience and literature on hollow masonry walling unit thermal performance, as highlighted in Section 3.2.

Figure 5-1 (a) shows the plan view of a 255 mm thick solid foam concrete wall and Figure 5-2 (b) shows the plan view of a foam concrete wall with a 185 mm air cavity with two 35 mm layers on either side of the cavity. After loading the solid wall with a heat flux of 342 W/m^2 on the outside surface and adding convection and radiation listed in Table 4-2 with an ambient temperature of 20°C on either side of the wall, the outside temperature is 40.31°C and the inside temperature is 21.4°C. When loading the wall with a 184mm air cavity with 342 W/m^2 on the outside surface and also applying radiation and convection as with the solid wall while ignoring radiation and convection effects of the cavity, the outside temperature is 42.07°C and the inside temperature is 20.10°C. These temperatures are measured at the midpoints of the outside and inside walls assuming that the cavities are never ending and independent of the small link at the top and bottom of the wall in Figure 5-1 (b) (indicated by the blue dotted line and crosses). In this case there is no heat transfer through the cavity due to the high thermal resistance across the wall which then explains the high outside temperature and low inside temperatures with respect to the outside and inside temperatures of the solid wall. When the solar heat enters the outside surface of the wall and the conduction resistance is high, the heat accumulates near the surface until the temperature of the outside surface is high enough to reject most of the heat back to the outside environment.

When adding cavity radiation to the hollow wall, the outside temperature is 39.85°C and the inside temperature is 22.47°C. Thus, the outside temperature decreases while the inside temperature increases significantly when adding cavity radiation to the hollow wall. When including cavity radiation, heat moves easier through the wall and thus heat is being transported away from the outer wall to the inside wall, hence the lower outside temperature and higher inside temperature than when adding no cavity radiation. Adding convection inside the cavities with a film condition of 2 W/m^{2}K, the outside temperature becomes 39.57°C and the inside temperature becomes 22.76°C. Once again, the outside temperature decreases while the inside temperature increases although not as much.

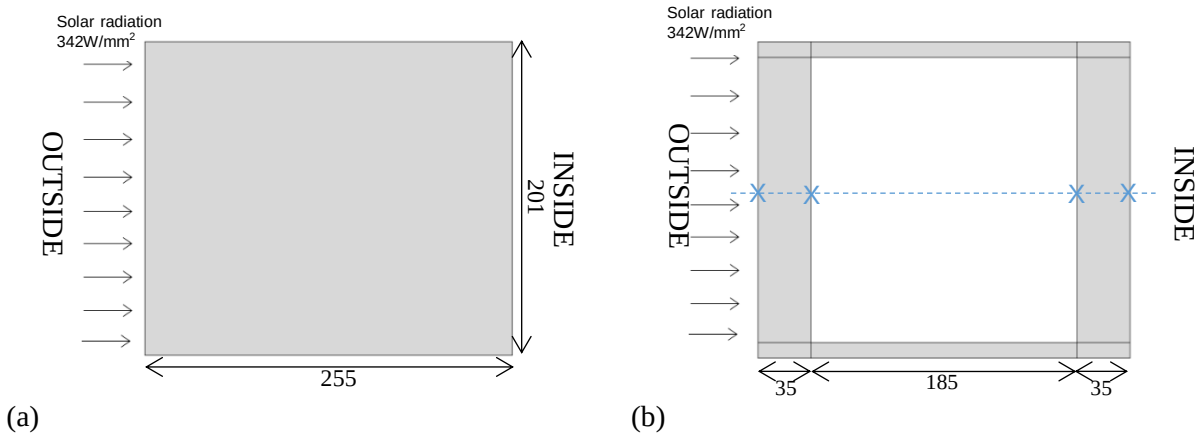

(a) (b)

Figure 5-1: Wall elements with (a) no voids and (b) a 185 mm void

According to Lorente et al. (1998) a wall system with more cavities, but smaller cavities results in a greater thermal resistance and thus a lower effective thermal conductivity. Al-Tamimi et al. (2017) inter alia compared the internal temperatures of wall elements with different rectangular cavities. The wall element with more rectangular cavities, but thinner cavity thicknesses resulted in a lower internal temperature than wall elements with less rectangular cavities but thicker cavity thicknesses with the same total cavity area.

Two different wall elements of 255x201 mm^2 dimensions shown in Figure 5-2 were modelled by FE. Foam concrete strips of 35 mm were chosen in order to be 3D printed. Both walls have the same area cavities, however Figure 5-2 (a) has three 181x38 mm^2 rectangular cavities and Figure 5-2 (b) has six 181x22 mm^2 rectangular cavities. Both models were analysed with properties shown in Table 4-2 during steady state and were loaded with 342 W/m^2 on the left side (outside). The outside and inside temperatures for the wall with three larger cavities were 40.84°C and 21.42 °C respectively and the outside and inside temperatures for the wall with six smaller cavities were 41.25°C and 20.98°C respectively. These temperatures were also measured at the midpoint as with Figure 5-1 (b) assuming that the cavities are infinite in length. Thus using smaller, but more cavities, decreases the inside temperature by 2.05%.

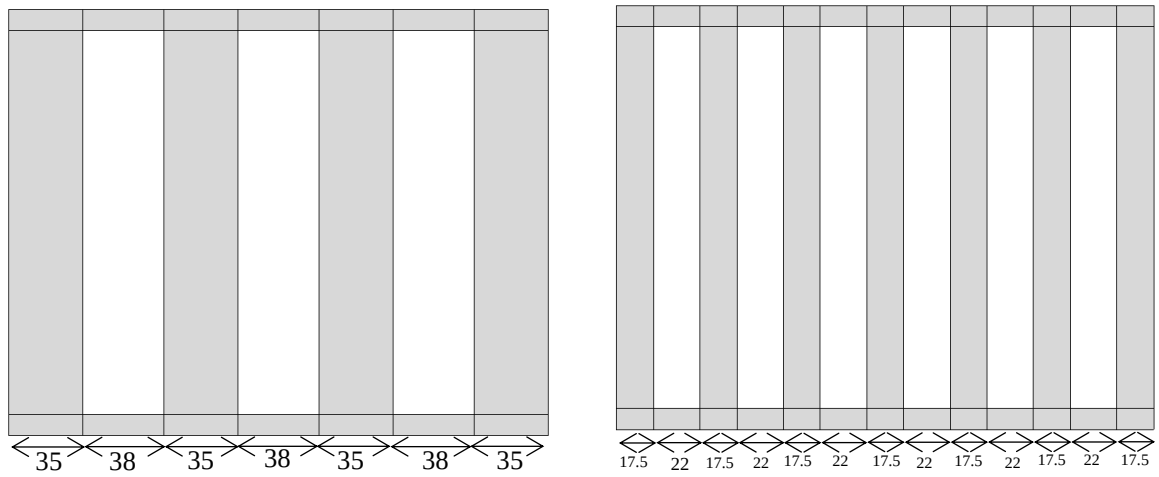

(a) (b)

Figure 5-2: Hollow wall elements with rectangular cavities with (a) 181x38 mm and (b) 181x22 mm cavity dimensions

Al-Tamimi et al. (2017) and Huang et al. (2018) analysed the void to material ratio of hollow core blocks. Both authors varied the void ratio up to 50% to determine what void ratio would yield the lowest internal temperature. Al-Tamimi et al. (2017) varied the shape of the voids between round, square and rectangular while also varying the void ratio from 0 to 51%. Huang et al. (2018) used varying round to

elliptic void shapes while varying the void ratio between 25 and 50%. Both concluded that the optimal ratio of concrete material to voids is 50% for a minimum temperature on the inside of the wall (see Figure 3-3).

The next analysis is done to compare the inside temperature results between a simple wall element with a good void ratio, but with fewer cavities that are wide versus a simple wall element with many thin cavities, but a bad void ratio. Figure 5-3 (a) shows a wall element with a 58.73% void ratio while Figure 5-3 (b) shows a wall element with 31.22% void ratio. Void ratios are taken as the percentage of void width over the total width of the wall. Both wall elements have overall dimensions of 255x201 mm^2 and have the same heat transfer properties as listed in Table 4-2.

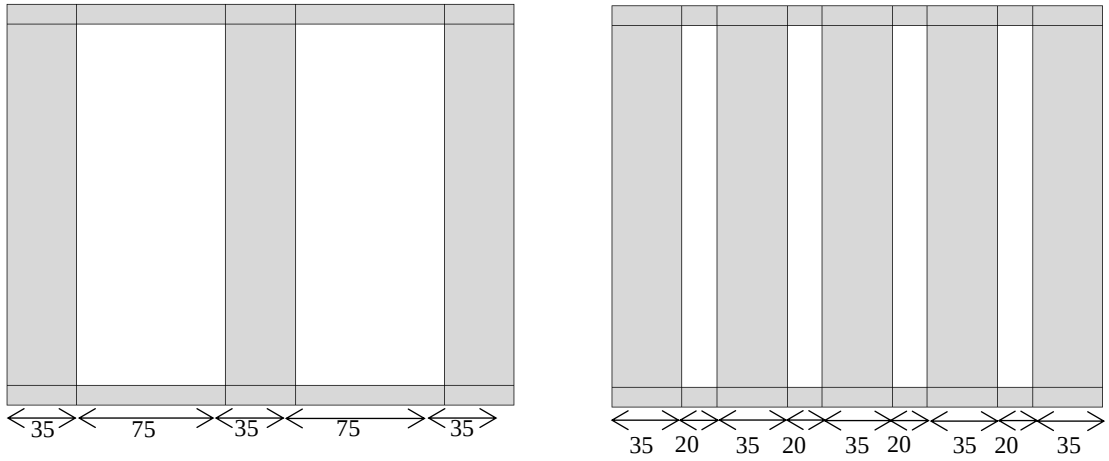

(a) (b)

Figure 5-3: Hollow wall element with (a) two rectangular cavities with dimensions of 181x75 mm and (b) four rectangular cavities with dimensions of 181x20 mm

The wall element in Figure 5-3 (a) has an outside temperature of 40.42°C and an inside temperature of 21.42°C and the wall element in Figure 5-3 (b) has an outside temperature of 41.09°C and an inside temperature of 21.15°C. Thus, in the case of simple rectangular cavities with foam concrete strips of 35 mm width, it can be concluded that thinner and more cavities, but a "bad" void ratio takes priority over thicker and less cavities, but a "good" void ratio.

The outside and inside temperature results for six wall sections with the same overall thickness, but with varying hole numbers are compared. All the walls have the same distance between each hole (35 mm) as seen in Figure 5-4. The temperature results measured at the midpoints of every wall are summarised in Table 5-1 for only conduction, Table 5-2 for conduction and cavity radiation and Table 5-3 for conduction and cavity radiation and convection.

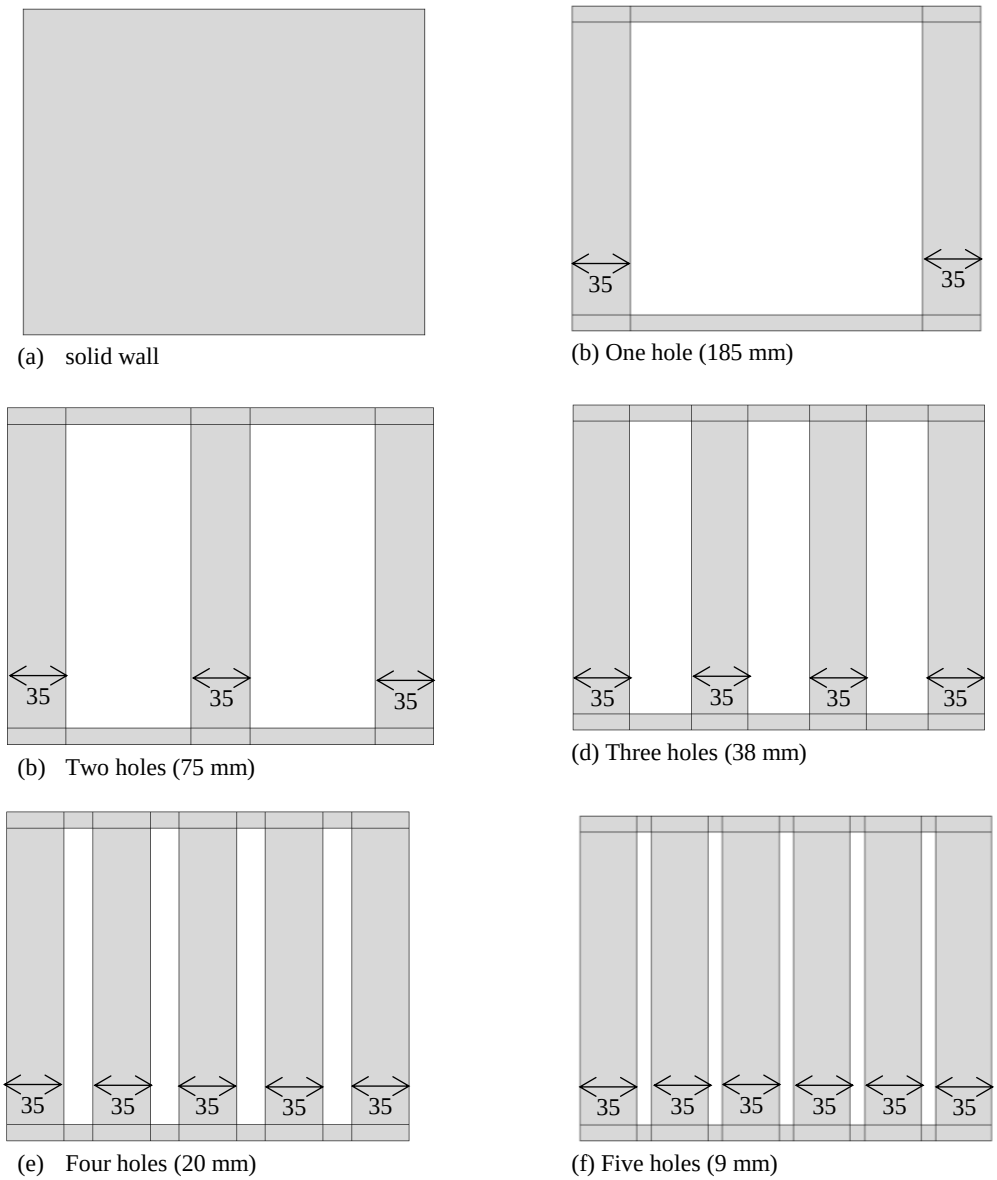

(a) solid wall

(b) One hole (185 mm)

(b) Two holes (75 mm)

(d) Three holes (38 mm)

(e) Four holes (20 mm)

(f) Five holes (9 mm)

Figure 5-4: Wall sections (a) solid wall, (b) one hole, (c) two holes, (d) three holes, (e) four holes and (f) five holes with 35 mm distances between holes.

Table 5-1: Outside and inside temperatures of wall sections with different cavity sizes and numbers when no cavity radiation or convection is taken into account.

No cavity radiation or convection		
	OUTSIDE (°C)	INSIDE (°C)
Solid	40.31	21.40
One Hole	42.07	20.10
Two Holes	42.06	20.11
Three Holes	42.05	20.12
Four Holes	42.04	20.13
Five Holes	42.92	20.13

Table 5-2: Outside and inside temperatures of wall sections with different cavity sizes and numbers when only cavity radiation is taken into account.

Adding cavity radiation		
	OUTSIDE (°C)	INSIDE (°C)
Solid	-	-
One Hole	39.85	22.47
Two Holes	40.58	21.70
Three Holes	40.94	21.30
Four Holes	41.17	21.06
Five Holes	41.19	20.90

Table 5-3: Outside and inside temperatures of wall sections with different cavity sizes and numbers when both cavity radiation and convection is taken into account.

Adding cavity radiation and convection		
	OUTSIDE (°C)	INSIDE (°C)
Solid	-	-
One Hole	39.57	22.76
Two Holes	40.42	21.87
Three Holes	40.84	21.42
Four Holes	41.09	21.15
Five Holes	41.32	20.98

Figures 5-5 and 5-6 illustrate the relationship between the inside temperature and the number of holes and the inside temperature and the void ratio respectively. The temperature results are also listed in Table 5-3. A clear relationship can be found between the number of cavities and the inside temperature and the void ratio and the inside temperature for cavity walls with equal thicknesses and distances between cavities. Thus, for a fixed distance between cavities, an increase in the number of holes and a decrease in the void ratio gives a lower inside temperature.

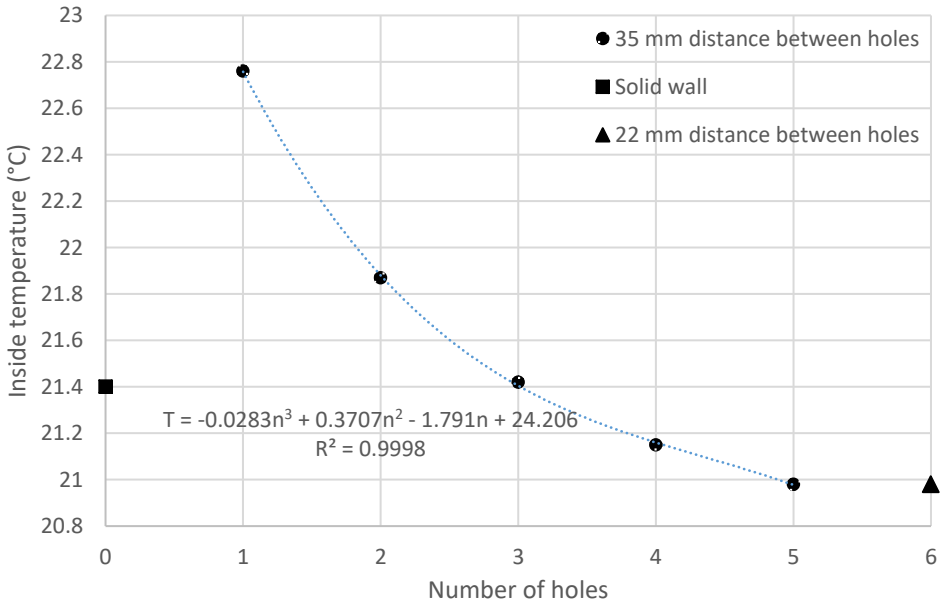

Figure 5-5: Inside temperatures of wall sections with different numbers of cavities that include cavity radiation and convection.

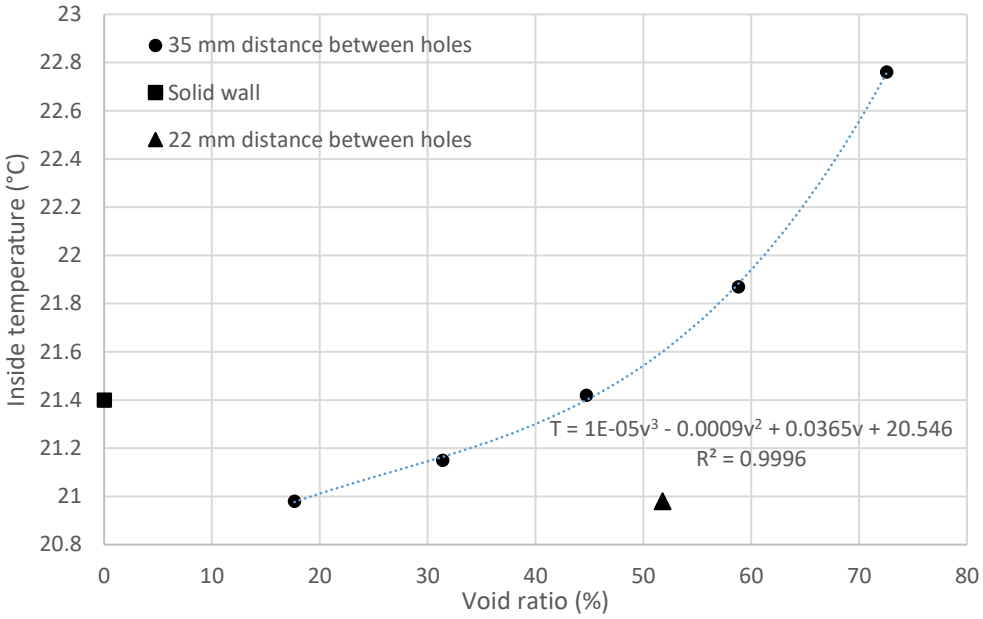

Figure 5-6: Inside temperature of wall sections with different void ratios that include cavity radiation and convection.

The 35 mm printing thickness shows a decreasing efficiency for large void ratio which is in contradiction with Figure 3-3 and the findings by Huang et al. (2018) stated in Section 3.2. For other printing thicknesses, such as the six holes of 22 mm in thickness shown in Figure 5-6, the trend deviates.

5.2 Analytical verification of numerical results

An analytical verification is done as a first step towards a design algorithm for the thermal performance of cavity walls. Therefore, a more effective design model can be developed in future. However, the use of a thermal resistance network that may still only account for the effects of thermal conduction shows that the problem is still intricate.

5.2.1 Background and assumptions

In order to perform hand calculations, it is assumed that heat transfer through a wall is perpendicular to the surface of the wall. There is no heat transfer in the direction where there is no change in temperature. Thus, the temperature in the plane parallel to the surface of the wall is constant.

The thermal resistance for conduction, convection and radiation can be expressed using Equations 5.1 to 5.3. The thermal resistance between two specific points with different temperatures can be expressed using Equation 5.4.

$$R_{cond} = \frac{L}{kA} \tag{5.1}$$

$$R_{conv} = \frac{1}{hA} \tag{5.2}$$

$$R_{rad} = \frac{1}{h_{rad}A} \tag{5.3}$$

$$R = \frac{\Delta T}{Q} \tag{5.4}$$

The radiation heat transfer coefficient, h_{rad}, is determined using Equation 5.5.

$$h_{rad} = \varepsilon\sigma(T_s^2 + T_a^2)(T_s + T_a) \tag{5.5}$$

Where T_s is the temperature of the surface of the wall and T_a is the ambient temperature to which the wall is exposed to. Both these temperature values should be Kelvin in the calculation of the radiation heat transfer coefficient.

Only the solid wall and wall with one 185 mm cavity is analytically verified with the FE results. It is assumed that the effect of radiation on the inside of the wall is negligible due to the small temperature changes seen in Table 5-4. This assumption also simplifies the analytical verification.

Table 5-4: FE temperatures results of the inside of a wall with no holes and with one hole with radiation only on the outside and radiation on the outside and inside

	Inside temperature of solid wall (°C)	**Inside temperature of wall with one hole (°C)**
Radiation on both sides	20	20.20
Radiation on outside only	20	20.30

Also, due to the addition of two extra unknown surface temperatures on either side of the air cavity on the inside of the outer and inner wall layers, it is assumed that heat is only transported through conduction in the air cavity for simplicity. It is thus not necessary to calculate the two extra unknown surface temperatures.

5.2.2 Thermal resistance network

A thermal resistance network is a representation of the heat flux through radiation, convection and conduction that travels through a system and is represented in the same way as an electric current flow as seen in Figure 5-7. Thus, the rate of heat transfer through a layer ($\dot{Q}$) is the parallel of the electric current (I) the thermal resistance (R) is the parallel of electrical resistance (R_e) and the temperature difference ($T_1 - T_2$) is the parallel of the voltage difference ($V_1 - V_2$) across the layer through which the heat is being transferred.

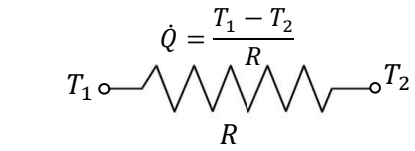

(a)

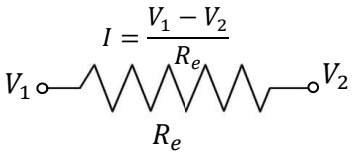

(b)

Figure 5-7: (a) heat flow and (b) electric current flow (reworked from Cengel & Ghajar, (2015)*)*

A thermal resistance network for a solid wall is shown in Figure 5-8 and for a wall with one hole is shown in Figure 5-9. The resistance due to convection and radiation on the outside of the wall is indicated in a parallel network and the resistance due to conduction of the wall is indicated in series with these parallel convection and radiation resistances.

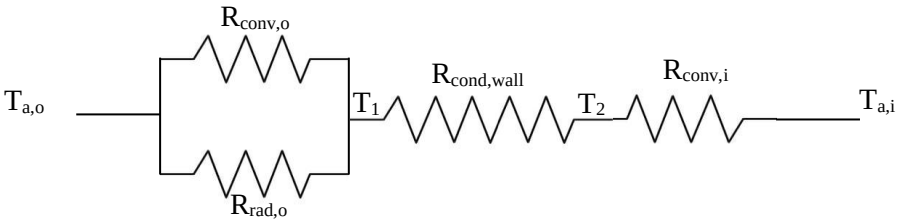

Figure 5-8: Thermal resistance network of a solid wall section.

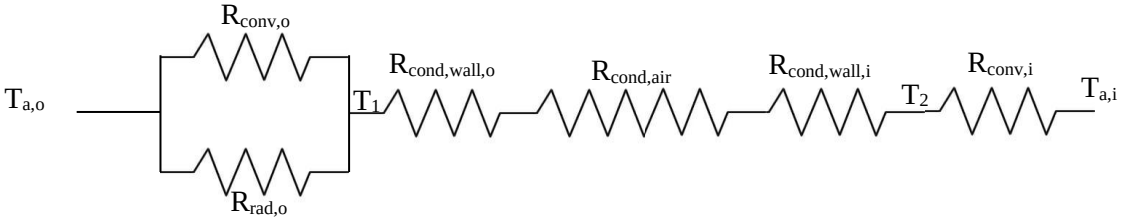

Figure 5-9: Thermal resistance network of a wall section with one cavity.

T_1 = temperature of the outside surface of the wall (°C)

T_2 = temperature of the inside surface of the wall (°C)

$T_{a,o}$ = ambient temperature of the outside environment (°C)

$T_{a,i}$ = ambient temperature of the inside environment (°C)

$R_{conv,o}$ = resistance due to convection of the outside environment (°C/W)

$R_{rad,o}$ = resistance due to radiation of the outside environment (°C/W)

$R_{conv,i}$ = resistance due to convection of the inside environment (°C/W)

$R_{rad,i}$ = resistance due to radiation of the inside environment (°C/W)

$R_{cond,wall}$ = resistance due to conduction of the wall (°C/W)

As seen from the radiation heat transfer coefficient equation, Equation 4.7, the temperatures of the wall surface and the ambient temperature have a large influence. When solving the heat transfer problem through a wall with the heat transfer principles, only the ambient temperatures outside and inside the wall are known while the temperatures of the surface of the wall on the outside and the inside are unknown. Thus, an iterative process is needed to solve the unknown temperatures.

First T_1 must be guessed in order to calculate the radiation heat transfer coefficient on the outside of the wall. Then the thermal resistances can be determined using Equations 5.1 to 5.3. Then a stepwise energy balance procedure is followed using Equations 5.6 to 5.12 in order to determine the surface temperature of the inside of the wall, T_2.

$$R_{combined,o} = \frac{1}{\frac{1}{R_{conv,o}} + \frac{1}{R_{rad,o}}} \tag{5.6}$$

$$Q_{loss,o} = \frac{T_1 - T_{a,o}}{R_{combined,o}} \tag{5.7}$$

$$Q_{net\ absorbed,o} = Q_{gross\ absorbed,o} - Q_{loss,o} \tag{5.8}$$

$$R_{combined,i} = R_{cond,wall} + R_{conv,i} \tag{5.9}$$

$$R_{combined,i} = R_{cond,wall,o} + R_{cond,wall,i} + R_{cond,air} + R_{conv,i} \tag{5.10}$$

$$T_{a,i} = T_1 - \frac{Q_{net\ absorbed,o}}{R_{combined,i}} \tag{5.11}$$

$$T_2 = T_{amb,i} - \frac{Q_{net\ absorbed,o}}{R_{combined,i}} \tag{5.12}$$

Tables 5-5 and 5-6 summarise the stepwise energy balance in order to determine the temperature of the inside of the wall with no cavities and one cavity respectively. When calculating the inside combined thermal resistance, for the wall with no cavities, Equation 5.9 is used and when calculating the inside combined resistance for the wall with one cavity, Equation 5.10 is used.

Table 5-5: Stepwise energy balance indicating heat flux, thermal resistances and temperatures of a solid wall.

Boundary conditions		
$\mathbf{Q_{incident}}$	342.02	W/m^2
$\mathbf{T_{a,o}}$	20	°C
$\mathbf{T_1}$	40.53	°C
Thermal resistances		
$\mathbf{R_{cond,wall}}$	0.687	°C/W
$\mathbf{R_{conv,o}}$	0.1	°C/W
$\mathbf{R_{conv,i}}$	0.1	°C/W
$\mathbf{R_{rad,o}}$	0.186	°C/W
Stepwise energy balance		
$\mathbf{Q_{gross\ absorbed,o}}$	342.02	W
$\mathbf{R_{combined,o}}$	0.065	°C/W
$\mathbf{Q_{loss,o}}$	315.813	W
$\mathbf{Q_{net\ absorbed,o}}$	26.207	W
$\mathbf{R_{combined,i}}$	0.787	°C/W
$\mathbf{T_{a,i}}$	19.897	°C
$\mathbf{T_2}$	22.517	°C

Table 5-6: Stepwise energy balance indicating heat flux, thermal resistances and temperatures of a wall with one air cavity.

Boundary conditions		
Incident heat flux	342.02	W/m^2
$\mathbf{T_{a,o}}$	20	°C
$\mathbf{T_1}$	41.98	°C
Thermal resistances		
$\mathbf{R_{cond,wall,o}}$	0.094	°C/W
$\mathbf{R_{cond,wall,i}}$	0.094	°C/W
$\mathbf{R_{cond,air}}$	7.061	°C/W
$\mathbf{R_{conv,o}}$	0.100	°C/W
$\mathbf{R_{conv,i}}$	0.100	°C/W
$\mathbf{R_{rad,o}}$	0.184	°C/W
Stepwise energy balance		
$\mathbf{Q_{gross\ absorbed,o}}$	342.02	W
$\mathbf{R_{combined,o}}$	0.06	°C/W
$\mathbf{Q_{loss,o}}$	339.02	W
$\mathbf{Q_{net\ absorbed,o}}$	3.00	W
$\mathbf{R_{combined,i}}$	7.35	°C/W
$\mathbf{T_{a,i}}$	19.94	°C
$\mathbf{T_2}$	20.24	°C

Tables 5-7 and 5-8 summarise the inside and outside temperatures of the solid wall and the wall with one large cavity.

Table 5-7: Difference in temperature of the ABAQUS results and the analytical verification of the inside of the solid wall.

	Numerical results	**Analytical verification**	**Difference (%)**
Outside wall surface temperature (°C)	40.458	40.53	0.178
Inside wall surface temperature (°C)	21.823	22.517	3.082

Table 5-8: Difference in temperature of the ABAQUS results and the analytical verification of the inside of the wall with one large cavity.

	Numerical results	**Analytical verification**	**Difference (%)**
Outside wall surface temperature (°C)	41.854	41.982	0.305
Inside wall surface temperature (°C)	20.397	20.24	0.780

5.3 Concluding summary

It is interesting to note that for a wall section with five cavities, the inside temperature is the same as for a wall section with six cavities (20.98°C). The wall with five cavities has a 17.65% void ratio with 9 mm thick cavities and the wall with six cavities has a 51.76% void ratio with 22 mm thick cavities. Furthermore, a too large void ratio such as 58.73% (Figure 5-3 (a)) influences the thermal performance negatively. Thus, a “good” void ratio does not take preference over more and thinner cavities. A cavity wall should have more cavities rather than less and cavities should be spaced close together for thermal performance. Thinner cavities also enhance the thermal performance.

The analytical verification gives a 3.082% higher temperature than the numerical results for the solid wall. For the cavity wall the analytical verification gives a 0.78% lower temperature than the numerical results. The lower temperature is probably due to the fact that the effect of cavity radiation and cavity convection is not taken into account in the cavity wall’s resistance network.

Chapter 6

6 Conclusions

6.1 General overview

The goal of this thesis was to investigate the thermal behaviour of foam concrete walls with different cavity sizes. In addition to solid foam concrete walls, 3D printed foam concrete wall sections were investigated to guide the geometrical design of the cross-sections containing cavities towards improved thermal performance

Chapter 1 mentioned that currently low and middle cost houses are built with CMU and that there are few set requirements and guidelines for housing projects in South Africa. An in depth study of foam concrete was therefore discussed in Chapter 2 in order to investigate the suitability of lightweight foam concrete as a building material. The different thermal parameters of foam concrete included the thermal heat transfer parameters, namely conduction, convection and radiation, the material density and porosity as well as the moisture content of foam concrete.

Chapter 3 dealt with case studies from literature to gain a better understanding of the application of the heat transfer mechanisms and how these mechanisms are applied in computational (FE) analysis. In Chapter 4 an existing 3D printed foam concrete wall section was analysed using the FEM. Simple rectangular cavities were then included in a wall with the same thickness of the 3D printed wall. The thickness and the number of these air cavities and the void ratio were varied to determine the lowest inside temperature of the wall. Lastly, numerical results were analytically verified using a thermal resistance network and iteratively solving for the temperatures of the outside and the inside surfaces of the wall.

6.2 Project findings

The conclusions derived from the results of the thesis are presented in this section. This includes the numerical and experimental results of different case studies and the comparison thereof with the author's findings. Conclusions on the size and number of holes are drawn in light of studies using pure conduction versus cavity radiation and convection inside the holes.

6.2.1 Heat transfer mechanisms in hollow walls

In Section 4.2 the heat transfer mechanisms, convection, conduction and radiation, were analysed in a hollow core wall section. Heat transfer through a wall with cavities is generally seen as being pure conduction which is correct only in cases where cavity radiation and convection are negligible. When assuming the heat transfers through the wall through pure conduction by using the conduction of air inside the cavities, namely Case D, the outside temperature is 42.022°C and the inside temperature is 20.145°C. When using cavity radiation rather than using the conduction of air, the outside temperature changes to 40.690°C and the inside temperature changes to 21.407°C (Case B). When adding cavity convection to the cavity radiation the outside temperature decreases to 40.540°C and the inside temperature increases to 21.573°C (Case C). Table 6-1 summarises the outside and inside temperature results for Cases B, C and D and shows the inside temperature as a percentage of the actual temperature for each case.

The difference in inside temperature between Case D and Case B is 5.9%. Thus, for triangular cavities with the specific dimensions assuming pure conduction through the cavities is not an accurate representation of the heat transfer through the wall and the effect of radiation inside the cavities needs to be taken into account. Therefore, care must be taken to verify whether cavity radiation and convection may be neglected, and only conduction considered in thermal analysis of a cavity wall section. For Cases B and C, the outside temperature decreases with 0.4% while the inside temperature increases with 0.8%. Thus, the addition of cavity convection is marginal.

Neglecting cavity radiation and convection may lead to significant under prediction, here 6.6%, of internal temperature in heat flow analysis of cavity walls as seen in Table 6-1.

Table 6-1: Outside and inside temperature results for heat transfer mechanisms.

Case	Outside Temperature (°C)	Inside Temperature (°C)	Percentage of actual	Mechanism
D	42.022	20.145	93.4	Conduction
B	40.690	21.407	99.2	+Radiation
C	40.540	21.573	100	+Convection

6.2.2 Size and number of holes

Different numbers and thicknesses of holes were analysed in Section 5.1. Two walls with the same total thickness of 255 mm were analysed. The one wall section had no air cavities while the other wall had one large cavity of 185 mm with a 35 mm foam concrete layer on either side of the cavity. It was found that the inside temperature for a solid wall was 21.4°C and for a wall with one hole of 185 mm the inside temperature was 22.76°C. Thus, although the thermal conductivity of air is lower than that of foam concrete, care should be taken when determining the size of the air cavities. Radiation and convection inside cavities decreases the air's thermal resistance.

Furthermore, the effective thermal conductivity can be decreased by adding more and smaller cavities to a wall which then increases the thermal resistance of the wall. This was proven by analysing two wall sections both with a total thickness of 255 mm. The first wall had three cavities of 38 mm in thickness with foam concrete layers of 35 mm. This wall had an inside temperature of 21.42°C. A wall with six holes of 22 mm in thickness with foam concrete layers of 17.5 mm had an inside temperature of 20.98°C.

In conclusion, care must be taken when considering hollow core walls above solid wall sections. Solid walls in some cases provide better thermal performance; that is lower inside temperatures, than walls with one, two or ever three larger cavities. Cavities should be thin and larger numbers of cavities should be considered for a wall to obtain better thermal performance. Also, when analysing hollow core walls, the effect of cavity radiation cannot be neglected even in thin cavities.

6.2.3 Void ratio

The influence of a large void ratio was also analysed. The void ratio is measured as the total thickness of the air cavities over the total thickness of the wall. A wall with a void ratio of 58.73% with two holes of 75 mm had an inside temperature of 22.76°C while a wall with a void ratio of 31.22% with four holes of 20 mm had an inside temperature of 21.15°C. A wall with a void ratio of 17.65% with five holes of 9 mm and a wall with a void ratio of 51.76% with six holes of 20 mm both had an inside temperature of 20.98°C.

Thus, when designing a wall for thermal efficiency the number of holes must first be increased before increasing the void ratio.

6.2.4 Analytical verification

The numerical results for the solid wall and the wall with a 185 mm air cavity were verified through heat transfer equations. The verifications were simplified so that radiation heat transfer was neglected on the inside of the walls and that the hollow wall was assumed to take on a pure conduction problem due to the various number of unknown temperatures inside the cavity and the complexity of heat traveling into the wall, but also being rejected back into the environment.

Due to the presence of convection radiation heat transfer on the outside of the wall and the difference in the outside ambient temperature and the temperature on the surface of the outside of the wall, not all the solar heat was absorbed by the wall. For both the solid wall and the wall with one air cavity, the wall accepted 7.662% of the total solar heat that the wall was exposed to.

The analytical results of the inside temperature of the solid wall was 22.517°C which was 3.082% higher than that of the numerical results. The analytical results of the inside temperature of the wall with one air cavity was 20.24°C which was 0.78% lower than that of the numerical results.

6.3 Recommendations and further research

6.3.1 Effect of small cavities on installation of reinforcement

This thesis only focussed on the thermal efficiency of foam concrete as a façade structure for middle cost housing. Further research must be done to determine the balance between thermal efficiency and strength of foam concrete walls with small and many air cavities. The effect of significantly small cavities on the difficulty of installation of reinforcement must further be researched as well as what the effect of reinforcement is on the effective thermal conductivity of the wall and thus the thermal efficiency of the wall.

6.3.2 Effect of ease of 3D printability

For better thermal performance of a foam concrete wall, small but many air cavities should be allowed in the wall. This has an effect on the ease and speed of 3D printing. The 3D printer at Stellenbosch University prints on average 15 mm high layers with an average thickness of 35 mm.

6.3.3 Further research on use of phase change material in cavities

The use of phase change material can absorb and release sufficient amounts of energy to heat or cool the inside environment of a building. The combination of phase change material (PCM) and the use of foam concrete walls with small, but many air cavities is a further research point to increase the thermal performance of these walls. Layers of foam concrete, PCM and air cavities can lead to a further decrease in internal temperature when used as a walling structure.

What is more, larger cavities in 3DP wall sections prone to cavity radiation and convection, could be filled with non-structural foam concrete of low density, whereby low conductivity replaces radiation and convection as heat transfer mechanism in the large cavities.

7 References

Act No. 103 (1977). National Building Regulations and Building Standards Act. Government Gazette of the Republic of South Africa, 6 July.145 (5640).

Agrément (2019). *Agrément South Africa*. [Online] Available at: www.agrement.co.za

Aldridge, D. (2005). Introduction to foamed concrete: what, why, how?. *Use of foamed concrete construction.* Scotland: Thomas Telford, p. 158.

Al-Tamimi, A. S., Al-Osta, M. A., Ben-mansour, R., & Al-Amoudi, O. S. B. (2017). Effect of Geometry of Holes on Heat Transfer of Concrete Masonry Bricks Using Numerical Analysis, 3733–3749. https://doi.org/10.1007/s13369-017-2482-6

Amran, Y. H. M., Farzadnia, N., & Ali, A. A. A. (2015). Properties and applications of foamed concrete; A review. *Construction and Building Materials*, *101*, 990–1005. https://doi.org/10.1016/j.conbuildmat.2015.10.112

Bekkouche, S. M. E. A., Benouaz, T., & Kamal, C. M. (2013). Thermal resistances of air in cavity walls and their effect upon the thermal insulation performance. *Energy and Environment*, *4*(3), 459–466.

Cengel, A. Y., & Ghajar, J. A. (2015). *Heat and Mass Transfer* (5th ed.). USA: McGraw-Hill Education.

Cho, S, Kruger, J., & Zeranka, S. (2019). 3D Printable concrete technology and mechanics, (c), 7–14.

Cho, S, Kruger, J., Zeranka, S., Van Rooyen, A. S., & Van Zijl, G. (2019). Mechanical evaluation of 3D printable nano-silica incorporated fibre-reinforced lightweight foam concrete. In Proceedings of the 10th International Conference on Fracture Mechanics of Concrete and Concrete Structures FraMCos-X, Editors: G. Pijaudier-Cabot, (b).

Cho, Seung, Kruger, J., Rooyen, A. Van, Zeranka, S., & Zijl, G. Van. (2019). Rheology of 3D printable lightweight foam concrete incorporating nano- silica (pp. 373–381). Dresden, Germany: SPRINGER.

De Villiers, J. P., Van Zijl, G., & Van Rooyen, A. S. (2017). Bond of deformed steel reinforcement in lightweight foamed concrete. *Wiley Fib*, (July 2016), 496–506. https://doi.org/10.1002/suco.201600019

De Villiers, W. I. (2019). *Computational and Experimental Modelling of Masonry Walling towards Performance - Based Standardisation of Alternative Masonry Units for Low - Income Housing*. Stellenbosch University.

Del Coz Diaz, J. J., Garcia-nieto, P. J., Alvarez-rabanal, F. P., Alonso-martínez, M., Dominguez-hernandez, J., & Perez-bella, J. M. (2014). The use of response surface methodology to improve the thermal transmittance of lightweight concrete hollow bricks by FEM, *52*, 331–344. https://doi.org/10.1016/j.conbuildmat.2013.11.056

del Coz Diaz, J. J., Garcia Nieto, P. J., Suarez Sierra, J. L., Alvarez Rabanal, F. P., Lozano, Martinez-Luengas, A., & Dominguez-Hernandez, J. (2012). Non-Linear Heat Transfer Analysis of the Performance of Light Concrete Hollow Brick Walls by the Finite Element Method (pp. 1–34). Saxe-Coburg Publications.

Do Amaral, D. R. (2019). *Dimensional Stability of Lightweight Foamed Concrete Thesis*. Stellenbosch University.

Dunn, T. P. A. (2017). *Precast Lightweight Foamed Concrete Walling , a Structural System for Low-Rise Residential Buildings by*. Stellenbosch University.

Dunn, T., Van Zijl, G., & Van Rooyen, A. S. (2017). Reinforced lightweight foamed concrete for seismically resistant low-rise residential buildings. In *International conference on advances in construction materials and systems, ICACMS*.

Ehlert, J. R. and Smith, T.F., 1993, "View Factors for Perpendicular and Parallel, Rectangular Plates," J. Thermophys. Heat Trans., vol. 7, no. 1, pp. 173-174.

Hilal, A. A., Thom, N. H., & Dawson, A. R. (2015). On entrained pore size distribution of foamed concrete. *Construction and Building Materials*, *75*, 227–233. https://doi.org/10.1016/j.conbuildmat.2014.09.117

Huang, S., Hu, M., Huang, Y., Cui, N., & Wang, W. (2018). A New Model for Optimal Mechanical and Thermal Performance of Cement-Based PartitionWall. *Materials*, *11*(615), 1–15. https://doi.org/10.3390/ma11040615

Jeffers, A., Wickström, U., & McGrattan, K. (2013). Documentation of the Solutions to the SFPE Heat Transfer Verification Cases. In *1ste SFPE Europe conference on fire safety engineering*. Copenhagen, Denmark.

Johnson, L., & Hasselman, D. (1987). Effective thermal conductivity of composites with interfacial thermal barrier resistance. *Journal of Composite Materials*. https://doi.org/10.1177/002199838702100602

Jones, M. R., & McCarthy, A. (2006). Heat of hydration in foamed concrete: Effect of mix constituents and plastic density. *Cement and Concrete Research*, *36*(6), 1032–1041. https://doi.org/10.1016/j.cemconres.2006.01.011

Just, A., & Middendorf, B. (2008). Microstructure of high-strength foam concrete. *Materials Characterization*, *60*(7), 741–748. https://doi.org/10.1016/j.matchar.2008.12.011

Kearsley, E, & Visagie, M. (2002). Properties of Foamed Concrete as Influenced by Air-Void Parameters. *Concrete Beton*, *101*, 9–13.

Kearsley, EP, & Wainwright, P. (2001). Porosity and permeability of shale.pdf, *31*. https://doi.org/10.1016/S0008-8846(01)00490-2

Lee, Y., Choi, M., Yi, S., & Kim, J. (2009). Cement & Concrete Composites Experimental study on the convective heat transfer coefficient of early-age concrete. *Cement and Concrete Composites*, *31*(1), 60–71. https://doi.org/10.1016/j.cemconcomp.2008.09.009

Liu, M. Y. J., Alengaram, U. J., Jumaat, M. Z., & Mo, K. H. (2014). Evaluation of thermal conductivity, mechanical and transport properties of lightweight aggregate foamed geopolymer concrete. *Energy and Buildings*, *72*, 238–245. https://doi.org/10.1016/j.enbuild.2013.12.029

Lorente, S., Petit, M., & Javelas, R. (1998). The effects of temperature conditions on the thermal resistance of walls made with different shapes vertical hollow bricks. *Energy And*, *28*, 237–240.

Marshall, A. L. (1972). The Thermal Properties of Concrete. *Building Science*, *7*, 167–174.

Marx, H. (2018). *Thermal behaviour of a novel cellular beam structural system in fire*. Stellenbosch University. Retrieved from https://scholar.sun.ac.za

Miled, K., & Limam, O. (2016). Effective thermal conductivity of foam concretes: Homogenization schemes vs experimental data and FEM simulations. *Mechanics Research Communications*, *76*, 96–100. https://doi.org/10.1016/j.mechrescom.2016.07.004

Mubatapasango, M. (2017). *Carbonation induced corrosion in integral and non - integral surface treated lightweight foam concrete*. Stellenbosch University. Retrieved from https://scholar.sun.ac.za

Mydin, M. A. O. (2011). Effective thermal conductivity of foamcrete of different densities. *Concrete*

Research Letters, *2*, 181–189.

Mydin, M. A. O. (2013). Modeling of transient heat transfer in foamed concrete slabs. *Journal of Engineering Science and Technology*, *8*(3), 326–343.

Mydin, M. A. O., Awang, H., & Roslan, A. F. (2012). Determination of lightweight foamed concrete thermal properties integrating various additives. *Elixir Cement & Con. Com.*, *48*, 9286–9291.

October, L. (2019). *Facade structural engineering of 3D printed housing facades*. *Thesis*. Stellenbosch University.

Oginni, F. A. (2017). Continental Application of Foamed Concrete Technology : Lessons for Infrastructural Development in Africa Continental Application of Foamed Concrete Technology : Lessons for Infrastructural Development in Africa, (January 2015). https://doi.org/10.9734/BJAST/2015/13063

Othuman, M. A., & Wang, Y. C. (2011). Elevated-temperature thermal properties of lightweight foamed concrete. *Construction and Building Materials*, *25*(2), 705–716. https://doi.org/10.1016/j.conbuildmat.2010.07.016

Panesar, D. K. (2013). Cellular concrete properties and the effect of synthetic and protein foaming agents. *Construction and Building Materials*, *44*, 575–584. https://doi.org/10.1016/j.conbuildmat.2013.03.024

Pietrak, K., & Winiewski, T. S. (2015). A review of models for effective thermal conductivity of composite materials. *Journal Journal of Power Technologies*, *95*(1), 14–24. https://doi.org/10.1109/TPAMI.1986.4767851

Ramamurthy, K., Kunhanandan Nambiar, E. K., & Indu Siva Ranjani, G. (2009). A classification of studies on properties of foam concrete. *Cement and Concrete Composites*, *31*(6), 388–396. https://doi.org/10.1016/j.cemconcomp.2009.04.006

Reddy, B. V. V., & Jagadish, K. S. (2003). Embodied energy of common and alternative building materials and technologies. *Energy and Buildings*, *35*, 129–137.

Sala, J. M., Urresti, A., Martin, K., Flores, I., & Apaolaza, A. (2008). Static and dynamic thermal characterisation of a hollow brick wall : Tests and numerical analysis. *Energy and Buildings*, *40*, 1513–1520. https://doi.org/10.1016/j.enbuild.2008.02.011

Silva, N., Mueller, U., Malaga, K., Hallingberg, P., & Cederquist, C. (2015). Foam concrete-aerogel composite for thermal insulation in lightweight sandwich facade elements. In *Concrete 2015* (pp. 1355–1362).

Tada, S. (1986). Material design of aerated concrete-An optimum performance design. *Materials and Structures*, *19*(1), 21–26. https://doi.org/10.1007/BF02472306

Tomlinson, M., & Jeffery, A. (2015). South Africa's Housing Conundrum. *South African Insitute of Race Relations*, *4*(20), 1–7.

Van Rooyen, A. S. (2013). *Structural lightweight aerated concrete*. University of Stellenbosch.

Van Zijl, G., & Van Rooyen, A. S. (2018). Developing Reinforced Foam Concrete As a Composite Material for Durable Structural Application. In *4th Brazilian Conference on Composite Materials* (pp. 216–224). Rio de Janeiro. https://doi.org/10.21452/bccm4.2018.02.22

Vinith Kumar, N., Arunkumar, C., & Srinivasa Senthil, S. (2018). Experimental Study on Mechanical and Thermal Behavior of Foamed Concrete. *Materials Today: Proceedings*, *5*(2), 8753–8760. https://doi.org/10.1016/j.matpr.2017.12.302

Wei, S., Yiqiang, C., Yunsheng, Z., & Jones, M. R. (2013). Characterization and simulation of microstructure and thermal properties of foamed concrete. *Construction and Building Materials*,

47, 1278–1291. https://doi.org/10.1016/j.conbuildmat.2013.06.027

Zhou, A., Wong, K., & Lau, D. (2014). Thermal Insulating Concrete Wall Panel Design for Sustainable Built Environment. *The Scientific World Journal*. Retrieved from http://dx.doi.org/10.1155/2014/279592